USING QB VLPS TO PACKAGE, PROTECT, AND DELIVER *IN VIVO* PRODUCED RNAS

A Dissertation
Presented to
The Academic Faculty

by

Po-Yu Fang

In Partial Fulfillment
of the Requirements for the Degree
Doctor of Philosophy in the
School of Chemistry & Biochemistry

Georgia Institute of Technology
August 2016

USING QB VLPS TO PACKAGE, PROTECT, AND DELIVER *IN VIVO* PRODUCED RNAS

Approved by:

Dr. Loren D. Williams, Advisor
School of Chemistry & Biochemistry
Georgia Institute of Technology

Dr. Nicholas V. Hud
School of Chemistry & Biochemistry
Georgia Institute of Technology

Dr. Adegboyega K. Oyelere
School of Chemistry & Biochemistry
Georgia Institute of Technology

Dr. Roger M. Wartell
School of Biology
Georgia Institute of Technology

Dr. George E. Fox
Department of Biology & Biochemistry
University of Houston

Date Approved: June 30th, 2016

ACKNOWLEDGEMENTS

TABLE OF CONTENTS

LIST OF TABLES

LIST OF FIGURES

LIST OF ABBREVIATIONS

AAV	Adeno-associated viruses
Ago	Argonaute
APOE	Apolipoprotein E
BBB	Blood brain barrier
CP	Coat protein
DNA	Deoxyribonucleic acid
Double stranded RNA	dsRNA
DTT	Dithiothreitol
E. coli	*Escherichia coli*
EDC	Ethyl-3-(3-dimethylaminopropyl) carbodiimide
EDTA	Ethylenediaminetetraacetic acid
GFP	Green fluorescent protein
HBV	Human papillomavirus
HIV	Human immunodeficiency virus
hp	Hairpin
LNPs	Lipid nanoparticles
MES	2-(N-morpholino)ethanesulfonic acid
miRNA	microRNA
mRNA	messenger RNA
MW	Molecular weight
NHS	N-hydroxysuccinimide
NoV	Nodamura virus
nt	Nucleotide
PACT	Protein kinase RNA activator

PDB	Protein Data Bank
PEG	Polyethylene glycol
PEI	Polyethyleneimine
PLL	Poly-L-lysine
Pre-miRNA	Precursor microRNAs
Pri-miRNA	Primary microRNAs
ₚVLP	Polymer-VLPs
RBS	Ribosomal binding site
RISC complex	RNA-induced silencing complex
RNA	Ribonucleic acid
RNAi	RNA interference
rRNA	Ribosomal RNA
RSV	Respiratory syncytial virus
shRNA	short hairpin RNA
SMCC	succinimidyl 4-(N-maleimidomethyl)cyclohexane-1-carboxylate
T. thermophilus	*Thermus thermophiles*
TRBP	Transactivation response RNA-binding protein
tRNA	Transfer RNA
UTR	Untransltated region
V. proteolytocus	*Vibrio proteolyticus*
VEGF	Vascular endothelial growth factor
VLPs	Virus-like particles

SUMMARY

This project focuses on Using Qβ VLPs to package, protect, and deliver recombinantly produced RNAs. The ultimate goal is to develop an RNA interference (RNAi) delivery platform to inhibit gene expression that is spontaneously assembling and scalable for potential medical applications. Preliminary studies suggested that this platform is amenable to efficient packaging of functional RNA and, most recently, simultaneous packaging with DNA plasmid. The principle goals were to i) determine the prevailing factors that affect efficient RNA assembly within VLPs, ii) demonstrate spontaneously intracellular uptake of VLP-cargos, iii) design a RNAi scaffold for one step *in vivo* VLP-RNA assembly, iv) deliver VLP-RNAi to human cancer cells for gene knockdown and expression, and vi) decorate RNA-containing VLP with polymer for plasmid delivery.

I have made significant progress in solving the VLP-RNA assembly problem and have discovered parameters that allow optimization of RNA production, packaging density and purity within Qβ VLPs. For the first time, to our knowledge, we can obtain Qβ VLP-RNAs containing a high density of homogeneous RNA. I also demonstrated that VLP offer substantial protection to packaged RNA against various types of metal-mediated cleavage.

I devised an RNAi scaffold that is a general utility single RNA molecule chimera that contains a functional RNA duplex with paired silencing and carrier sequences linked by and stabilized by a RNA stem-loop. The scaffold is a single molecule of RNA with the hairpin on the 5' end that confers affinity for the viral coat protein (CP). The free 3' end

of the scaffold allows for recognition by Dicer and transfer of the processed RNA to Argonaute (Ago). Silencing sequences can include mature miRNAs and siRNAs, and can target any mRNA.

I claim a single-step and scalable method for recombinantly produced RNAs and folding of functional RNAs in a novel RNAi scaffold, packaged within VLPs. The VLP-RNAi assembles in *E. coli*, or other expression systems, upon co-expression of CP and the RNAi scaffold. The annealing of the scaffold to form functional RNAs is intramolecular, because the scaffold is a single RNA molecule, and therefore annealing is concentration independent and is efficient in the *in vivo* assembly environment.

I introduced a VLP surface decorating method using cationic polymers that is generally applicable, scalable, spontaneously assembling at the level of molecules, deliverable, targetable and potential orally available. Capsid protein and functional RNA or protein co-produce and co-assemble to produce VLP assembles *in vivo*. With this decorating method, VLPs can attract plasmid DNA on the exterior of the VLP surface. The method is amenable to packaging of a broad array of plasmid DNA and negatively charged drug molecules.

The ultimate goal is to deliver multifunctional VLPs against brain tumor growth in mice. The new RNAi scaffold we designe can carry different target siRNAs and self-assemble into stable RNA nanoparticles. The RNA nanoparticles with Qβ hp can then be encapsulated into Qβ VLP. We believe this multifunctional VLPs platform has potential

to overcome impediments as mentioned earlier and is well suited for nucleic acid-based tools.

All together, this dissertation expands our current knowledge on RNA packaging in VLPs and demonstrates proof of concept of combining VLPs with novel RNAi scaffold and cationic polymer as a delivery tool for multiple cargos to mammalian cells.

CHAPTER 1

1. INTRODUCTION

1.1 Qβ Virus-Like Particles and Current Applications

1.1.1 *General background of Qβ virus-like particles*

Qβ Virus-like particles (VLPs) are macromolecule self-assemblies, composed of 180 copies of a 14.4 kDa coat proteins that form three-dimensional structures resembling native single-stranded RNA bacteriophage Qβ viruses at the nanometer level. The coat protein monomer forms Qβ dimer spontaneously under physiological conditions (Figure 1.1-1).[1,2] Dimers further assemble into pentamer and hexamer by disulfide bonds and hydrogen bond interactions that eventually form Qβ VLP (Figure 1.1-2). The size of Qβ VLPs ranges from 25 to 30 nm with icosahedral structure and have pores of around 14 Å and 7 Å in diameter.[1] Although the morphology of Qβ VLPs is similar to infectious viruses, they are benign and noninfectious due to the absence of viral nucleic acid. Qβ VLPs have shown substantial tolerance against hostile organic solvents,[2,3] extreme pH conditions,[4] and high temperature stress,[5,6] due to their inherent structural stability. Qβ VLPs have also been gaining a lot of attention in recent years because of their biocompatibility, biodegradability, and low toxicity.[7,8] Nowadays, Qβ VLPs can be obtained from different recombinant organisms. The genes encoding viral coat protein are cloned, recombinantly expressed, and self-assembled in microbial, yeast, and cell-free protein synthesis reaction.[4,9,10]
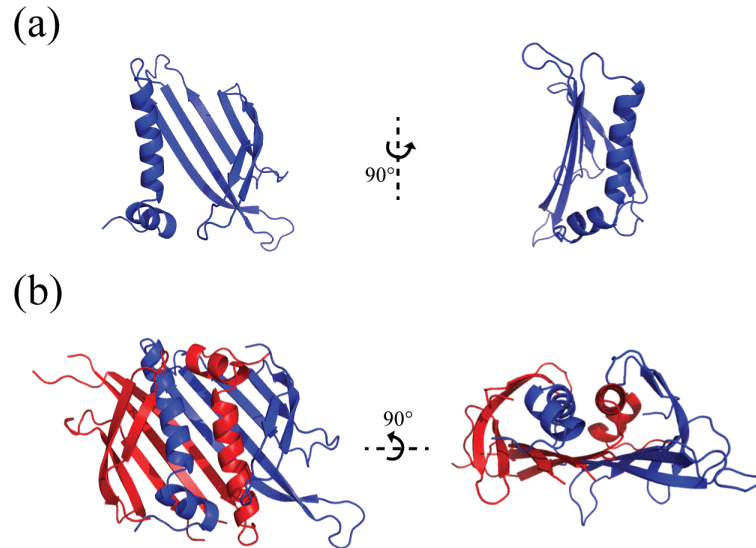
Figure 1.1-1 The structure of (a) Qβ coat protein monomer and (b) noncovalent coat protein dimer (PDB: 1qbe).
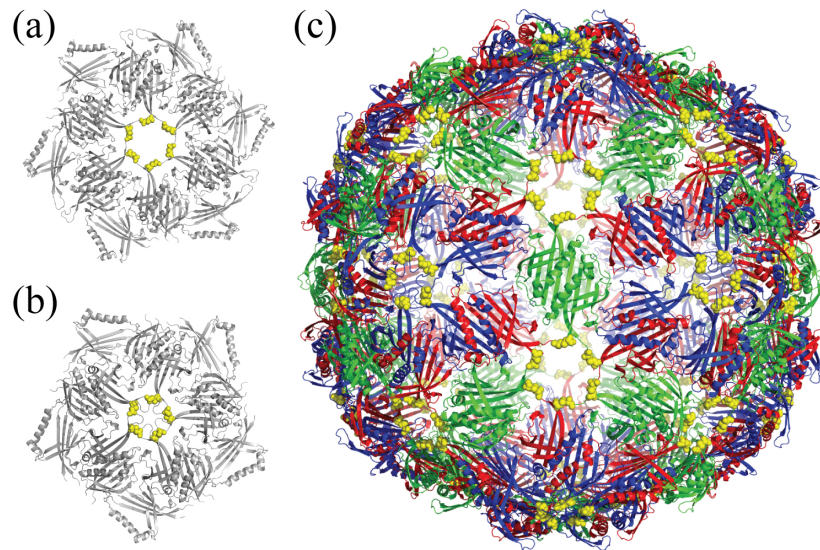
Figure 1.1-2 Self-Assembly of Qβ VLP shown in cartoon representation. (a and b) Qβ dimers self-assemble into hexamer and pentamer by the disulfide bonds in yellow. (c) The structure of Qβ capsid consists of 20 hexamers and 12 pentamers. (PDB: 1qbe)

1.1.2 *Surface modification of Qβ VLPs*

Qβ VLPs have potential for several biomedical applications. The composition and highly ordered repetitive structure of Qβ VLPs allow conventional protein conjugation strategies.[11,12] For example, VLPs, which bear lysines, glutamic or aspartic acids, cysteines, and tyrosines on their surface, can be conjugated covalently with ligand and small molecules to generate chimeric VLPs *in vitro* (Figure 1.1-3).[8,13] Chemical modification allows the conjugation of VLPs to multiple molecules, such as antigens, peptides, fluorescent dyes, protein, and complex carbohydrates.[14] The surface functionalization of VLP with different functional molecules has been integrated to produce multifunctional bio-nanoparticles that may be used for drug delivery, bioimaging, and cell targeting.[15]
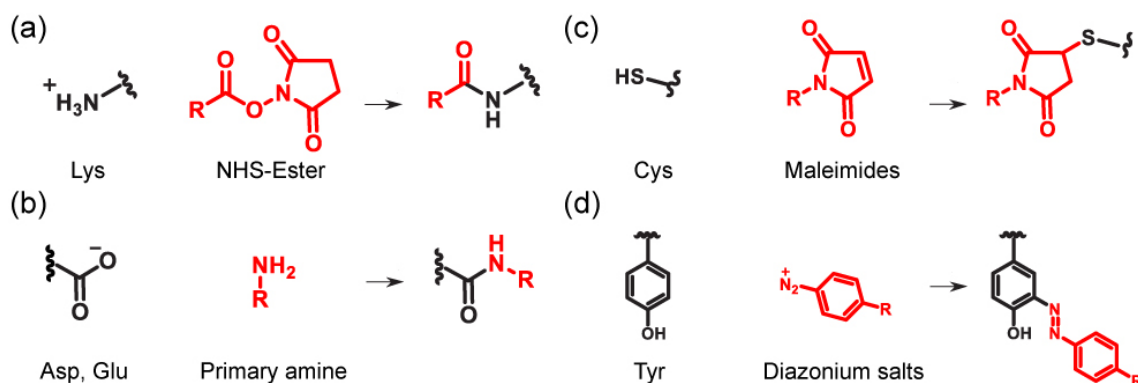
Figure 1.1-3 Conventional bioconjugation strategies targeting the functional groups of natural amino acids of Qβ VLPs.

In addition to the chemical modification, viral coat proteins can tolerate extensive genetic modification. Heterologous peptides are capable of being inserted into coat protein using recombinant nucleic acid technique.[16,17] Introducing single or multiple mutations into the sequence of the Qβ coat protein gene allow production of chimeric VLPs in distinct

3

structural forms.[2] In addition, dual expression of Qβ coat protein and Qβ coat protein-peptide fusion in *E. coli* results in the assembly of hybrid VLPs. It is the most common method for displaying proteinaceous ligands on the exterior surface of VLPs. (Figure 1.1-4).[18,19] However, genetic insertion of long heterologous peptides (more than 20 amino acids) may lead to failed self-assembly.
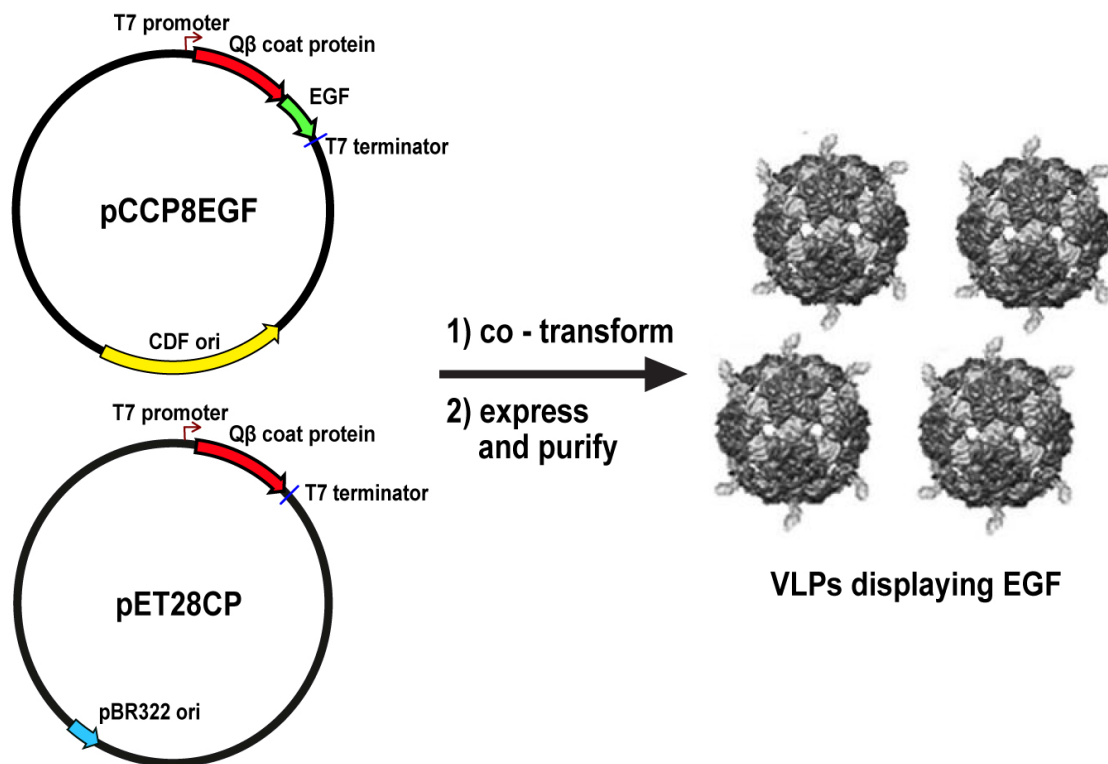
Figure 1.1-4 Genetic insertion of epidermal growth factor on the exterior surface of hybrid Qβ VLPs. Figure adapted from Pokorski et al.[18]

1.1.3 *In vitro and in vivo packaging of cargo into Qβ VLPs*

In addition to the applications of exterior surface modification of VLPs, packaging capacity of VLPs has lately generated interest as a way to develop of new drug delivery vehicles that can encapsulate nucleic acids,[20-22] proteins,[23,24] and small molecules.[25,26] VLPs have been successfully employed as multifunctional bio-nanoparticles to conjugate targeting ligands and selectively deliver quantum dots, chemotherapeutic drugs, siRNA molecules, and protein toxins to mammalian cells (Figure 1.1-5).[15] The major problems of using VLPs as nanocarriers is based on *in vivo* expression of viral coat protein and *in vitro* self-assembly and encapsulation of cargo. This *in vitro* packaging approach has a number of impediments, such as coat protein re-assembly difficulties, and inefficient encapsulation. Thus, a general, efficient and robust strategy for the *in vivo* production of protein-filled or RNA-filled VLPs has been developed to overcome the inconveniences of *in vitro* self-assembly and encapsulation of cargos.

In comparison to *in vitro* packaging method, *in vivo* packaging approaches are attractive for the following reasons: (i) All cargos are produced with VLPs simultaneously *in vivo*. (ii) Decreased chance of failure to fold cargos (protein and RNA) into native structure. (iii) Cargos expressed in recombinant organisms are selectively encapsulated into particles within cells. (iv) Coat proteins can efficiently self-assemble to form VLP-cargo complexes. (v) VLPs offer *in vivo* packaged cargos substantial protection from thermal inactivation, enzyme degradation, and non-specific protein adsorption. Finn, et al, has demonstrated the RNA-mediated packaging method to encapsulate active enzymes within VLPs *in vivo* (Figure 1.6).[23,24] Recently, Ponchon, et al, exhibited encapsulation of tRNA

fusions in VLPs to form RNA-protein complexes using *E. coli.*[21] *In vivo* packaging may increase the yield of fragile RNA molecules and proteins, enable rapid purification of stabilized recombinant RNA molecules, and provide new delivery tools for targeted cancer therapy.
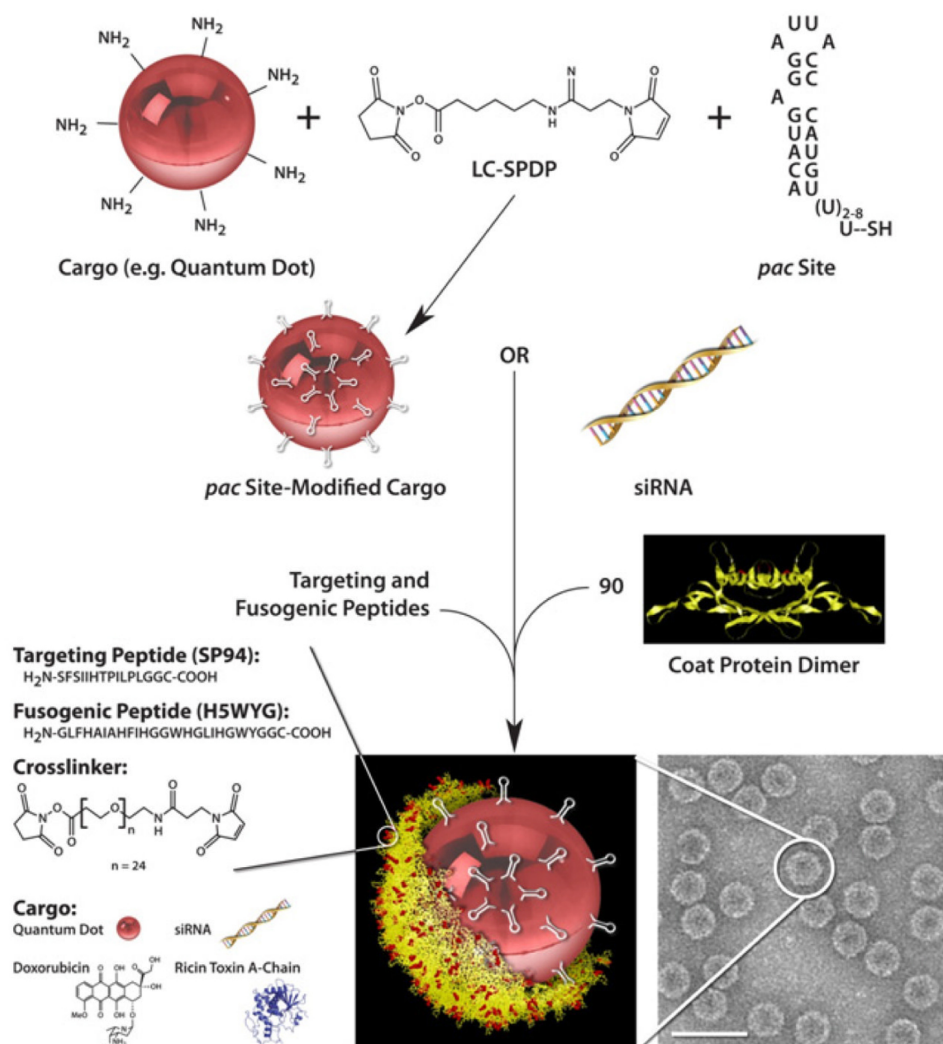
Figure 1.1-5 Using conjugation strategies and *in vitro* assembly method on MS2 VLPs to selectively deliver quantum dots, anticancer drugs, siRNA molecules to human hepatocellular carcinoma. Figure adapted from Ashley et al.[15]

Impediments to broadly applicable RNA-based therapeutics remain. Cellular uptake is inhibited by the high anionic charge of RNA. Chemical and biological stability of RNA is low.[27,28] RNA production on large scales by *in vitro* RNA transcription [29] or solid-phase synthesis [30] is problematic.[31,32] The packaging of RNA by protein(s) in coupled RNA production/packaging systems *in vivo* may be effective for overcoming at least a subset of these challenges. RNA expression *in vivo* [33-35] employs recombinant viral RNAs containing polymerase promoters upstream from target sequences.

Coupled RNA production/protein packaging are achievable because non-viral RNA can be encapsulated in VLPs upon co-expression of RNA and CP in systems such as *E. coli*.[36] RNA packaging into VLPs is promoted by incorporation of RNA hairpins with high affinity for CP.[37,38] These hairpins, with specific Qβ or MS2 sequences, are derived from the genomes of the viral RNAs. CP binds to the viral RNA hairpins during virus assembly *in vivo*.[39] Secondary structure also promotes viral assembly; RNA stem-loops promote capsid formation.[40] Biological stability of RNA is increased by scaffold systems in which target RNA is fused to stable folds such as 5S rRNA or tRNA. These fusions allow simultaneous production and purification of active RNA in fermentation-based systems.[41-46]
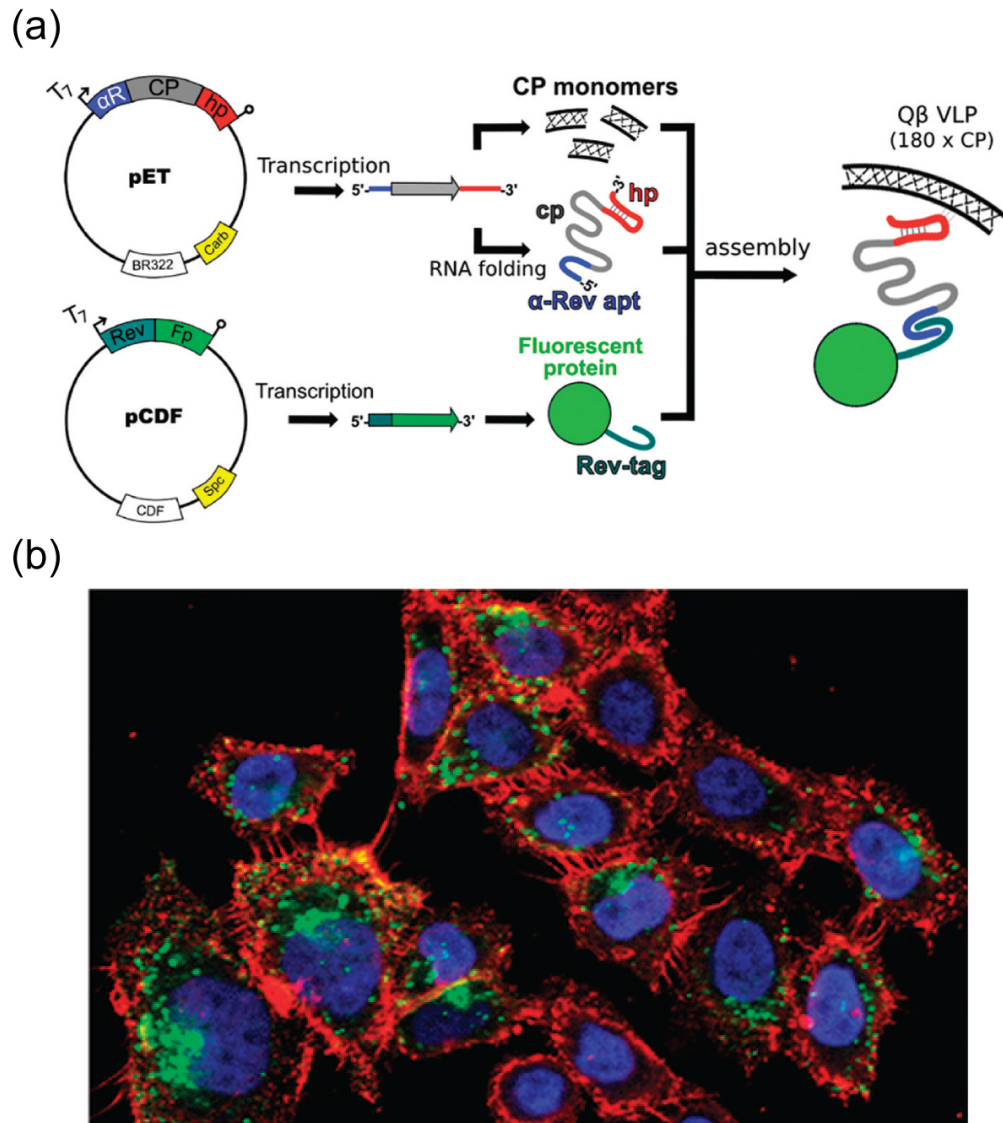
Figure 1.1-6 (a) Using dual plasmid strategies to encapsulate green fluorescent protein inside Qβ VLPs. (b) Chemically derivatized fluorescent VLP were internalized by Chinese hamster ovary cells. Figure adapted from Rhee et al [23].

1.2 RNA Interference

1.2.1 *General background of RNAi*

The discovery of double stranded RNA (dsRNA) inducing repression of endogenously expressed protein in *Caenorhabditis elegans* was one of the most important discoveries in cell biology.[47] This unique gene silencing effect was later shown to be carried out in mammalian cells transfected with 21 nucleotide (nt) RNA duplexes [48] known as small interfering RNAs (siRNAs). This biological mechanism, termed RNA interference (RNAi), has potential utility in fundamental research, in drug discovery, and in treatment of genetic disorders. In 2004, introduction of a siRNA molecule by intravitreal injection demonstrated great success in targeting the vascular endothelial growth factor (VEGF) mRNA. In recent years, using RNAi based tools for therapeutic applications has been applied to a wide range of human diseases, including genetic diseases, cancers, and viral infections.[49,50] An intriguing property of RNAi-based tools is the specificity of target gene knockdown, taking advantage of base-pairing interactions for target recognition. The main types of RNA molecules involved in RNAi are microRNAs (miRNAs) and siRNAs.

1.2.2 *The miRNA processing pathway*

miRNAs are naturally occurring biological molecules. Numerous miRNAs have been identified in insects,[51] plants,[52] and humans.[53] In contrast to siRNAs, miRNAs are usually ~21-25 nt asymmetric RNA duplexes. They are partially complementary to the mRNA target usually located within the 3' untranslated region (UTR) to mediate post-transcriptional gene silencing. miRNAs require extensive processing from their

transcribed precursors in order to form mature RISC, which inhibits translation initiation (Figure 1.2-1, right).[54,55] First, primary microRNAs (pri-miRNAs) are expressed from genomic DNA in nucleus,[56,57] and are processed by microprocessor complex (Drosha and *DGCR8*) into ~70 nt precursor miRNAs (pre-miRNAs).[58,59] The pre-miRNAs are further exported to cytoplasm by exportin 5. Dicer associates with trans-activation response RNA-binding protein (*TRBP*) and protein kinase RNA activator (*PACT*) processes exported pre-miRNAs into miRNA duplexes. miRNA duplex is then loaded into Argonaute (Ago) protein-containing complex to form precursor RNAi-induced silencing complex (pre-RISC). To form activated RISC, one strand of the duplex, where it serves as "passenger strand" is removed. Finally, the "guide strand" of the duplex in activated RISC directs the complex to target gene and inhibits protein translation. RISC dissociates from cleaved mRNA and is recycled for additional rounds of gene silencing. Synthetic siRNA and short hairpin RNA (shRNA), which mimics Dicer substrates, can be loaded into Dicers and allows RISC complex to trigger site-specific cleavage.[60,61]

1.2.3 *The siRNA processing pathway*

Chemically synthesized siRNA is one of the most common approaches to effectively down-regulating gene expression through the RNAi mechanism. siRNAs are ~21-23 nt duplexes that mimic the Dicer products. In general, siRNAs show perfect complementary to the target sequences. Once exogenously supplied siRNAs associate with RNAi-induced silencing complex (RISC), one strand serves as "guide strand" that directs mature RISC to mediate site-specific cleavage of mRNA, and, hence, inhibition of protein translation (Figure 1.2-1, right).[62] Newly published results show "dicer-ready

siRNA" is 100-fold more potent than conventional siRNAs. Dicer-ready siRNAs are double stranded RNA, 25-27 nt in length. On administration, these longer version siRNA moleculess are readily processed by dicer into siRNAs, and then initiates a RNAi pathway as mentioned in the previous section.[60]

1.2.4 *Anticancer and antiviral activities*

Currently, RNAi-based tools are also considered as a potential therapeutic candidate directed against common oncogenes in human cancer.[63-65] The use of viral vector expressing siRNA has successfully inhibited tumor progression in mice models.[66] Additional findings have suggested that RNAi may be considered as one of innate antiviral defense mechanisms. RNAi has recently been developed as a potential antiviral therapeutic agents. For example, several specific human immunodeficiency virus (HIV) mRNAs and HIV genome have been effectively degraded via RNAi-mediated cleavage.[50] Promising results have shown that RNAi can inhibit various pathogenic viruses *in vivo*, including Nodamura virus (NoV),[67] human respiratory syncytial virus (RSV),[68] and HIV.[69,70] Moreover, a similar antiviral mechanism has been demonstrated and observed from honeybee.[71,72]
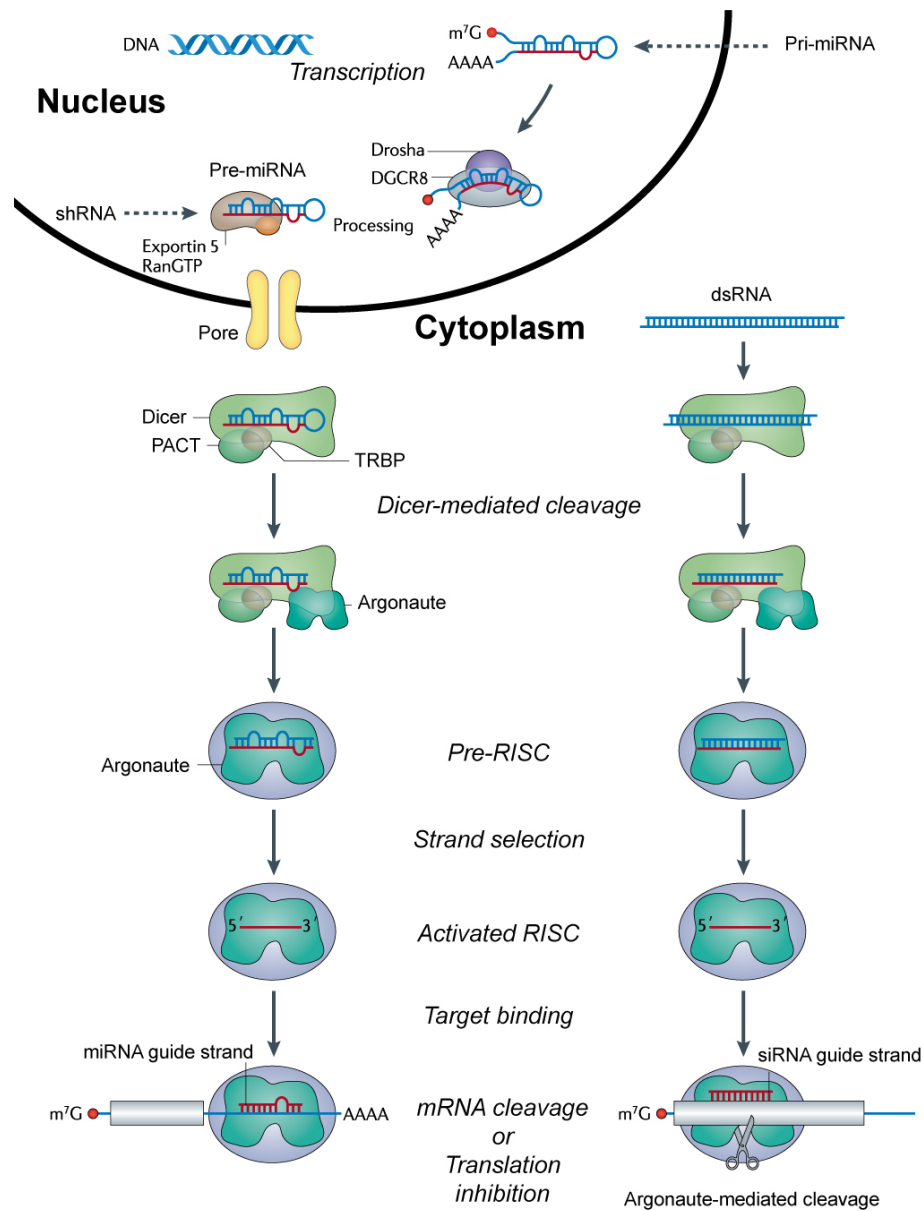
Figure 1.2-1 The RNAi processing pathway overview in mammals. Left: miRNA pathway. Right: siRNA pathway. Figure adapted from Davidson et al.[73]

1.3 RNA-Based tools delivery strategies

Although numbers of RNAi-based therapeutic agents are involved in ongoing clinical studies (Table 1.3-1), numerous barriers, including biological and chemical stability and intracellular uptake of RNA must be overcome before RNAi-based tools become an effective strategy for gene therapy. Owing to the high anionic charge of the RNA backbone, and low inherent stability of RNA, small molecules, polymers, lipids, peptides, aptamers and proteins are most commonly used for effective delivery and reinforcing stability of RNAi therapeutics.[74]

Table 1.3-1 Clinical trials for RNAi-based therapeutics*

Diseases	Drug	Indication	Target	Phase	Sponsor
Ocular and retinal disorders	AGN211745	Age-related macular degeneration (AMD)	VEGF-R1	Completed, I/II	Allergan
	Bevasiranib	Diabetic macular edema (DME)	VEGF	Completed, II	Opko Health, Inc
	PF-655	AMD; DME	RTP801	Active, I	Quark Pharm., Inc
Cancers	CALAA-01	Solid tumor	RRM2	Active, I	Calando Pharm.
	Atu027	Metastatic solid malignancies	PKN3	Active, I	Silence Theraputics
	ALN-PLK1	Liver tumors	PLK1	Active, I	Alnyam Pharm.
	NTC00672542	Metastatic melanoma	LMP2, LMP7, and MECL1	Active, I	Duke University
Viral infection	pHIV7-shl-TAR-CCR5RZ	Human immunodeficiency virus (HIV)	HIV Tat and Rev proteins, TAR RNA, and human CCR5	Active, 0	City of Hope Medical Center/Benitec
	SPC3649	Hepatitis C virus (HCV)	miR-122	Active, II	Santaris Pharm
	ALN-RSV01	Respiratory syncytial virus (RSV)	RSV nucleocapsid	Active, II	Alnylam Pharm

*From ClinicalTrials.gov

1.3.1 *Non-viral vector delivery systems*

Small molecules, polymers, lipids, peptides, aptamers and antibodies have been employed to facilitate RNA-based tools delivery (Figure 1.3-1).[75] The most common carriers are lipid nanoparticles (LNPs) which have shown encouraging results in clinical trials with solid tumor and hypercholesterolemia.[76,77] It is striking that using the same RNAi delivery approach can provide substantial protection against Ebola virus in non-human primates.[78] Recent studies have developed aptamer-siRNA chimeras capable of selectively delivering functional siRNA into prostate cancer cells and HIV-infected cells and demonstrated more potent inhibition.[79,80] Cationic polymers (e.g., polyaminoester (PAS), poly-L-lysine (PLL), and polyethyleneimine (PEI)) have also been widely used to deliver anionic DNA plasmid or siRNA molecules through electrostatic interactions.[81,82] In addition, amine functional groups in cationic polymers allow for covalent conjugation of targeting ligands, small molecules, and polymers to increase specificity and potency. These polymer-based systems protect encapsulated RNA from degradation in serum, and provide highly efficient transfection of RNA into cells.[83,84]

Cholesterol-conjugated siRNA

siRNA

Lipid nanoparticles

siRNA

Aptamer-siRNA chimera

Aptamer

siRNA

Peptide-mediated siRNA

Peptide

Antibody-targeted siRNA

Fragment antigen-binding

siRNA

siRNA

Protamine

Cationic polymer-based nanoparticles

small molecule

Ligand

PEG

siRNA

Cationic polymer
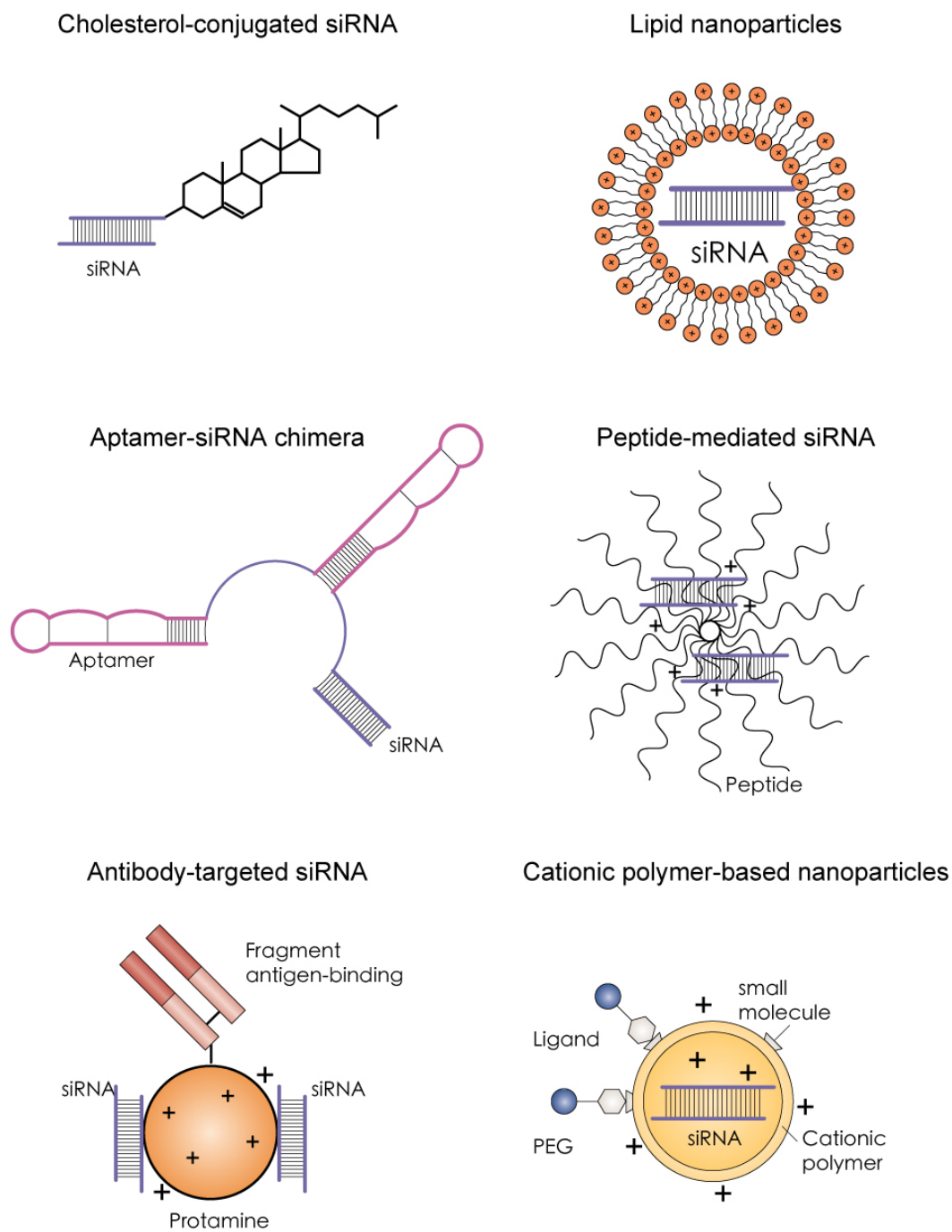
Figure 1.3-1 Common strategies for RNA-based tool delivery. Figure adapted from Järver et al,[85] Kim et al,[55] and Kanasty et al.[74]

1.3.2 *Viral vector delivery systems*

Another approach for delivering of nuclieci acid into cells is to use non-pathogenic viruses for DNA plasmid delivery. Viruses that have been used include adeno-associated viruses (AAV), adenoviruses, and lentivirus (Figure 1.3-2).[86-88] Targeting RNA molecules (e.g., shRNA or miRNA) are produced in virally infected cells by encapsulated DNA plasmid and are processed into siRNA which leads to gene silencing. In general, this system shows greater efficiencies for cellular delivery and gene expression, compared to non-viral mediated systems [81]. This viral vector delivery system has several limitations, such as plasmid DNA packaging capacity, unwanted immune response, and the availability of lack of efficient large-scale preparation impede viral-mediated delivery.[89-91]
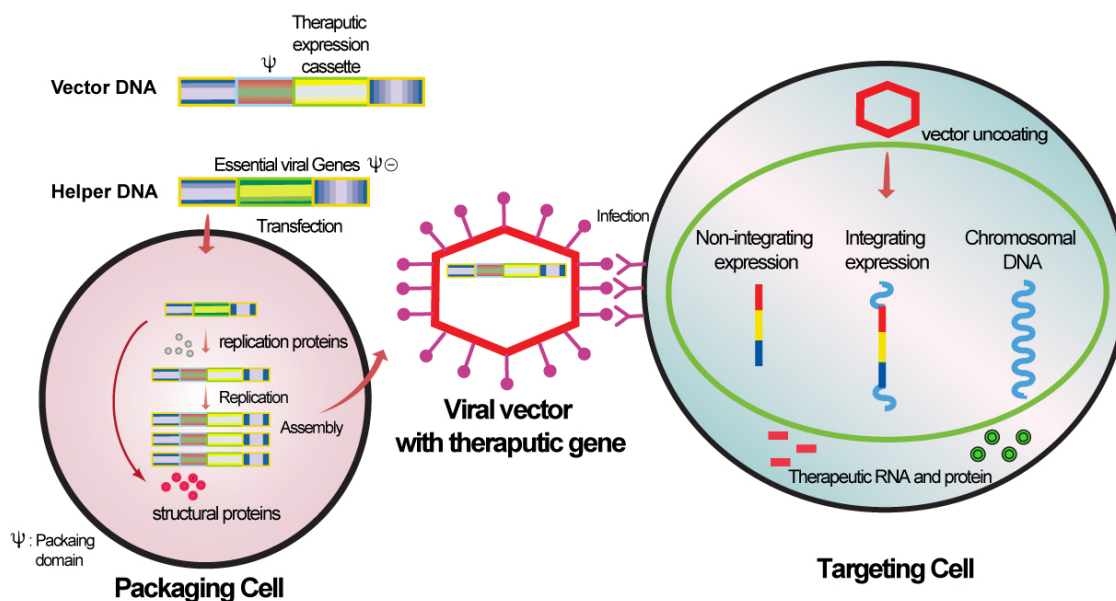
Figure 1.3-2 Generic strategy for engineered viral vector mediated delivery of genes. Figure adapted from Kay et al.[92]

1.4 Recombinant RNA Technology

1.4.1 *General background of recombinant RNA technology*

In the past decade, RNA has been transformed into new powerful therapeutic agents in pharmaceutical sciences. Many RNAi-based tools have demonstrated promising efficacy *in vitro* and *in vivo*, and so far over 20 potential RNA therapeutic candidates have made into clinical studies. In order to optimize sequence and RNA structure design, improve RNAi target prediction, and enhance cellular delivery of RNAi therapeutics, scalable production of large quantities of RNA is necessary for further pharmacological testing and investigation. To date, RNA has mostly been prepared using either *in vitro* RNA transcription [93] or solid-phase synthesis.[94] However, both enzymatic and chemically synthesized RNAs are not capable of providing a large quantity of RNA. Using bacteria to produce and accumulate high levels of naturally stable recombinant RNA in the cytoplasm might become a cost-effective strategy.[21,95] *In vivo* RNA expression has been extensively studied using viral infection and promoter to produce heterologous messenger RNA (mRNA) in bacteria.[34,96,97] Unfortunately, this recombinant RNA approach has been plagued by several limitations. For example, heterologous transcripts are subject to spontaneous degradation and cleavage due to innate instability and ribonucleases (RNAse) in cellular environments.

1.4.2 *New approaches for recombinant RNA technology*

Non-coding RNAs, including rRNA and tRNA are considered stable RNA molecules in cells. Stable RNA molecules are generally able to form secondary and tertiary structures by either RNA folding or RNA-protein assemblies. Stable RNAs show longer half-lives and are protected against cellular nucleases under normal growth conditions, compared to mRNAs.[98] Until

recently, relatively few research groups have adopted stable RNAs as part of their strategy in recombinant RNA synthesis. Different RNA scaffold systems have been invented to produce stable recombinant RNA in *E. coli* and overcome obstacles as mentioned above, for instance as rRNA variants [99,100] and transfer RNA (tRNA).[43,101-103] 5S rRNA and tRNA scaffold are two of the most successful recombinant RNA expression that can produce and purify target RNA molecules from a fermentation-based system.

1.4.3 *5S rRNA scaffold*

The 5S rRNA structure derived from the marine bacterium, *Vibrio proteolyticus* and its variants have been extensively studied and characterized by Fox group.[99,104,105] In previous studies, they have identified and created a plasmid-borne mutant of *V. proteolytocus* 5S rRNA that can be produced and accumulated in high levels in cells without being incorporated into *E. coli* 70S ribosomes (Figure 1.4-1).[106] Thus, 5S rRNA chimera is an ideal RNA molecule to serve as a RNA carrier, to stabilize RNA insert in cellular conditions without any unanticipated side effects.[107] By using the plasmid-encoded artificial 5S rRNA scaffold, various RNA sequences, especially those less than 100 nucleotides, can be expressed and purified without loss of functionality from *E. coli*.[106,108-110] Moreover, Fox et al, have described a method for excision of RNA insert from 5S rRNA scaffold using biotinylated DNAzyme. The excised RNA products were then recovered through DNA-RNA hybridization.[109]
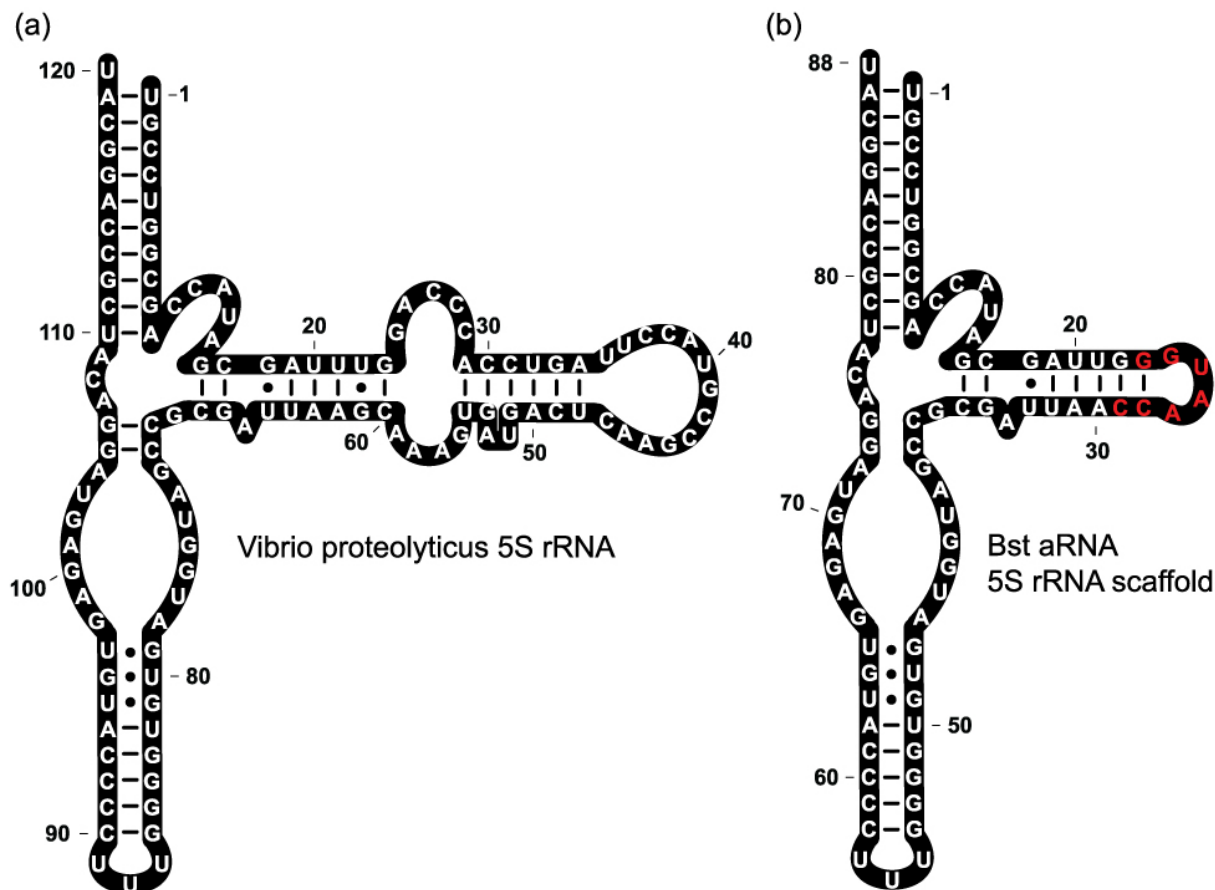
Figure 1.4-1 Sequence and predicted secondary structure of (a) the *V. proteolyticus* 5S rRNA and (b) the 88-base *Bst* 5S rRNA scaffold. The RNA of interest could be inserted into the *Bst* site at the DNA level. *Bst* recognition sites are highlighted with red letters. Figure adapted from Pitulle et al[106] and Liu et al.[109]

1.4.4 *tRNA scaffold*

Cellular tRNA is subjected to a series of post-transcriptional modifications to avoid RNA degradation in cells.[111] The advantage of using tRNA as an alternative scaffold is that tRNA serves as a protective scaffold that is resistant to nucleases. Thus, recombinant tRNA can masquerade as a natural tRNA, and allow RNA insert within the tRNA to fold into native confirmation in the cellular environment. The tRNA scaffold approach exploits both human and *E. coli* tRNA to accommodate the insert RNA sequence and produce tRNA fusions. Various

RNA sequences have been successfully incorporated in the tRNA scaffold and been produced in *E. coli.*[102,103] By incorporating ribozymes and affinity aptamer within the tRNA scaffold, the insert RNA can be easily isolated by standard chromatography and denaturing PAGE.[95]
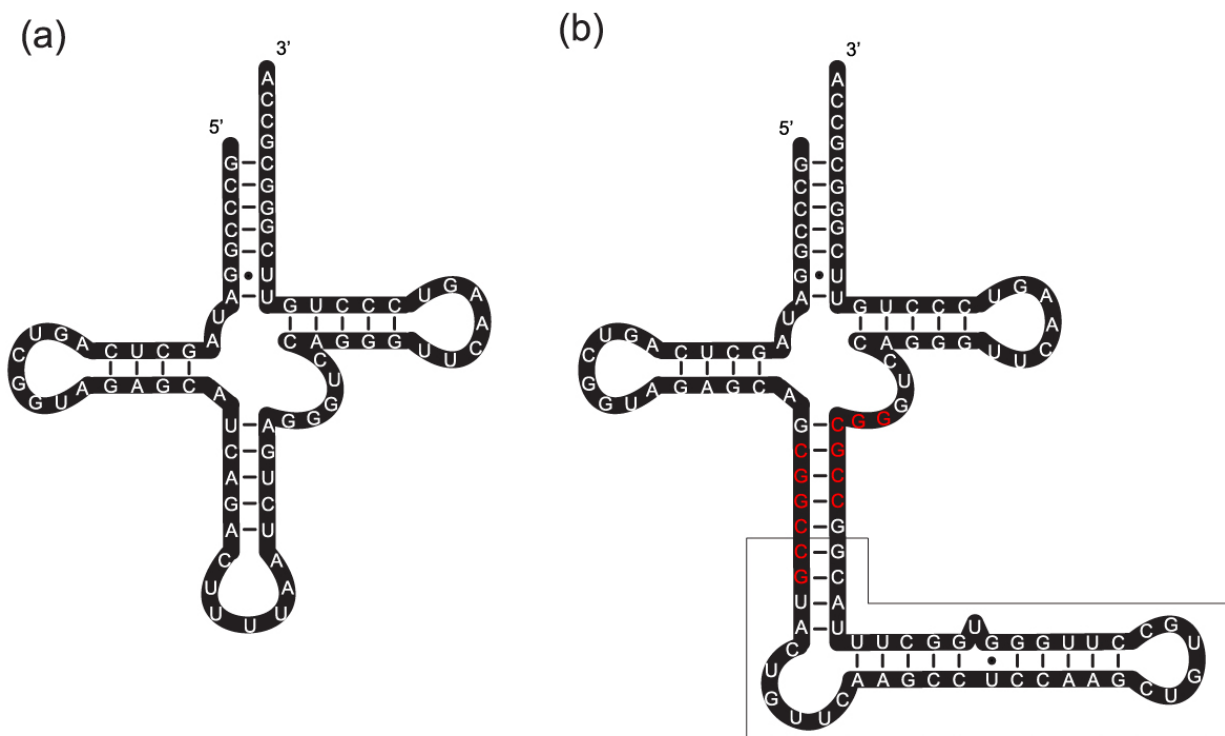
Figure 1.4-2 Schematic structure of (a) unmodified human tRNA$^{Lys, 3}$ and (b) tRNA-HBV chimera with the epsilon sequence from human HBV virus (boxed). RNA insertion sites are highlighted with red letters. Figure adapted from Ponchon et al.[103]

1.5 Aims and Organization of the Dissertation

This project focuses on production, packaging, protection and delivery of functional RNA molecules using Qβ VLP. To understand parameters affecting the non-viral RNA packaging within VLPs *in vivo*, structural differences and aptamer affinity of RNA have been thoroughly probed by co-expression and co-assembly with Qβ coat proteins in bacteria. Also, the stability of packaged RNA from a series of chemical assaults was investigated (**Chapter 2**).

To develop a single-step, *in vivo* method for production of functional RNAs packaged within Qβ VLPs, a general utility RNAi scaffold has been designed. Cellular uptake of VLPs was assessed with various cancer cell lines. The RNAi activities of functional VLPs against different target genes were demonstrated. (**Chapter 3**)

We have initiated the development of compatible cationic polymers for Qβ VLPs to deliver plasmid DNA with RNA-filled VLP simultaneously by electrostatic interactions. Particle size and surface potential of polymer-conjugated VLP were studied. The feasibility of using polymer-VLP to deliver DNA plasmid to mammalian cells was examined (**Chapter 4**).

CHAPTER 2

2. RNA: PACKAGED AND PROTECTED BY VLPS

2.1 Introduction & Motivation

RNA-based tools have utility in fundamental research, drug discovery, and disease treatment [49,112,113] in part because of the programmable specificity inherent in base-pairing interactions. Small interfering RNAs (siRNAs) and microRNAs (miRNAs) can modulate gene expression by directly inhibiting translation or by stimulating degradation of mRNA.[114,115] RNAi's can be active as antibacterial or antiviral agents.[116,117]

Virus Like Particles (VLPs) are devices that can package, protect and deliver RNA. Qβ/MS2 VLPs are a hollow non-replicative icosahedral nanoparticles with diameters of 30 nm, formed of 180 copies of the Coat Protein (CP).[118,119] Qβ and MS2 are $T = 3$ icosahedral positive-sense single-strand RNA bacteriophages with a small mRNA genomes that encode four open reading frames.[120] We hypothesize that an optimization of both packaging and protection of RNA within these particles has taken place over billions of years of evolution.

Here, focusing on Qβ, explore factors that influence the purity and amount of target RNA that is packaged *in vivo*. We show that intrinsic compaction of RNA increases the efficiency of assembly. Intrinsically compact RNA, here derived from rRNA, appears to package with high efficiency *in vivo*. We also characterize the stability of RNA within VLPs and report that VLPs chemically protect RNA from metals that can readily penetrate the VLP. VLPs chemically stabilize packaged RNA by mechanisms beyond direct exclusion of reactive species from proximity to the RNA.

2.2 Materials & Methods

2.2.1 *Reagents*

DNA oligos were ordered from Eurofins MWG Operon, Inc. NZY broth media was purchased from TEKNOVA. Sec-Butanol and Chloroform and Magnesium Chloride hexahydrate were purchased from Fisher Scientific. Ferrous Ammonium Sulfate Hexahydrate was obtained from EM Science. Ammonium sulfate was purchased from ICN Biomedicals. Sucrose, RNase- and DNase-free, were purchased from Amresco. Dithiothreitol (DTT) was purchased from Research Products International Corp. Polyethylene glycol 8000 was purchased from J. T. Baker. (+)-sodium L-ascorbate was purchased from Sigma-Aldrich. Sodium dodecyl sulfate was purchased from Shelton Scientific, Inc. 30% hydrogen peroxide was purchased from Fisher Scientific. BCA protein assay kit was purchased from Thermo Scientific. Low range ssRNA ladder was purchased from New England Biolabs. Ultra-Pure SequGel was purchased from National Diagnostics. Polyallomer centrifuge tubes were purchased from Beckman Coulter. Agilent RNA 6000 Nano Kit was purchased from Agilent Technologies. Amicon® Ultra centrifugal filters (100 kDa MWCO) were purchased from Millipore. Spectra/Por® dialysis tubing (15 KDa MWCO) was purchased from Spectrum® Laboratories, Inc. All other reagents were analytical grade. All DNA constructs were confirmed by sequence analysis (Eurofins MWG Operon).

2.2.2 *Construction of Qβ CP and Qβ VLP-RNA expression vector*

In this study, we used a two-plasmid expression system for the production of Qβ VLP and non-viral RNA in *E. coli*. Thus, two compatible origins of replication and antibiotic resistance markers are required within the same host strain. The pBR322 origin of replication and kanamycin resistance gene of pET-28b (+) is compatible with the CloDF13 origin and

streptomycin resistance gene in pCDF-1b, allowing for co-transformation in the same bacterial cell. Therefore, we chose pCDF-1b as a coat protein expression vector (pCDF-CP) (Figure 2.3-1a,c) and pET-28b (+) as an RNA expression vector (pET-RNA) (Figure 2.3-1b). The non-viral RNAs and Qβ CP were cloned downstream of the T7 promoter/lac operator.

2.2.3 *Qβ coat protein expression vector*

DNA encoding Qβ CP monomer (NCBI reference sequence: NC_001890.1) was synthesized by recursive-PCR (R-PCR)[121] with restriction sites *Nco* I and *Avr* II (Table 5.1-1) and cloned into pCDF-1b (Novagen) to generate plasmid pCDF-CP. *E. coli* BL21(DE3) transformants were selected based on LB streptomycin resistance (50μg mL^{-1}) and screened for inserts by colony PCR. All constructs were sequence confirmed (MWG Operon).

2.2.4 *RNA expression vector*

a-rRNA [122] and *Thermus thermophiles* 23S rRNA (NCBI reference sequence: 3169129) were chosen as highly structural RNA. GFP mRNA derived from gWizGFP (Genlantis) was chosen as non-structural RNA. Template DNAs, including the corresponding Qβ hp, spacer region, and RBS were synthesized by R-PCR [121]. The template DNAs (Table 5.2-2) flanked by *Xba*I and *Blp*I were then cloned into pET28-b (+) (Novagen) to generate the Qβ VLP-RNA expression vectors. *E. coli* BL21(DE3) pCDF-CP/pET28-b (+)-VLP-RNA transformants were selected based on LB streptomycin/kanamycin resistance (50μg mL^{-1}). The insert sequence was further confirmed by sequencing analysis (MWG Operon).

2.2.5 *Expression of Qβ VLP and VLP-RNA complexes*

E. coli containing pCDF-Qβ CP vector was inoculated in NZY medium with streptomycin (50μg mL^{-1}) and incubated overnight at 37°C. Qβ-VLP production started with the addition of 1% overnight culture to the ZYM-5052 auto-induction medium [123]. Production culture was incubated 24 h at 37°C. Cells were collected by centrifugation at 4°C and 6500xg for 30 minnutes. Cells were resuspended in equal volume of Qβ buffer (10 mM MgCl$_2$ and 20 mM Tris-HCl, pH7.5) and lysed by sonication at 40 watts for three minutes with 10s on/off intervals. The lysate was centrifuged to remove cell debris for 30 minutes at 23,430xg. 2M Ammonium sulfate precipitation followed by 30-minute centrifugation at 23,430xg was performed to obtain crude VLP. Crude VLPs were then suspended in 1 mL Qβ buffer and extracted with 1:1 n-butanol:chloroform. Organic extraction was repeated three times. The aqueous layer was subsequently purified by step sucrose gradient ultracentrifugation (10-40% w:v) in a SW41Ti rotor (Beckman) at 40K RPM for two hours. Qβ VLPs were precipitated from the sucrose fraction with 20% w:v PEG8000. Resuspended Qβ VLPs were combined and dialyzed against 2 L dialysis buffer (20 mM Tris-HCl, pH 7.5 and 50 mM NaCl) for two hours. This procedure was repeated three times prior to the use of particles in further analyses. Qβ VLPs were characterized by SDS polyacrylamide gel electrophoresis. VLP-RNA complexes were obtained as described above using co-expression strategy in *E. coli* BL21 (DE3) pCDF-CP/pET28-b(+)-GFP strain selected with streptomycin/kanamycin (50μg mL^{-1}).

2.2.6 *Recombinant RNA extraction from Qβ VLPs*

VLPs and VLP-RNA complexes were expressed and purified as described above. An amount of 50 μg VLP was added to 250 μL of the extraction buffer (5% SDS, 25 mM DTT, 20mM Tris-

HCl, pH 7.5, and 50 mM NaCl). The solution was incubated at room temperature for 20 minutes. Equal volume of low pH phenol-chloroform was then added to the solution. The RNA extracts were centrifuged to remove protein and DNA for 15 minutes at 16,300xg. RNA retained in aqueous phase was precipitated. Ammonium acetate precipitation was performed at -20 °C for at least 24 h followed by 15-minute centrifugation at 16,300xg. The RNA pellet was washed with 80% ethanol at least three times to remove excess salt. The RNA was dissolved in nuclease free water and stored at -80 °C. Using this extraction method, RNA yield was about 4-5 μg for every 50 μg VLP or VLP-RNA complexes. RNA samples were analyzed by denaturing urea polyacrylamide gel electrophoresis or Agilent 2100 Bioanalyzer.

2.2.7 *Transmission electron microscopy*

All TEM images were obtained using a Hitachi H-7500 electron microscope. Samples were prepared by fixing with 250 μL of glutaraldehyde (8%) per 500 μL of sample (1μg/mL). A drop of the sample, ~15 μL, was dropped on the copper grid and incubated for five minutes. Excess sample was wicked off the grid using filter paper. The grid was then placed face down on a drop of 2% ammonium molybdate stain for two minutes. Excess stain was wicked off using filter paper and the grid was dried for two hours before imaging.

2.2.8 *Hydroxyl radical cleavage generated from Fenton reaction*

This method was adopted from hydroxyl radical footprinting methodology [124] with slightly modifications. For various time points in uniform amounts of hydroxyl radical generated from the Fenton reaction, VLP-RNA complexes (250 μg) or packaged RNA alone (25 μg) was added to pre-cleavage solution (0.3% H_2O_2, 3.3 mM sodium ascorbate, 20 mM Tris-HCl, pH 7.4) to 50

μL. The hydroxyl radical cleavage initiates when 10 μL of freshly prepared 200 μM iron (II) EDTA solution was introduced. For mixture of iron (II) EDTA solution, the ratio of $(NH4)_2Fe(SO_4)_2 \bullet 6H_2O$ to EDTA solution is 2:1 (e.g. 200 μM $(NH4)_2Fe(SO_4)_2 \bullet 6H_2O$/ 400 μM EDTA). The cleavage reaction was then quenched after various times (0-180 minutes) by treating 20 μL of 0.1 M thiourea. In varying concentrations of hydroxyl radical incubated for uniform time increments, 10 μL of different concentrations of iron (II) EDTA solution (0-1500 μM) were prepared and added to individual pre-cleavage solution with VLP-RNA complexes (250 μg) or packaged RNA alone (25 μg). The cleavage reactions were terminated after 15 minutes by addition of 20 μL of 0.1 M thiourea. RNA extraction was performed according to the procedures mentioned above.

2.2.9 *Inline cleavage induced by magnesium ions*

The methodology originated from the previous work on the inline probing analysis of riboswitches [125]. For different incubation periods at a constant magnesium ion concentration that promote inline cleavage, VLP-RNA complexes (250 μg) or packaged RNA alone (25 μg) was added to Mg cleavage solution (25 mM $MgCl_2 \bullet 6H_2O$, 20 mM Tris-HCl, pH 7.4) to 60 μL. Samples were incubated at 37 °C for different time periods (0-120 hours). In varying concentrations of Mg^{2+} ions at constant periods of time, VLP-RNA complexes (250 μg) or packaged RNA alone (25 μg) was added to Mg cleavage solution with elevated concentrations of $MgCl_2$ (0-300 mM). All samples were incubated at 37 °C for 15 minutes. The inline cleavage reactions were paused by storing at -80°C. RNA extractions from the different incubation periods or different Mg^{2+} ions concentrations were performed according to the procedures mentioned above.

2.2.10 *Slow unmediated cleavage*

VLP-RNA complexes (250 μg) or packaged RNA alone (25 μg) was added to unmediated cleavage solution (20 mM Tris-HCl, pH 7.4) to a final volume of 60 μL. All samples were incubated at room temperature for different time periods. The slow unmediated cleavage reactions were halted by storing at -80°C. RNA extractions from the different incubation periods were performed according to the procedures mentioned above.

2.2.11 *RNA integrity analysis*

The packaged a-rRNA-hp samples were run on a denaturing urea polyacrylamide gel with SYBR® Green II RNA gel stain and quantitated with AlphaView® software. The integrated pixel intensity for the area under major RNA band was used to represent a-rRNA-hp band intensity. Here, the band intensity representing the % uncleaved a-rRNA-hp by various conditions was normalized to control a-rRNA-hp samples. The values of % uncleaved a-rRNA-hp were calculated by dividing the remaining a-rRNA-hp band intensity by the control a-rRNA-hp band intensity. The control a-rRNA-hp was purified from purified VLPs without Fenton and in-line cleavage treatment.

2.3 Results

2.3.1 *Design of RNAs for studying VLP packaging efficiency*

A series of RNAs were constructed here to determine the effects of various RNA properties and sequences, separately and in combination, on the efficiency of VLP packaging. The series of RNAs allows us to investigate effects of RNA size, structure and degree of intrinsic compaction, effects of competition with binding to the ribosome, and the effect of Qβ hp on the amount of target RNA and amount of contaminating RNA packaged into VLPs *in vivo*.

To investigate VLP packaging of a highly structured and compacted RNA, and to determine the effect of the Qβ hp on packing of such RNAs, VLPs containing a-rRNA [126] with and without the Qβ hp were characterized. a-RNA is a well-characterized RNA derived from the core of the *Thermus thermophilus* large ribosomal subunit rRNA.

To determine the effect of RNA size, a large RNA, the intact *T. thermophilus* 23S rRNA was also fused to the Qβ hp (Figure 2.3-1d-e). To characterize the effect of competition from ribosomal binding, the RNA ribosomal binding site RBS, [127] was fused to a-rRNA Qβ-hp. To characterize packaging of a flexible and extended RNA, an mRNA (encoding green fluorescent protein (GFP)) was fused to the Qβ hp (Figure 2.3-1g). To further characterize the effect of competing RNA binding factors, the RBS was added upstream of the mRNA$_{GFP}$ Qβ-hp (Figure 2.3-1f). Throughout this series of experiments coat protein was expressed in pCDF-1b (pCDF-CP) (Figure 2.3-1a, c) and RNA was expressed in pET-28b (+) (pET-RNA, Figure 2.3-1b).
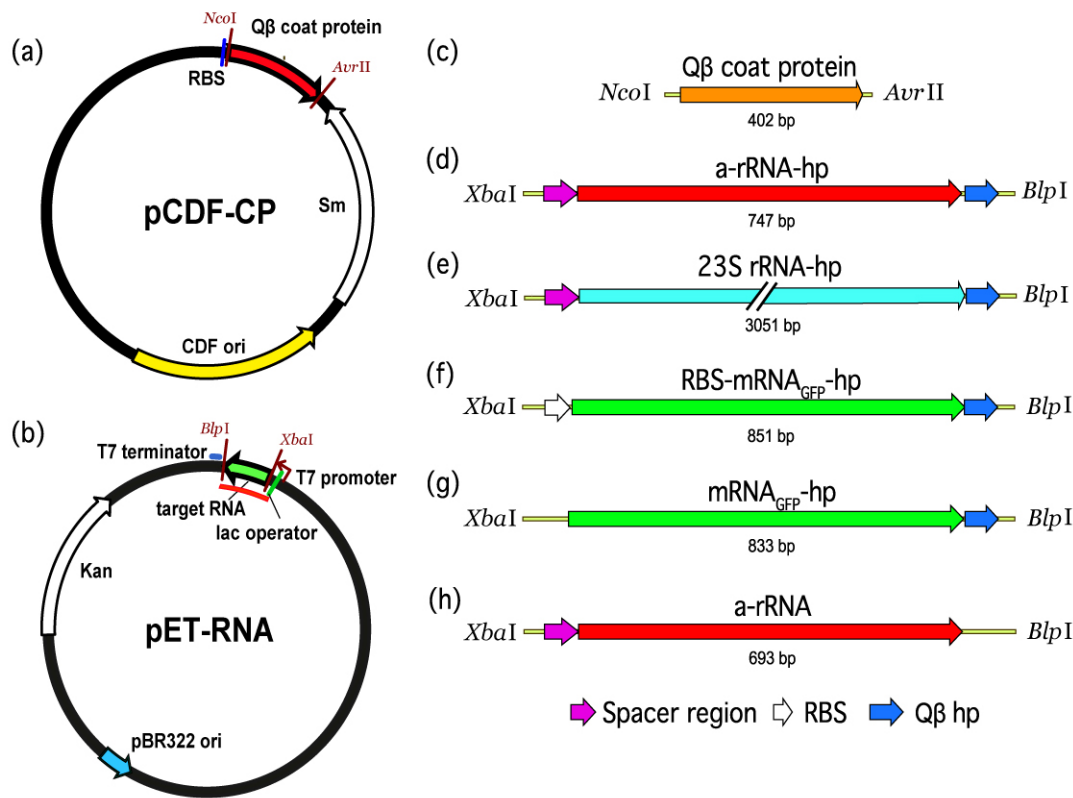
Figure 2.3-1 The protein expression vector (pCDF-CP), RNA production vector (pET-RNA), and the series of RNA constructs used in this study. (a-b) The pCDF-CP and pET-RNA plasmids used to co-express protein and RNA in E. coli. The red line on pET-RNA plasmid (b) indicates the RNA transcript. Genes that encode the desired protein or RNA product for co-expression are (c) Qβ coat protein, (d) a-rRNA-hp, (e) 23S rRNA-hp, (f) RBS-mRNAGFP-hp, (g) mRNAGFP-hp, and (h) a-rRNA.

2.3.2 *Packaging of short and long RNAs*

CP and various target RNAs were co-expressed, and the resulting VLPs were purified. SDS-PAGE analysis and transmission electron microscopy (Figure 2.3-2a-b) confirmed co-expression of CP and RNA leads to formation of canonical VLPs that contain the target RNA. Amount of target RNA incorporated into the VLP was quantitated and normalized to amount of CP mRNA. The results show that RNAs of up to 3,051 nucleotides can be efficiently packaged in Qb VLPs. The a-rRNA-hp (747 nucleotides) is efficiently packaged within VLPs (Figure 2.3-2c). The 23S

rRNA-hp (3,051 nucleotides), which is four times larger than a-rRNA-hp, is packaged within VLPs with similar efficiency (Figure 2.3-2d). Both of these VLPs contain a small amount of contaminating mRNA encoding Qβ CP, as observed previously.[36]

We used amount of packaged CP mRNA as a reference to estimate packaging efficiency of other RNAs. RNAs that packaged in great excess of CP mRNA are considered to be efficiently packaged. RNAs that are incorporated to levels equivalent to CP mRNA are considered to be inefficiently packaged. Packaged RNA impurities of molecular weight less than than 23S rRNA-hp are observed. These species may be 23S rRNA degradation products or endogenous *E. coli* sourced impurities, which are also observed with a-RNA-hp VLPs.

2.3.3 *Packaging of RNAs with varying structure and compaction*

Intrinsic RNA structure appears to play a significant role in packaging efficiency within VLPs in *E. coli*. It has been shown that a-rRNA [126] and 23S rRNA [128] fold to compact secondary and tertiary structures in the presence of magnesium. We compared VLP packaging of a-rRNA-hp to mRNA$_{GFP}$-hp. The lengths of mRNA$_{GFP}$-hp and a-rRNA-hp are similar, and both contain the Qβ hairpin. However, mRNA$_{GFP}$-hp differs from a-rRNA-hp in that mRNAs are less structured, less compact and more dynamic than rRNAs. The results show that a-rRNA-hp is packaged more efficiently than mRNA$_{GFP}$-hp (Figure 2.3-1d,f, Figure 2.3-3a), suggesting that in general highly structured RNAs are packaged more efficiently than non-structured RNAs.

2.3.4 *Packaging of RNAs is influenced by competing RNA binding factors*

We determined whether ribosomes can compete with VLP assembly by binding to target RNA. Comparing mRNA$_{GFP}$-hp bearing an RBS (figure 2.3-1f) with mRNA$_{GFP}$-hp lacking an RBS

(figure 2.3-1g) shows that RNA packaging efficiency in VLPs decreases slightly when the RNA contains an RBS (Figure 2.3-3a). This result suggests competition between ribosomal binding and Qβ assembly *in vivo*.

2.3.5 *Packaging of RNAs required the Qβ hairpin*

The Qβ hp is necessary for efficient packaging of essentially any RNA within a Qβ VLP. a-rRNA fused to the Qβ hp shows the highest packaging efficiency of any RNA tested here. We investigated the importance of the Qβ hp to packaging of a highly structured RNA by removing Qβ hp from a-rRNA (Figure 2.3-1h). Removal of the Qβ hp essentially abolishes packaging of a-RNA (Figure 2.3-3b). These results indicate that efficient packaging of RNA within the VLPs *in vivo* is dependent upon both RNA structure and the Qβ hp.

(a)

kDa   1   2

116

45

25

14

(b)

(c)

nt   1   2   3

1000

500

300

(d)

nt   1   2   3

6000
4000

2000

1000

500

200

25

33
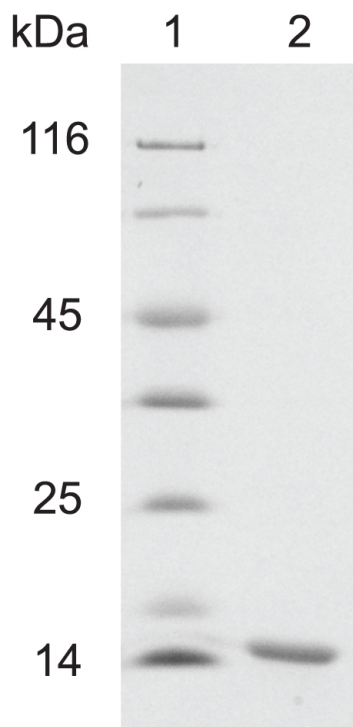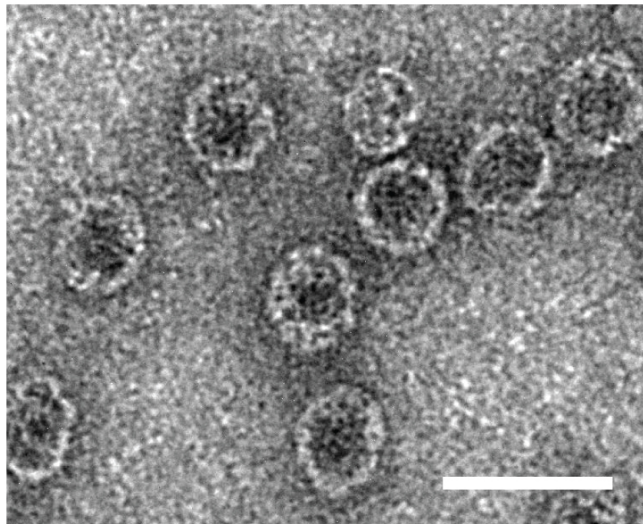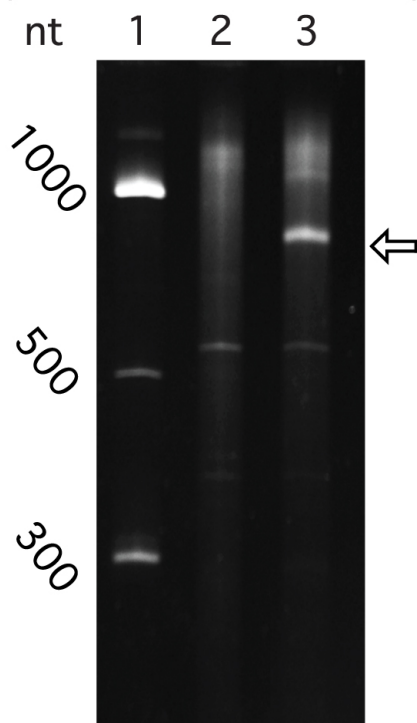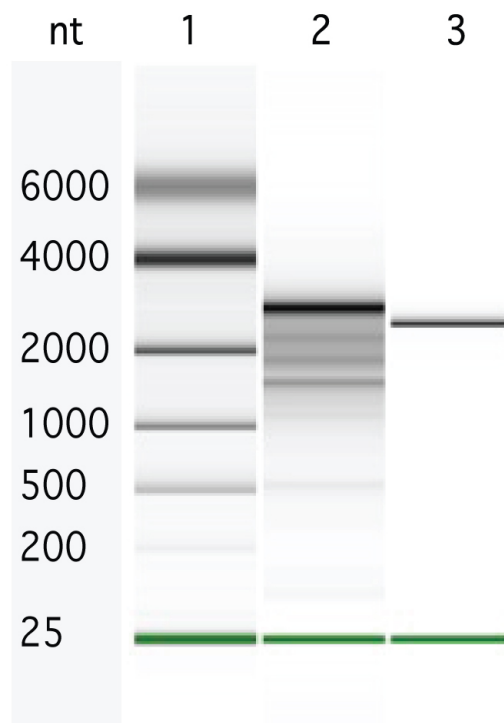
Figure 2.3-2 in vivo expressed RNA is packaged within VLPs to form VLP-RNA assemblies. (a) Purified Qβ -VLPs were analyzed by SDS-PAGE. The Qβ CP monomer is 14.5 kDa. Lane 1: Protein Sizing Ladder. Lane 2: Qβ CP monomer from purified Qβ - VLPs. (b) Transmission electron microscope images of Qβ -VLP containing a-rRNA-hp. Scale bar= 50 nm. (c) in vivo expressed a-rRNA-hp, extracted from purified Qβ –VLPs, subjected to electrophoresis on denaturing Urea PAGE. Lane 1: RNA ladder, Lane 2: RNAs of Qβ CP expressed alone. Lane 3: RNAs of purified Qβ CP co-expressed with a-rRNA-hp. The arrow indicates the a-rRNA-hp (747 nt). (d) in vivo expressed 23S rRNA-hp, extracted from purified Qβ –VLP, subjected to microfluidic-based chip electrophoresis. Lane 1: RNA sizing ladder, Lane 2: RNAs extracted from purified Qβ CP co-expressed with 23S rRNA-hp (3051 nt). Lane 3: 23S rRNA prepared by in vitro transcription (2966 nt).
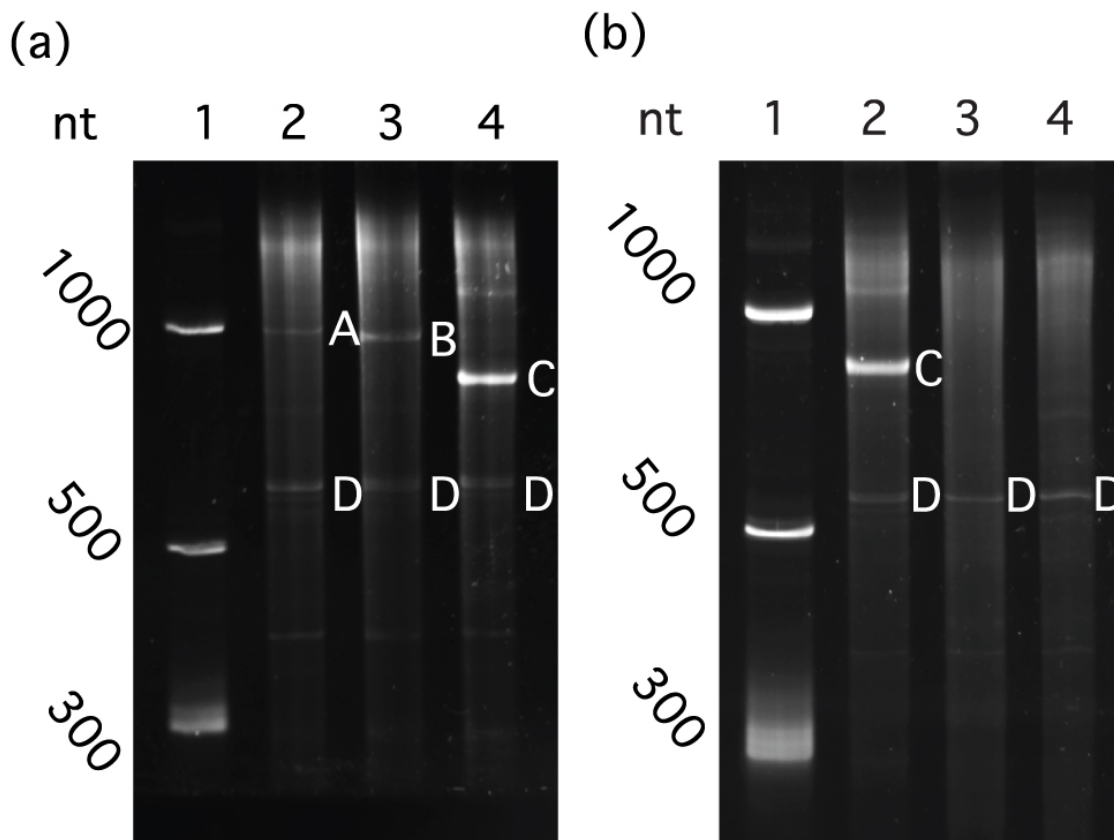
Figure 2.3-3 Highly structured RNA and a high affinity RNA aptamer are two critical elements for efficient in vivo non-viral RNA packaging. (a) structured and unstructured RNAs, packaged in vivo by Qβ CP. Lane 1: RNA Ladder. Lane 2: RNAs extracted from purified Qβ CP co-expressed with RBS-mRNAGFP-hp. Lane 3: RNAs from purified Qβ CP co-expressed with mRNAGFP-hp. Lane 4: RNAs from purified Qβ CP co-expressed with a-rRNA-hp. (b) RNAs with and without the Qβ hp, co-expressed in vivo with Qβ CP. Lane 1: RNA Ladder. Lane 2: RNAs of purified Qβ CP co-expressed with a-rRNA-hp. Lane 3: RNAs of purified Qβ CP co-expressed with a-rRNA (without Qβ hp). Lane 4: RNAs of Qβ CP expressed alone. One hundred nanograms of total VLP-extracted RNA was loaded to each well for denaturing PAGE. Band A: RBS-mRNAGFP-hp (851 nt). Band B: mRNAGFP-hp (833 nt, without the RBS). Band C: a-rRNA-hp (747 nt). Band D: Qβ CP mRNA.

2.3.6 *VLPs protect RNA from Fenton chemistry*

VLPs have previously been shown to protect RNA from nucleases.[129] Here, we investigated the

ability of Qβ VLPs to protect packaged RNA from chemical assault. We compared the rates of

degradation of a-rRNA-hp, which packages efficiently, when it is packaged in VLPs or free in

solution. The percent of uncleaved RNA was determined after RNA extraction and separation on urea gel.

Qβ VLPs protect RNAs against attack by hydroxyl radical. After incubation in Fe-EDTA, O_2 and H_2O_2, conditions known to generate hydroxyl radical,[130] a-rRNA-hp packaged within VLPs remains about 60% intact after three hours. In contrast, only 30% of the same RNA, unprotected by VLPs (free a-rRNA-hp), remains intact under the same conditions (Figure 2.3-4a). The relative extent of protection increases with time. Similarly, protection of a-rRNA-hp within VLPs can be observed in a series of experiments in which Fe-EDTA concentration is varied at fixed time. After 15 minutes in 1500 μM Fe-EDTA and H_2O_2, about 80% of VLP-packaged RNA remains intact, while less than 50% of free RNA remains (Figure 2.3-4b).

2.3.7 *VLPs protect RNA from in-line cleavage*

VLPs protect a-rRNA-hp against magnesium-mediated in-line cleavage. In-line cleavage is intramolecular attack by the nucleophilic 2' hydroxyl on the proximal phosphate. Magnesium is known to catalyze in-line cleavage of RNA.[131,132] After 36 hours of incubation in 25 mM $MgCl_2$ at 37°C, the RNA within VLPs is about 90% intact. By contrast, only 5% of free a-rRNA-hp is intact under the same conditions (Figure 2.3-4c). Similarly, VLP packaging increases the concentration of $MgCl_2$ required to cleave RNA over specific periods of time. About 35% of VLP-packaged a-rRNA-hp remains intact after 24 hours at an $MgCl_2$ concentration of 100 mM. There is no detectable free RNA remaining after the same incubation time under the same cleavage conditions (Figure 2.3-4d).

2.3.8 *VLPs cannot protect RNA from slow unmediated cleavage*

Here we assayed rates of unmediated cleavage of VLP-packaged RNA in comparison to free RNA. RNA in the presence of buffer and monovalent cations degrades slowly at room temperature. Rates of unmediated cleavage are an order of magnitude less than rates by magnesium-mediated in-line cleavage or Fenton cleavage. Our results show that both VLP-packaged and free a-rRNA-hp slowly degrade at 37°C in the absence of Mg^{2+}. There is no significant difference between rates of degradation of VLP-packaged RNA and free RNA. The VLP does not appear to retard the rate of unmediated RNA degradation over extended periods of time at 37°C (Figure 2.3-4e).

(a) Hydroxyl radical cleavage

(b) Hydroxyl radical cleavage

(c) Inline cleavage

(d) Inline cleavage

(e) Slow unmediated cleavage
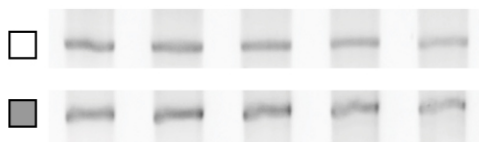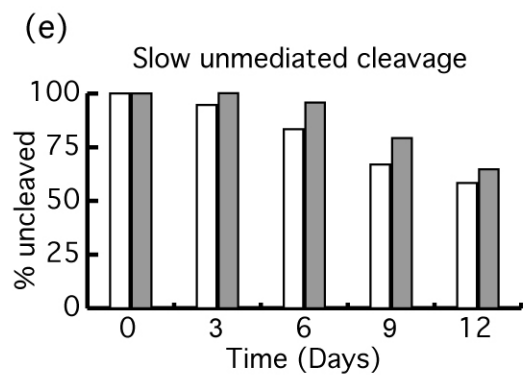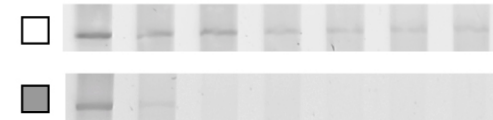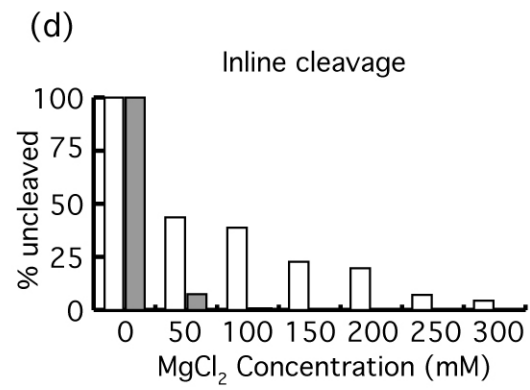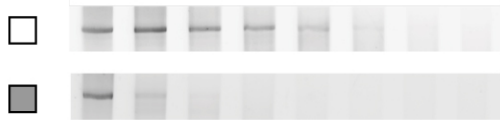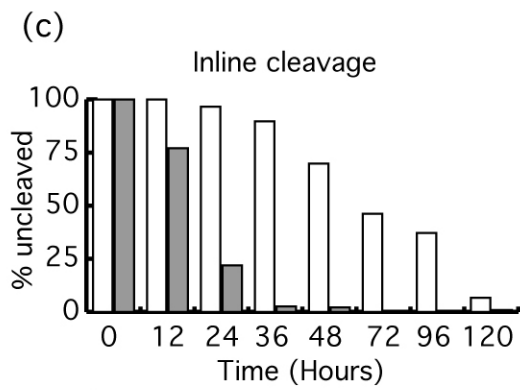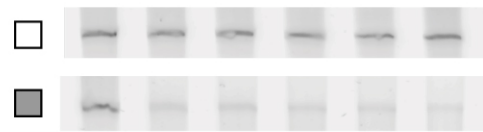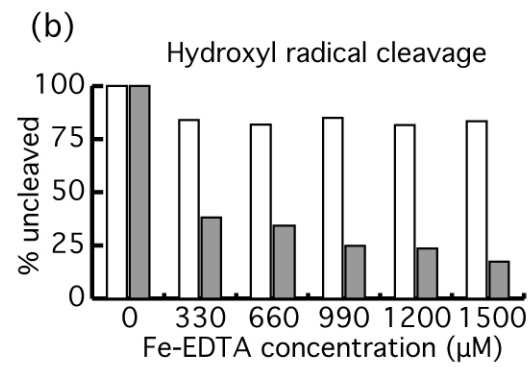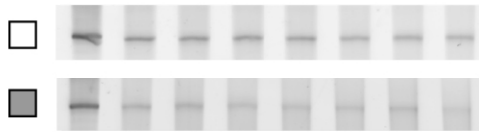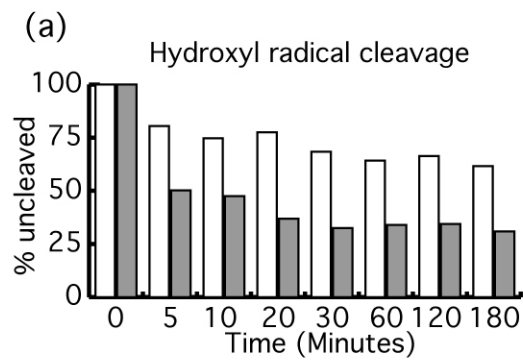
□ VLP Packaged a-rRNA

■ Free a-rRNA

Figure 2.3-4 VLP packaging confers chemical stability to RNA. VLP-packaged a-rRNA-hp and free a-rRNA-hp were incubated (a) for various time in 200 μM Fe-EDTA and 1% H2O2 in the presence of atmospheric oxygen at 37°C, which promotes Fenton cleavage (b) in varying [Fe-EDTA], incubated for 15 minutes at 37°C, (c) for variable time in 25 mM MgCl2 at 37°C, which promotes in-line cleavage, (d) in varying [Mg2+] for 24 hours at 37°C, and (e) for variable time at neutral pH in the absence of divalent cations. For all experiments here, the uncleaved a-rRNA-hp was isolated by denaturing urea PAGE and quantitated with AlphaView® software for FluorChem systems.

2.4 Discussion

Potency and efficacy of VLPs that act via delivery of functional RNAs are related to initial functionality, purity and quantity of the packaged RNA and to the chemical stability of the RNA within the VLP. Using *E. coli* for combined expression and packaging of RNA into Qβ VLPs, we probed relationships between packaging efficiency and RNA size, sequence and intrinsic compaction. We characterized the degree of RNA protection conferred by VLPs from small diffusible agents such as hydroxyl radical and magnesium cations. The results indicate that *in vivo* RNA packaging of RNA within VLPs is most efficient for intrinsically compact RNAs such as rRNA and is less efficient for dynamic, elongated RNAs such as mRNAs. The Qβ hp is necessary but not sufficient for efficient packaging. Qβ VLPs protect RNA not only against nucleases [133] but against assault by small diffusible species.

Stockley previously suggested that for viral RNA, stem-loops dispersed through the MS2 viral genome interact with CP during assembly [134-136] and tentatively identified 60 RNA stem-loops in the MS2 genome.[40] Initial RNA collapse during assembly *in vitro* depends initially on RNA-protein interactions, followed by CP-CP interactions.[137] Packaging involves multiple weak RNA-CP interactions along the length of the viral RNA and a single strong interaction with the MS2 hp.[39] MS2 and Qβ CP share about 25% amino acid sequence identity,[138-140] with highly similar three-dimensional structures and RNA binding sites.

We conclude that *in vivo* packaging efficiency of non-viral RNA within Qβ VLPs is high when the RNA (i) is intrinsically compact, (ii) includes the Qβ hp, (iii) lacks binding sites for assemblies that compete with CP (e.g., the RBS), and (vi) is as large as the 23S rRNA (2,970 nt). We prepared a series of RNAs (Figure 1) and co-expressed the RNA with Qβ CP in *E. coli*. The expressed RNAs contain i) a-rRNA, a ~650 nt intrinsically compact RNA stabilized by 11 GNRA tetraloops,[126] ii) 23S rRNA, a ~2,970 nt intrinsically compact RNA containing over forty stem-loops, and iii) mRNA$_{GFP}$, an unstructured ~780 nt RNA. The expressed RNAs either incorporated or lacked the Qβ hp, and/or an RBS. The results show that both a-rRNA-hp and 23S rRNA-hp are efficiently packaged within Qβ VLP *in vivo* (Figure 2.3-2), suggesting that within the limits explored here RNA length is not a strong predictor of packaging efficiency. We compared the packaging efficiency of intrinsically compact a-rRNA-hp and unstructured mRNA$_{GFP}$-hp. The results of these experiments show higher packaging of intrinsically compacted rRNA than unstructured mRNA (Figure 2.3-3a). We conclude that intrinsic RNA compaction has significant influence on the efficiency of *in vivo* RNA packaging in Qβ VLPs.

The Qβ hp is necessary but not sufficient for efficient packaging of RNA into VLPs within *E. coli* (Figure 2.3-3b). This finding is consistent with previous work showing that RNAs lacking the MS2 hairpin do not interact with MS2 CP *in vitro*.[137] The MS2 hairpin is thought to be the initiation trigger for viral capsid formation.[141-144] Our results confirm that numerous GNRA tetraloops, as found on the surface of a-rRNA, do not substitute for the Qβ hp during RNA packaging *in vivo*.

Finn and coworkers found VLP packaging of CP mRNA competes with CP expression. When the Qβ hp is fused the 3' end of the CP mRNA, expression of Qβ CP decreases.[2] Our results, showing that RBS decreases mRNA$_{GFP}$–hp packaging in the VLP, confirm that Qβ CP and the ribosome compete binding to mRNA$_{GFP}$–hp. RNA packaging efficiency in VLPs is slightly decreased when an RBS is introduced upstream of the mRNA$_{GFP}$-hp (Figure 2.3-3a). Based on previous studies and our current findings, we expect that introduction of additional high-affinity RNA binding sites on RNA to be packaged *in vivo* could facilitate or attenuate RNA packaging efficiency consistent with the inherent affinity for the RNA.

We and others observe that non-target RNAs, including Qb CP mRNA. tRNAs, etc., are packaged within VLPs along with target RNA. Contaminating RNAs compete with target RNA during co-assembly. The absolute amount of contaminating RNA depends of the extent of packaging of the target RNA. If target RNA is expressed at low levels, or lacks the Qb hp, then the amount of contaminating RNA is increased. In total, it appears that sufficient RNA is packaged in the VLP to fully compensate for the cationic charge of Qb CP.[145] It is possible that RNA is required within the VLP for charge neutralization of positive charge [146]. In our two-plasmid expression system, T7 RNA polymerase was used to induce high-level expression of both Qβ CP and target RNAs. Without the simultaneous expression of RNA *in vivo*, high concentrations of positively charged viral CP may form non-specific RNA-CP interactions that serve to stabilize the protein structure and neutralize RNA charge.[147]

RNAs packaged within MS2 VLPs are completely protected from digestion from plasma ribonucleases.[129] The mechanism of this protection is steric; the enzymes are significantly larger

than the pores in the VLP capsid. Here we determine whether VLPs protect RNA against small diffusible damaging agents.

We determine the level of protection afforded by Qβ VLP against strand cleavage by metal ions. Mechanisms and levels of protection against small reactive molecules such as metal ions are expected to be distinctive from those of nucleases because Qβ VLPs contain holes [119] that are significantly larger than the metal ions and their hydrates. Pores in VLPs allow entry and exit of metal ions and species such as hydroxyl radical. Diffusion of metal ions into Qβ VLPs has been demonstrated by Finn, who showed that RNA packaged in VLPs is degraded by lead(II) acetate.[148] It has been shown that RNA within MS2 VLPs is degraded by high pH.[12]

Our results demonstrate as expected that Mg^{2+} and Fe^{2+} enter VLPs and degrade RNA. The results are consistent with expectations that rates of RNA cleavage in the interior of VLPs caused these metals are highly attenuated compared to rates of cleavage of free RNA in solution. RNA is substantially protected by VLPs against hydroxyl radical and magnesium-mediated in-line cleavage (Figure 2.3-4). It is known that rates of hydroxyl radical [149] and magnesium-mediated in-line cleavage [131] of RNA are influenced by RNA compaction and dynamics. RNA is more compact and less dynamic within VLPs than RNA that is free in solution.[150]

The RNA backbone is cleaved spontaneously in the presence and absence of magnesium.[131,132] The mechanism is thought to be the same for both reactions; intramolecular in-line cleavage with a linear arrangement of the nucleophile (the 2' oxygen), the electrophile (the P) and the leaving group (the 5' oxygen). The reaction is faster in the presence of magnesium because it stabilizes

the transition state by accepting a proton from the 2'oxygen and/or by withdrawing electon density from the phosphorous. Flexible regions of RNA are most labile to in-line cleavage because they more frequently occupy transient conformational states similar to in the transition state.[131,132] As expected, in the presence of magnesium the rate of cleavage decreases when RNA is packaged in the VLP. The reaction rate decreases because dynamics of RNA within the VLP are suppressed by confinement and association with CP.

CHAPTER 3

3. FUNCTIONAL RNAS: COMBINED ASSEMBLY AND PACKAGING IN VLPS

3.1 Introduction & Motivation

In **chapter 2**, we probed relationships between packaging efficiency and RNA size, sequence and intrinsic compaction. We also investigated the extent of chemical protection conferred by VLPs on RNA. These finding may allow us to further develop potential RNAi platform. In this chapter, we describe combined co-expression and assembly of a designed RNA molecule and its protective particle in *E. coli*. The particles are stable and readily absorbed by cells, where RNAs are released and processed to functional states. The RNA production, packaging and delivery system described here is based on bacteriophage Qβ. A high affinity CP binding site on Qβ genomic RNA has been isolated as a 29-nucleotide RNA hairpin, known as the Qβ hairpin.[37,38] CP and target RNA can be co-expressed in *E. coli* to spontaneously form VLPs.[36,37] The Qβ CP can encapsulate molecular cargo during *in vitro* or *in vivo* assembly.[137,151,152] Qβ VLPs are robust, retaining and protecting enzymes that remain catalytically active over broad ranges of temperatures.[151] They contain pores,[153] by which small substrate and product molecules can enter and exit.[151] Qβ VLPs lack components of the phage genome and are replication-incompetent.[154]

Functional RNAs such as small interfering RNA (siRNA), microRNA (miRNA), and short hairpin RNA (shRNA) have utility in therapeutic [155] and research applications.[156,157] Increased adoption of RNA-based therapeutics would be assisted by improved production and delivery processes, some of which currently employ small molecules, polymers, lipids, peptides, aptamers

and proteins.[75] Here we demonstrate a single-step *in vivo* method for production and packaging of functional RNA molecules in Qβ VLPs. The method employs our designed RNAi scaffold that folds by intramolecular processes. The assembly occurs within *E. coli* and produces VLP-RNAi particles. The RNAi scaffold (Figure 3.1-1) is a general utility chimera that contains a functional sequence paired to a carrier sequence combined with stability, packaging and processing elements. The scaffold contains the Qβ hairpin [37,38] on the 5' end to confer affinity for the CP, and a miR-30 stem-loop [158,159] that is demonstrated to be of utility for inhibition of gene expression.[158,160] With our scaffold, functional duplex RNAs form by an intramolecular process,
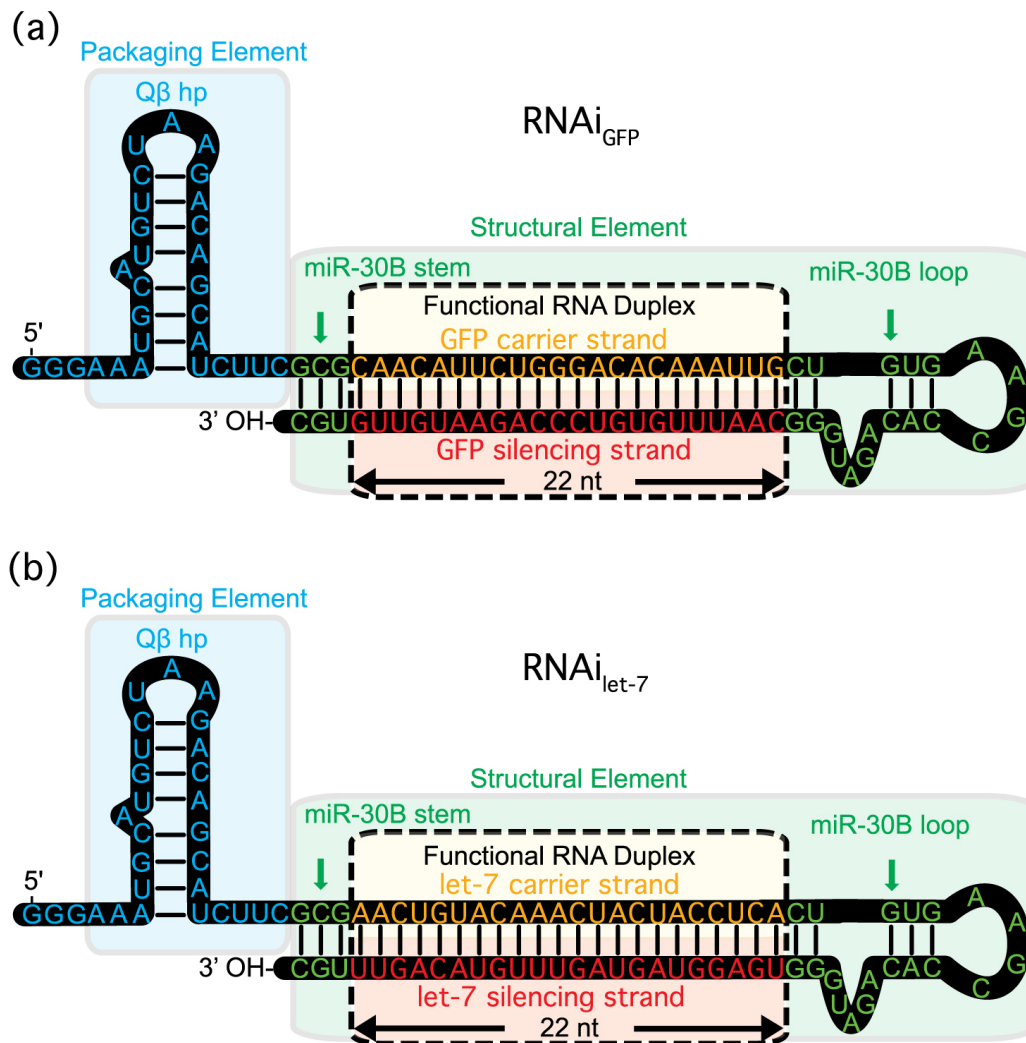
Figure 3.1-1 The Qβ RNAi scaffold is designed to fold and assemble with CP *in vivo*. A single RNA molecule folds to form a Qβ hairpin (blue) linked to a miR-30B stem loop (green), which caps the functional RNA duplex (yellow/red). The functional RNA duplex can encode miRNA or siRNA. The scaffold can incorporate any 22 base pair sequence, depending on the desired target. (a) An RNAi scaffold that targets GFP mRNA. (b) An RNAi scaffold that targets the Pan-ras 3' UTR.

which is concentration independent and efficient *in vivo*. The silencing RNA component remains in the duplex state [161,162] within the VLP and is therefore functional when delivered to the cytoplasm. The RNA is released from the VLP in the cell, were it is expected that dicer protein would liberate the functional ~22 nucleotide element from the scaffold.[163,164] The functional RNA enters the RNA-induced silencing complex (RISC complex) to induce RNA interference.[158-160]

3.2 Materials & Methods

3.2.1 *Reagents*

GFP was purchased from EMD Millipore. DyLight 633 Amine-Reactive kit was purchased from Thermo Scientific. DNA oligos were ordered from Eurofins MWG Operon, Inc. NZY broth media was purchased from TEKNOVA. Polyallomer centrifuge tubes were purchased from Beckman Coulter. Amicon® Ultra centrifugal filters (100 kDa MWCO) were purchased from Millipore. Spectra/Por® dialysis tubing (15 KDa MWCO) was purchased from Spectrum® Laboratories, Inc. sec-Butanol and Chloroform were purchased from Fisher Scientific. Ammonium sulfate was purchased from ICN Biomedicals. Sucrose, RNase- and DNase-free, was purchased from Amresco. HeLa cells were obtained from the American Type Culture Collection (Manassas, VA, USA), U87 human glioblastoma cells were a gift from Dr. Kuo-Chen Wei at the Department of Neurosurgery (Chang Gung Memorial Hospital, Taiwan) and were maintained in Dulbecco's modified Eagle's medium (DMEM) supplemented with 10% fetal

bovine serum (FBS). Primary Pan-Ras antibodies were purchased from Santa Cruz biotechnology. Secondary antibody, horseradish peroxidase-conjugated goat anti-mouse IgG was purchased from PerkinElmer. Glass bottom microwell dishes were purchased from MatTek. XTT kit was purchased from Sigma. All other reagents were analytical grade. All DNA constructs were confirmed by sequence analysis (Eurofins MWG Operon).

3.2.2 *Construction of Qβ-VLP, VLP-RNAi and GFP-containing VLP expression vectors*

Qβ coat protein expression vector. DNA encoding Qβ CP monomer (NCBI reference sequence: NC_001890.1) was synthesized by recursive-PCR (R-PCR) [121] with restriction sites *Nco* I and *Avr* II (Table 5.2-3) and cloned into pCDF-1b (Novagen) to generate plasmid pCDF-CP. *E. coli* BL21(DE3) transformants were selected based on LB streptomycin resistance (50μg mL^{-1}) and screened for inserts by colony PCR.

RNAi scaffold expression vector. Human miR-30B pre-miRNA was used as a scaffold for 22 bases of GFP (GenBank: AB038602.1, 5'-CAA CAT TCT GGG ACA CAA ATT G-3') or let-7 (NCBI reference sequence: NR_029660.1, 5'-TGA GGT AGT AGT TTG TAC AGT T-3') RNAi sequences and their complements. Template DNAs, including the T7 promoter and T7 terminator regions needed for RNA transcription, were synthesized by R-PCR.[121] The DNA sequences encoding RNAi scaffold containing RNAi$_{GFP}$ or RNAi$_{let-7}$ (Table 5.2-4) were cloned into pET28-b(+) (Novagen) to generate the Qβ VLP-RNAi scaffold expression vectors. *E. coli* BL21(DE3) pCDF-CP/pET28-b(+)-VLP-RNAi transformants were selected based on LB streptomycin/kanamycin resistance (50μg mL^{-1}).

GFP expression vector. The DNA gene encoding GFP was amplified by PCR from gWizGFP (Genlantis) with restriction sites BglII and BlpI (Table 5.2-3) and cloned into pET28-b (+) (Novagen) to generate plasmid pET28-b (+)-GFP. *E. coli* BL21 (DE3) pCDF-CP/ pET28-b (+)-GFP transformants were selected based on LB streptomycin/kanamycin resistance (50µg mL^{-1}).

3.2.3 *Expression of Qβ VLP and GFP-containing VLP*

E. coli containing pCDF-CP vector was inoculated in NZY medium with streptomycin (50µg mL^{-1}) and incubated overnight at 37 °C. Expression was induced by 1:100 dilution of overnight culture in 500 mL of ZYM-5052 auto-induction medium.[123] Production culture was incubated 24 h at 37 °C. Cells were collected by centrifugation at 4 °C and 6500xg for 30 min. Cells were resuspended in an equal volume of Qβ buffer (10 mM MgCl$_2$ and 20 mM Tris-HCl, pH7.5) and lysed by sonication at 40 watts for three minutes with 10s on/off intervals. The lysate was centrifuged to remove cell debris for 30 minutes at 23,430xg. 2M Ammonium sulfate precipitation followed by a 30-minute centrifugation at 23,430xg was used to obtain crude VLPs. Crude VLPs were resuspended in 1 mL Qβ buffer and extracted with 1:1 n-butanol:chloroform. Organic extraction was repeated three times. The aqueous layer was subsequently purified by step sucrose gradient ultracentrifugation (10-40% w:v) in a SW41Ti rotor (Beckman) at 40K RPM for two hours. VLPs were precipitated from the sucrose fraction with 20% w:v PEG8000. VLPs were resuspended in 25 mL of Qβ buffer, combined, and dialyzed against 2L dialysis buffer (20 mM Tris, pH 7.5 and 50 mM NaCl) overnight. This procedure was repeated an extra three times for 2 h prior to the use of VLPs in analyses. VLP concentration was assessed by Pierce BCA Protein Assay kit. GFP-containing VLP was expressed as described above using *E.*

coli BL21(DE3) pCDF-CP/pET28-b(+)-GFP strain selected with streptomycin/kanamycin (50μg mL^{-1}).

3.2.4 *Conjugation of Dylight 633 NHS Ester to Qβ-VLPs pression of Qβ VLP and GFP-containing VLP*

Conjugation of DyLight 633 N-hydroxysuccinimide (NHS) ester to VLPs was performed according to manufacturer protocols with slight modifications. VLPs were dialyzed against 0.05 M sodium borate buffer at pH 8.5 (labeling buffer) to remove the Tris present in Qβ buffer. VLPs (100 μL of 1 mg mL^{-1}) were incubated with 200 μL DyLight 633 NHS ester reagent (1 mg mL^{-1}) at room temperature for one hour. Buffer exchange was performed to remove non-reacted reagent using centrifugal filter unit with a 100 kDa molecular-weight cutoff. DyLight 633-labeled Qβ-VLPs were stored at -80 °C following GFP *in vitro* encapsidation.

3.2.5 *In vitro encapsulation of GFP within Qβ-VLPs*

VLPs were expressed and purified as described above. DyLight 633-labeled VLPs (10mg/mL) were incubated in disassembly buffer (20 mM Tris-HCl, 50 mM NaCl, 6M urea and 10 mM dithiothreitol) at 4 °C for one hour to disassemble VLP into CP dimers and posteriorly dialyzed against 10 mM acetic acid with 50 mM NaCl. Dialyzed CP dimers were then applied to a Sephadex G75 column and concentrated by a centrifugal filter unit (3.5 kDa MWCO). Subsequently, DyLight 633 labeled Qβ-VLPs were combined with a five-fold molar excess of GFP in dialysis tubing (3.5 kDa MWCO). VLP dimers and GFP were dialyzed against 2L of reassembling buffer (20 mM Tris-HCl, pH 7.5, 50 mM NaCl) three times at 4 °C for at least 24 h. Excess GFP and unassembled dimers were removed by centrifugation (100 kDa MWCO).

3.2.6 *Confocal microscopy*

HeLa cells (2 x 10^5 cells) were seeded into glass bottom microwell dishes (MatTek) and grown for 24 h in DMEM with 2.2 mg mL^{-1} sodium carbonate, 10% fetal bovine serum, 50 µg mL^{-1} gentamicin, 50 µg mL^{-1} penicillin, and 50 µg mL^{-1} streptomycin at 37 °C and 5% CO_2. VLP_{633}-GFP were prepared in Tris buffer at pH 7.4 (20 mM Tris-HCl, 50 mM NaCl). VLP_{633}-GFP was added to cells to a final concentration of 45 nM. Treated cells were further incubated at 37 °C with 5% CO_2 for 0, 24, and 48 h. After incubation, cells were rinsed three times with PBS. Nuclei were stained with Hoechst for 20 min at 37 °C, and washed three times with PBS. Images were acquired on a Zeiss LSM 700 Confocal Microscope with 63x oil immersion objective. Images were processed with Zeiss Zen software.

3.2.7 *Fluorescence microscopy*

To confirm that internalization is not affected by either attachment of fluorescent probes to the exterior or *in vitro* reassembly of VLP, *in vivo* prepared GFP-containing VLP was added to PC3 cells to a final concentration of 360 nM and cells incubated without transfection reagent at 37 °C and 5% CO_2 for 48 h. After incubation, the cells were washed three times with PBS to remove residual VLPs. Fluorescence images of PC3 cells were captured using a fluorescence microscope (Olympus U-LH100HG, Japan).

3.2.8 *In vitro transcription of RNAi$_{let7}$*

DNA containing the T7 promoter, the RNAi$_{let7}$, and T7 terminator generated by PCR was used as template for *in vitro* transcription (Primer: RNAi-Fwd and RNAi-Rev, Table S1). The DNA was purified with the QIAquick PCR Purification Kit (Qiagen). Approximately 1000 ng of DNA per

20 μL reaction volume was transcribed for 4 h at 37 °C with the MEGAscript High Yield Transcription Kit (Applied Biosystems), followed by incubation with TURBO DNase for 15 min to 1 h at 37 °C. RNA was pelleted by ammonium acetate precipitation, and the pellet was washed with 80% ethanol before drying via Speedvac or lyophilization. Pellets were resuspended in nuclease-free water and further purified by illustra™ NAP-5™ columns to remove unincorporated nucleotides.

3.2.9 *In vitro dicer RNAi scaffold cleavage assay*

Dicer cleavage assay was performed follow the kit protocol. Ten-microliter reactions including recombinant human dicer enzyme (1 Unit) and i*n vitro* transcribed RNAi scaffold (RNAi$_{let7}$, 1 µg) were incubated at 37°C for 16 h. Reactions were stopped by adding Dicer Stop Solution. *In vitro* Digested samples were directly analyzed by 16% denaturing urea gel. Images were acquired using Typhoon™ FLA 9500 biomolecular imager (GE Healthcare).

3.2.10 *In vitro gene transfection GFP inhibition studies*

To test for GFP inhibition in HeLa and U87 glioma cells, 12-well plates were seeded with ~ 2 x 10^5 cells per well and incubated 24 h before transfection. Cells (HeLa or U87) were transfected with GFP-expressing plasmid, gWiz-GFP, carried out by adding 1 µg of gWiz-GFP/lipofectamine 2000 complexes to each well. After incubation for 18 h at 37 °C and 5% CO_2, the media was removed, cells washed three times with DI-water to remove residual media, and then wells were filled with fresh media. Transgene expression was tested by fluorescence microscopy, western blot, and flow cytometry. To test GFP inhibition efficiency, different concentration of VLP or VLP-RNAi$_{GFP}$ was added to GFP-expressing cells and cells incubated

without transfection reagent at 37 °C for 48 h. After incubation, the cells were washed three times with PBS to remove residual VLPs. Fluorescence images of cells were captured using a fluorescence microscope (Olympus U-LH100HG, Japan). Expression of GFP proteins was determined by Western blot to confirm the inhibition efficiency. All images were collected using the same parameters.

3.2.11 *Flow cytometry data analysis*

The gWiz-GFP transfected HeLa cells were incubated with different concentrations of VLP-$RNAi_{GFP}$ (45, 90, 180, 270, 360, 540, 720 nM, 50 μL each) or VLP (360, 720 nM, 50 μL each as negative control) at 37 °C and 5% CO_2 for 24 h and 48 h. After washing three times with PBS to remove residual VLPs, samples were detached, pelleted and resuspended in PBS. Data on inhibition of GFP expression was acquired with a BD™ LSR II flow cytometer (BD Biosciences), and analyzed using FACSDiva™ software (BD Biosciences).

3.2.12 *Pan-Ras expression western blots*

For Western blot analysis, U87 glioma cells were added to 12-well plates, at a density of about 2 x 10^5 cells per well, 24 h before transfection. For Pan-Ras expression western blot anaylsis, the study was carried out by adding 100 μL of VLP or VLP-$RNAi_{let7g}$ with concentration of 750 nM to each well. After incubation at 37 °C and 5% CO_2 for 48 h, the media was removed and cells washed three times with serum-free DMEM medium to remove residual VLPs before addition of 750 μL formal DMEM growth medium containing 10% FBS. An additional 24 h incubation period was needed for efficient reaction of let-7 inside the cells. Chemically synthesized let-7

miRNA without any transfection agent was used as a negative control. Expression of Pan-Ras and GFP proteins was determined by Western blot to confirm the inhibition efficiency.

3.2.13 *VLP-RNAi$_{let7}$ U87 cell in vitro cytotoxicity assay*

U87 glioma cells were cultured in DMEM supplemented with 2.2 mg mL^{-1} sodium carbonate, 10% fetal bovine serum, 50 μg mL^{-1} gentamicin, 50 μg mL^{-1} penicillin, and 50 μg mL^{-1} streptomycin at 37 °C and 5% CO$_2$. Approximately 10,000 cells (i.e., 150 μL of a suspension of 6.67 × 10^4 cells/mL) were placed in each well of 96-well culture plates and incubated in a humidified chamber at 37 °C and 5% CO$_2$ for 24 h. Variable concentrations of samples (62.5, 125, 250, 500,1000 nM, 50 μL each) were co-cultured with U87 cells without transfection reagent and incubated for 24 and 48 h. After 24 or 48 h of incubation, the culture medium was removed from plate, and the cells were incubated in 120 μL of XTT solution for 2 hours. Subsequently, 100 μL of the XTT solution was removed from each well and transferred to a 96-well counting plate. The cytotoxicity toward U87 cells *in vitro* for different time points was evaluated by measuring the OD at 490 nm using an ELISA reader.

3.3 Results

3.3.1 *The CP and RNAi scaffold co-express and assemble into functional VLPs*

We have co-expressed Qβ CP and the RNAi scaffold in *E. coli*. The resulting RNAi scaffold and VLPs were purified and analyzed by gel electrophoresis, transmission electron microscopy, and dynamic light scattering (Figure 3.3-1). The RNAi scaffold is overexpressed and accumulated in *E. coli* (Figure 3.3-1a, lane 3) and is successfully packaged inside VLPs (Figure 3.3-1a, lane 4, red arrow). VLPs also package background RNA from *E. coli* during the *in vivo* self-assembly

process. We have observed RNAi scaffold read-through product from *in vitro* transcription (Figure 3.3-1b, lane 5, blue arrow), but not from *E. coli* total RNA and extracted RNA from VLPs. By *in vitro* Dicer cleavage assay, we have demonstrated that the recombinant human dicer can cleave *in vitro* transcribed RNAi scaffold, to produce oligomers ranging from 21-mers to 25-mers (Figure 3.3-1b, lane 3, black arrows). Packaging of the RNAi scaffold in the capsid does not change the morphology of the VLP (Figure 3.3-1c). Externally our VLPs are indistinguishable from previous Qβ VLPs.[151,165]

To further confirm that the RNAi scaffold assembles with Qβ CP *in vivo* to form functional VLPs, we assayed activities of scaffold-containing and control VLPs. RNA sequences inserted into the scaffold were directed against well-characterized targets whose expression levels can be readily monitored. The targets included green fluorescent protein (GFP) or the oncogenic Pan-Ras protein. VLP-RNAi$_{GFP}$ (Figure 3.1-1a) is designed to cause degradation of the mRNA of GFP. VLP-RNAi$_{let-7}$ (Figure 3.1-1b) is designed to decrease Pan-Ras expression at the level of translation.[166] Both of these VLP-RNAis are seen to be active against their targets but do not cross react. Control experiments confirm that neither VLPs containing endogenouse *E. coli* RNA nor VLP-RNAi with off-target RNAi are active. Therefore, the results are most consistent with VLP-RNAi activity against specified RNAi targets.

To further confirm that the RNA scaffold assembles with Qβ CP *in vivo* to form functional VLPs, we assayed activities of scaffold-containing and control VLPs. RNA sequences inserted into the scaffold were directed against well-characterized targets whose expression levels can be readily monitored. The targets included green fluorescent protein (GFP) or the oncogenic Pan-

Ras protein. VLP-RNAi$_{GFP}$ (Figure 3.1-1a) is designed to cause degradation of the mRNA of GFP. VLP-RNAi$_{let-7}$ (Figure 3.1-1b) is designed to decrease Pan-Ras expression at the level of translation.[166] Both of these VLP-RNAis are seen to be active against their targets but do not cross react. Control experiments confirm that neither the VLP alone nor non-specific VLP-RNA is active. Therefore, the results confirm that VLP-RNAi are active against RNAi targets, and that the RNA scaffold containing functional sequences is packaged into VLPs.
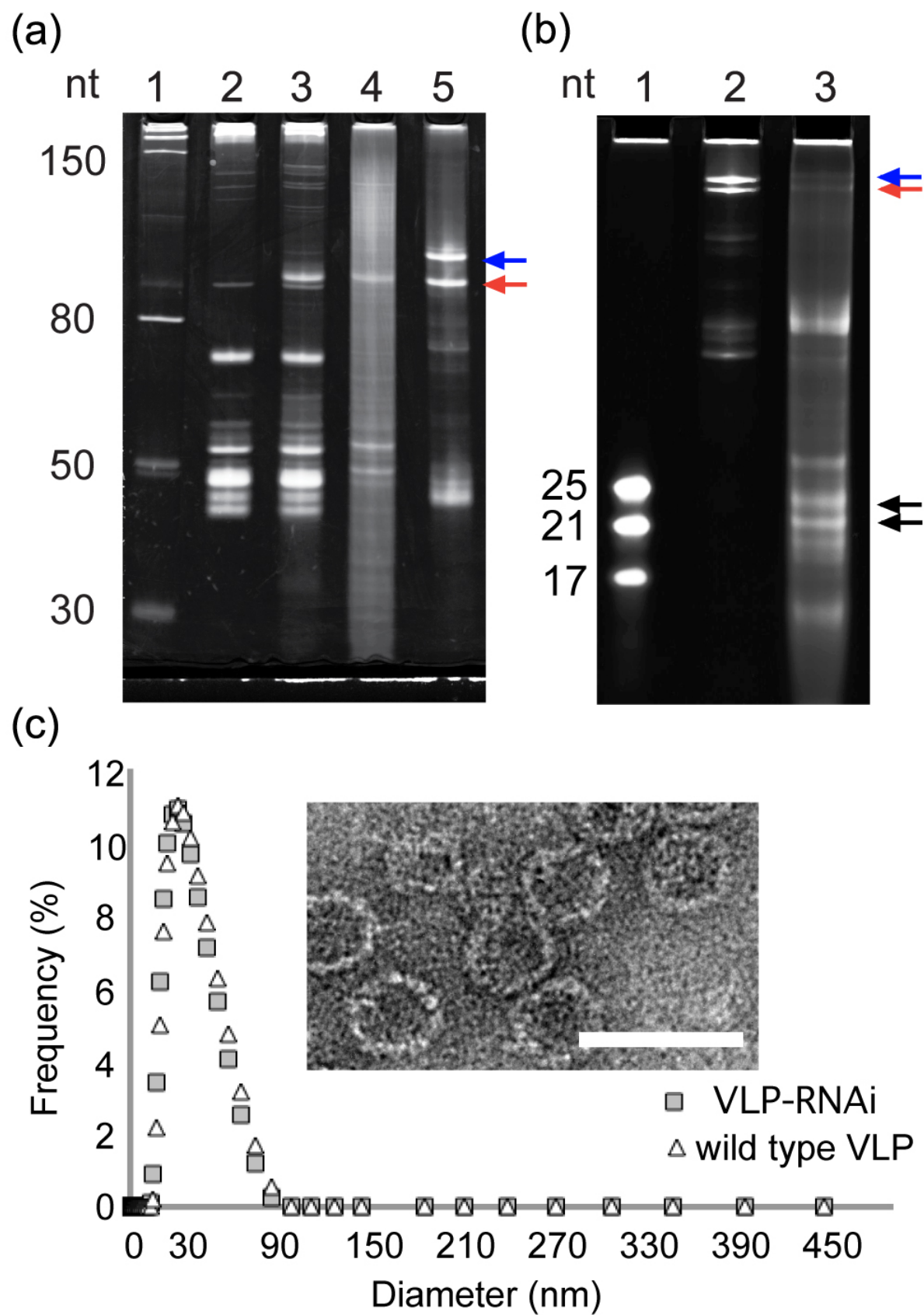
Figure 3.3-1 Characterization of the RNAi scaffold and Qβ-VLPs by electrophoresis, microscopy, and dynamic light scattering. (a) The *in vivo* transcribed RNAi scaffold was subject to electrophoresis on a 10% denaturing urea gel. Lane 1: ladder, Lane 2: Total *E. coli* RNA before induction of the scaffold and CP. Lane 3: Total E. coli RNA after induction, Lane 4: RNA extracted from purified VLPs, Lane 5: RNAi scaffold prepared by in vitro transcription (red arrow) with a length of ~98nt. The blue arrow indicates terminator read-through product. (b) RNAi scaffold prepared by in vitro transcription, processed by the human dicer enzyme (16% denaturing urea gel). Lane 1: siRNA ladder, Lane 2: RNAi scaffold (control). Lane 3: RNAi scaffold treated with human dicer. The black arrows indicate processed siRNAs ranging from 21-mers to 25-mers. (c) Size characterization of Qβ -VLP with RNAi scaffold (gray rectangle) and wild type Qβ -VLP (white triangle) by dynamic light scattering. Inset: Transmission electron microscope images of Qβ -VLP containing the RNAi scaffold. Scale bar= 50 nm.

3.3.2 *VLPs are taken up by human cells*

Finn and coworkers has previously shown that Qβ VLPs decorated with epidermal growth factor domain are rapidly internalized (within an hour in their experiments) in epidermoid carcinoma cell line A431 by receptor-mediated endocytosis.[167] During those relatively short incubation times, undecorated Qβ VLPs associate weakly with A431 cells but are not internalized. Here we asked if extending the time period allows internalization of undecorated Qβ VLPs.

The results show that undecorated Qβ VLPs, like undecorated MS2 VLPs,[168] are internalized by human HeLa cervical and PC3 prostate cancer cell lines over 24 to 48 h (Figure 3.3-2). We prepared dual-color VLP_{633}-GFP that can be tracked and monitored for cellular internalization and distribution, particle integrity, and cargo release using confocal laser scanning microscopy. VLP_{633}-GFP fluoresces at two different wavelengths (Figure 3.3-2) due to the presence of GFP in the VLP interior and covalent attachment of DyLight 633 on the VLP exterior. Yellow signal microscopy indicates intact VLP_{633}-GFP particles, where green GFP and red DyLight 633 emissions are co-localized. Green emission alone indicates free GFP that has been released by

the VLP, presumably upon VLP dissociation. Red emission alone indicates VLP capsid protein in isolation of cargo.

The results show VLP_{633}-GFP particles are internalized by the human epithelial cell line HeLa cells in a time-dependent manner. The internalization of VLP_{633}-GFP after 48 h of incubation is greater than after 24 h (Figure 3.3-2b-c). Yellow fluorescent particles within the cytoplasm slowly resolve, over 24 h, into points of distinct regions of green and red emission, indicating that the GFP cargo is released from the VLP_{633}-GFP particles. The particles appear to be excluded from the nucleus. Experiments show that VLP internalization is not affected by attachment of fluorescent probes to the exterior (Figure 3.3-2b-c and Figure 5.2-1) or by packaging of GFP into the interior of VLPs (Figure 3.3-2b-c, Figure 3.3-2e-f). VLP-GFP particles are internalized by human prostate cancer cell line PC3 to the same extent as VLP_{633}-GFP after 48 h.
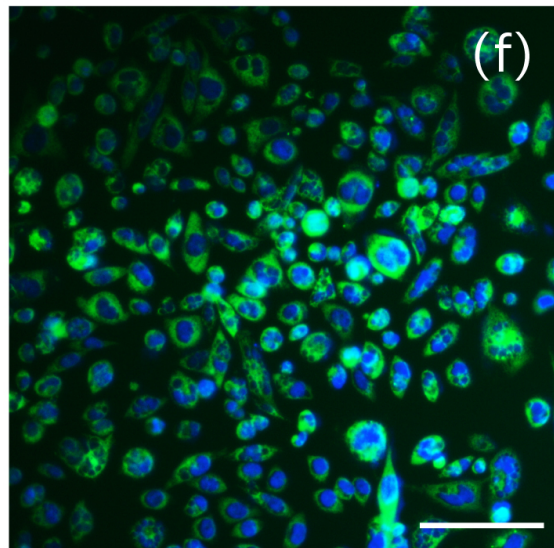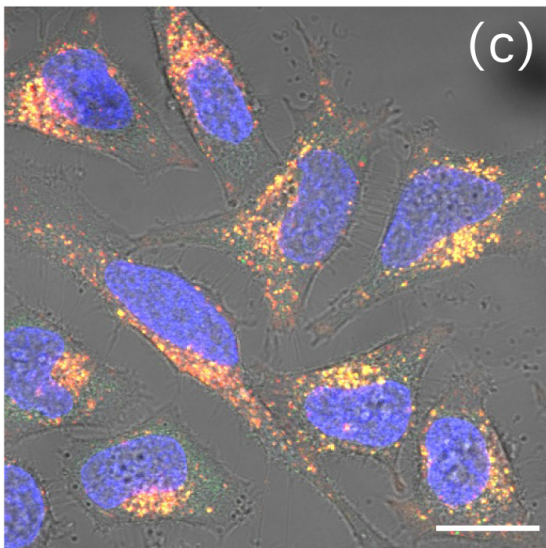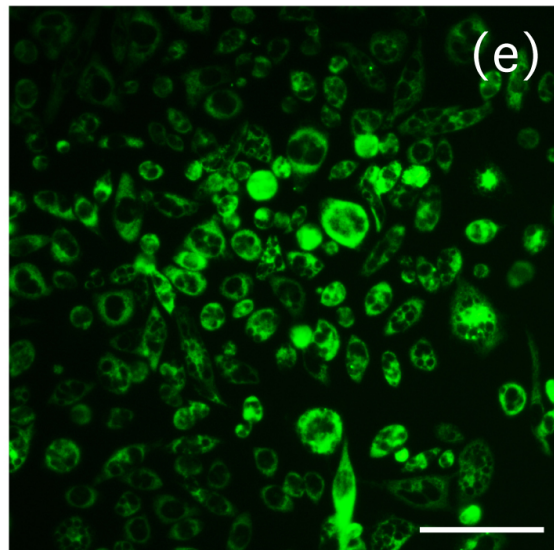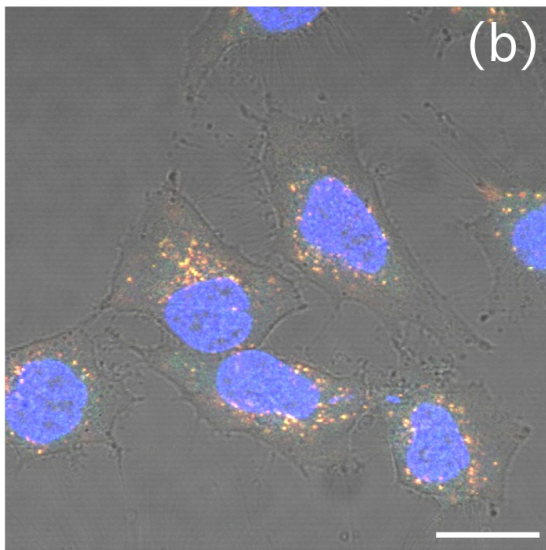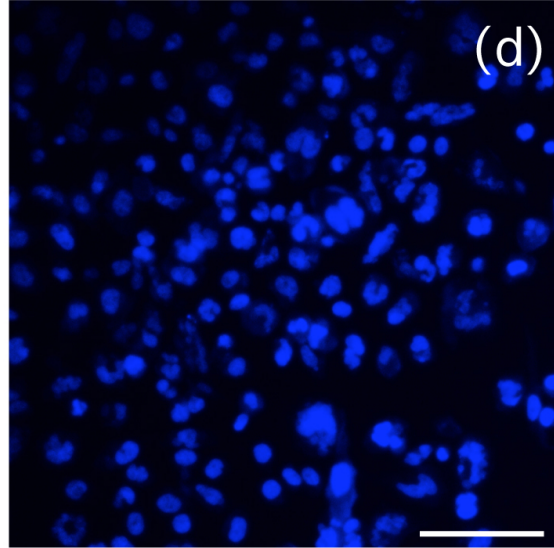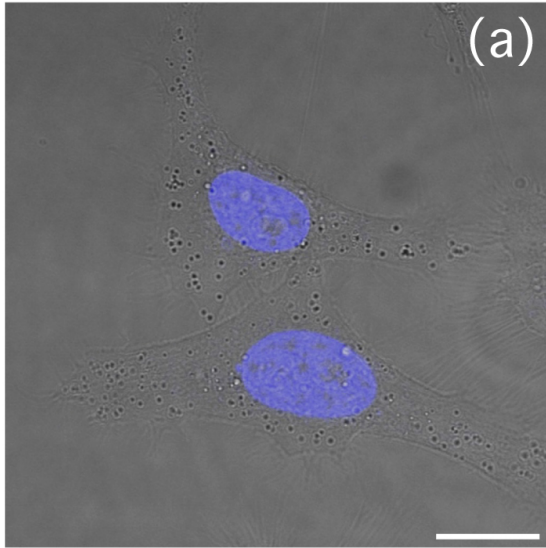
Figure 3.3-2 The internalization of *in vitro* - assembled, dual-color VLP$_{633}$-GFP (panels a-c, confocal microscopy) and *in vivo* - assembled, VLP-GFP (panels d-f, fluorescence microscopy) by cancer cell lines. HeLa cells were incubated with VLP$_{633}$-GFP (100 nM) for (a) 0 h, (b) 24 h, and (c) 48 h. VLP conjugated with Dylight 633 is red, GFP is green, and VLP$_{633}$-GFP complexes are yellow due to the co-localization of red and green emissions. Green color at 24 h indicates that the VLPs have opened and released the GFP. PC3 cells incubated with VLP-GFP (360 nM) for 48 h show (d) nuclei, (e) GFP-containing VLPs, and (f) merged fluorescent signals. Scale bar (a-c) = 20 μm or (d-f) = 300 μm. The nuclei are stained blue with DAPI.

3.3.3 *The RNAi scaffold is functional upon delivery by VLP*

VLP-RNAi$_{GFP}$ targets GFP mRNA in HeLa cells. A 22 base pair duplex containing a sequence from GFP mRNA was incorporated into the RNAi scaffold (RNAi$_{GFP}$, Figure 3.1-1a). RNAi$_{GFP,}$ was transcribed in *E. coli* expressing CP, and packaged into VLPs in a single step. To assay their activity, the VLPs were purified and co-cultured with HeLa cells transfected with GFP-expressing plasmid.

GFP expression is inhibited by VLP-RNAi$_{GFP}$. Incubation of the transfected U87 cells with VLP-RNAi$_{GFP}$ decreases expression of GFP, as shown by fluorescence microscopy (Figure 3.3-3a-d) and western blot analysis (Figure 3.3-3e). The results show VLP-RNAi$_{GFP}$ can efficiently inhibit expression levels of GFP by incubation in 300 nM of VLP-RNAi$_{GFP}$ for 48 h (Figure 3.3-3d and 3.3-3e, lane 4). High concentrations of VLPs containing endogenous RNAs from *E. coli*, which lack sequences that target GFP mRNA, do not affect GFP expression (Figure 3.3-3c and Figure 3.3-3e, lane 3). These experiments confirm that inhibition is caused by the VLP-RNAi$_{GFP}$ complexes, but not VLP.

This experiment was repeated with the HeLa cells, where similar levels of inhibition of GFP expression were observed (Figure 5.2-4). VLP-RNAi$_{GFP}$ induces dose-dependent and time-

dependent inhibition of GFP expression. Levels of inhibition of GFP expression in HeLa cells were analyzed quantitatively by flow cytometry (Figure 5.2-5). For cells transfected with GFP-expressing plasmid in the absence of VLP-RNAi$_{GFP}$, 23% of cells fluoresce after 24 h and 21% fluoresce after 48 h. In transfected cells that were also treated with 45 nM of VLP-RNAi$_{GFP}$, 15% fluoresce after 24 h and 10% fluoresce after 48 h. The results indicate fluorescence in 50% of cells expressing GFP is inhibited by 360 nM of VLP-RNAi$_{GFP}$ after 48 h.

3.3.4 *VLP-RNAi$_{let-7}$ targets the 3'UTR of Ras mRNA in U87 cells*

We constructed a version of the RNAi scaffold containing a sequence from let-7 mRNA (Figure 3.1-1b). The RNAi$_{let-7}$ was transcribed and assembled in *E. coli* with CP to form VLP-RNAi$_{let-7}$. Pan-Ras expression is suppressed by VLP-RNAi$_{let-7}$ (Figure 3.3-4). U87 cells were treated with purified VLP-RNAi$_{let-7}$ and assayed for Pan-Ras expression. Expression levels of Pan-Ras were significantly reduced (>70%) by incubation in 750 nM of VLP-RNAi$_{let-7}$ for 48 h (Figure 3.3-4a, lane 1 and 3). The observed decrease of expression is similar to that observed after treatment with chemically synthesized let-7 siRNA associated with a transfection agent (Figure 3.3-4a, lane 2). The effect of let-7 siRNA associated with a transfection agent was demonstrated previously.[169] Our results indicate that VLP-RNAi$_{let-7}$ is taken up by U87 cells and that functional RNAi$_{let-7}$ is released from the VLP to trigger RNAi. We have also performed a series of control experiments that minimize the chance that RNAi is caused here from off-target effects. Pan-Ras expression levels from U87 cells are unaltered by VLPs containing endogenous *E. coli* RNA or by VLP-RNAi$_{GFP}$ (Figure 3.3-4a, lane 4 and 5). These control experiments are most consistent with a model in which activity of VLP-RNAi$_{let-7}$ arises from the expected mechanism.

3.3.5 *VLP-RNAilet-7 attenuates U87 cell proliferation and promotes cell death*

Cell viability decreases in a time and dose-dependent fashion consistent with delivery of RNAi$_{\text{let-7}}$ (Figure 3.3-4b). We confirm previous work[169] showing that chemically synthesized let-7 miRNA alone was not functional in the absence of a transfection reagent. We investigated the viability of U87 cells upon treatment with VLP-RNAi$_{\text{let7}}$ and VLP-RNAi$_{\text{GFP}}$ (control) for 24 and 48 h. VLP-RNAi$_{\textit{let-7}}$ promotes U87 cell death in a dose-dependent and time-dependent manner as observed for GFP inhibition. The concentration required for 50% inhibition of growth (IC$_{50}$) for VLP-RNAi$_{\text{let-7}}$ is greater than 1000 nM after 24 h of incubation but is only 202 nM when the incubation period is extended to 48 h. The extended time for function presumably arises in part from the time-dependence of processes downstream of Ras expression or the processing of the VLP to release RNAi$_{\text{let-7}}$ scaffold. Control experiments confirm that cell death is caused by the VLP-RNAi$_{\text{let-7}}$. VLP-RNAi$_{\text{GFP}}$ does not promote death of U87 cells (Figure 3.3-4b).
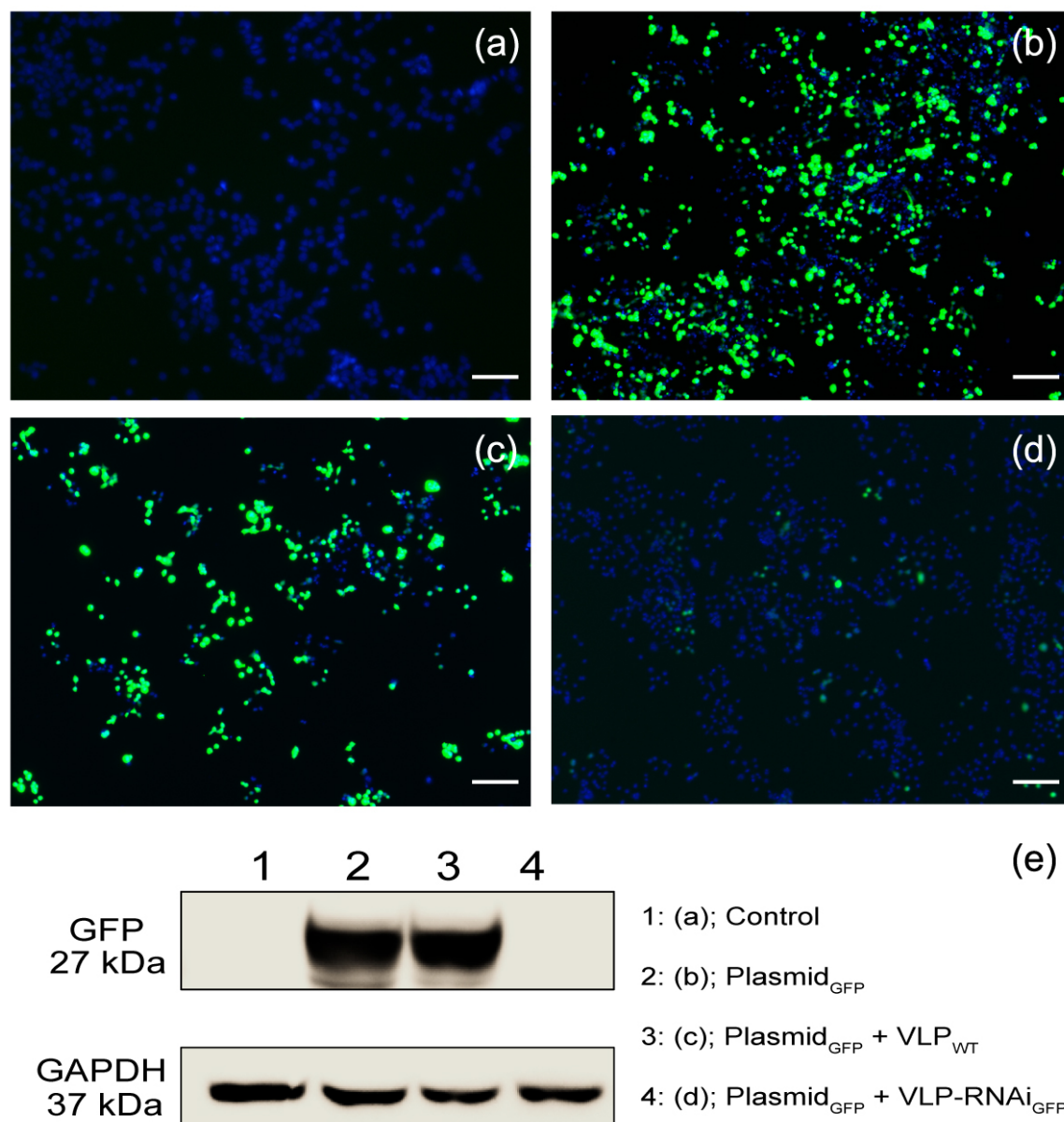
Figure 3.3-3 Suppression of gene expression by VLP-RNAi$_{GFP}$ in human glioblastoma cell line U87. Cells were treated with (a) PBS, (b) Transfection agent along with a plasmid expressing GFP, (c) Transfection agent/plasmid expressing GFP followed after 18 hours by treatment with 300 nM VLP$_{WT}$ (negative control containing endogenous *E. coli* RNA), (d) Transfection agent/plasmid expressing GFP followed after 18 hours by treatment with by 300 nM of VLP-RNAi$_{GFP}$. (e) Western blot analysis of GFP expression. Lane 1 shows the GFP expression in the cells corresponding to panel (a). Lane 2 shows expression in panel (b). Lane 3 shows expression in panel (c). Lane 4 shows expression in panel (d). In the images, green shows GFP expressions; blue shows nuclei. Images were obtained 48 hours after plasmid transfection. Scale bar = 200 μm.

(a)

	1	2	3	4	5	
Pan-Ras						34 kDa
β-actin						45 kDa

(1) Control   (4) VLP
(2) let-7 siRNA   (5) VLP-RNAi$_{GFP}$
(3) VLP-RNAi$_{let-7}$

(b)

IC$_{50}$ after 48 h (202 nM)

Percentage of Live Cells

VLP-RNAi concentration (nM)
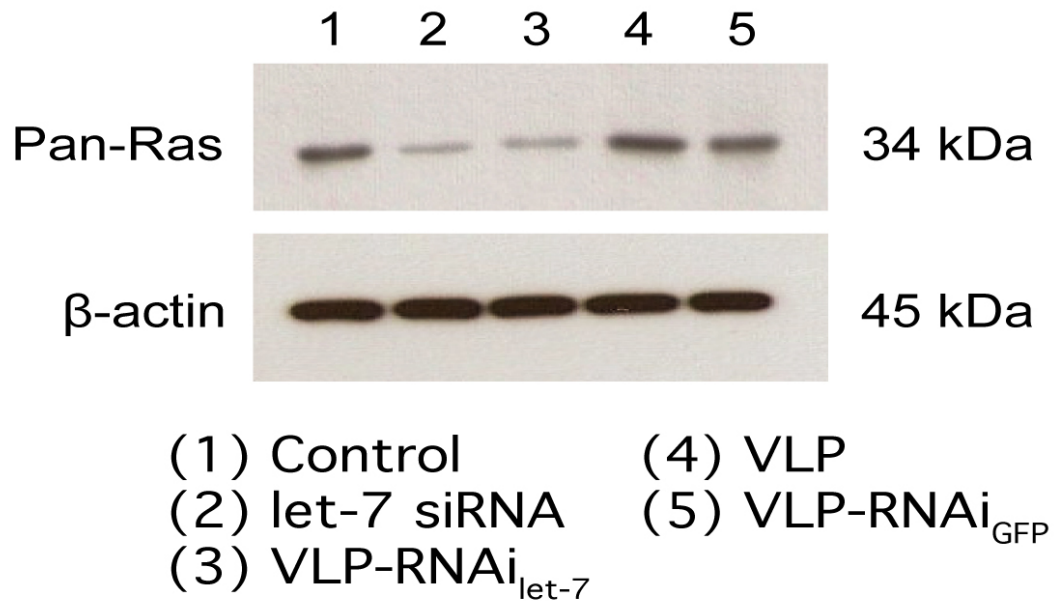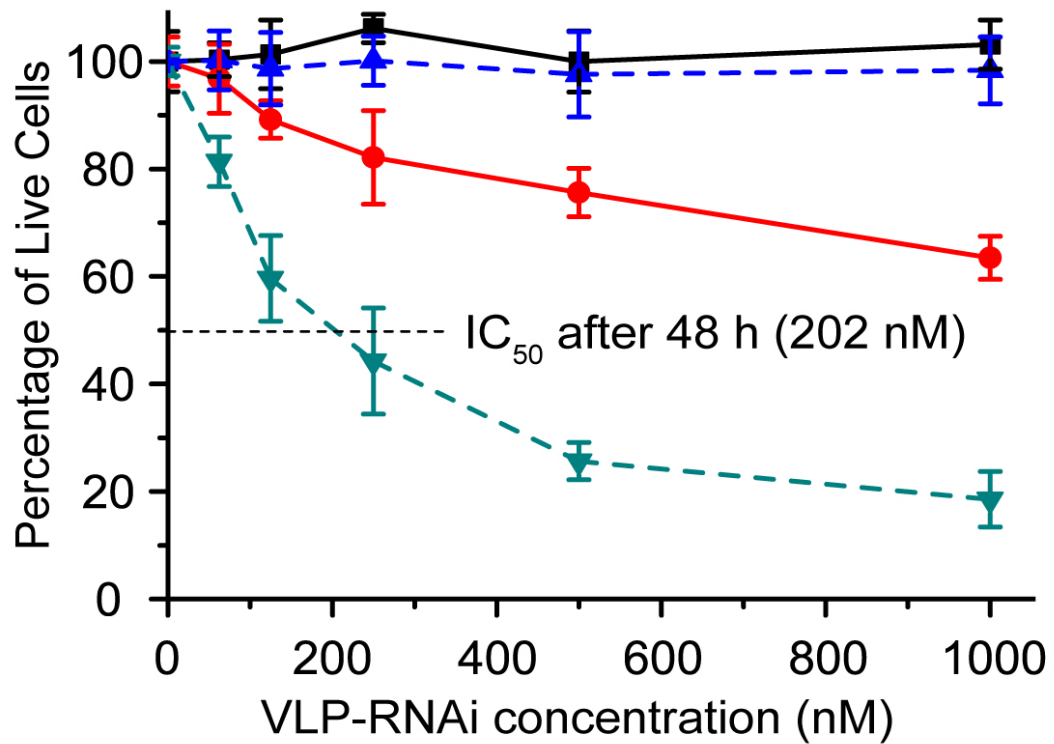
Figure 3.3-4 VLP-RNAi$_{let-7}$ inhibits Pan-Ras expression and demonstrates *in vitro* cytotoxicity in U87 cells. (a) Western blot analysis of Pan-Ras levels in U87 after 48 h with no treatment (lane 1), chemically synthesized let7 RNA delivered by the transfection agent lipofectamine (lane 2), VLP-RNAi$_{let-7}$ (lane 3), VLP (lane 4) and VLP-RNAi$_{GFP}$ (lane 5). U87 cells were incubated with 750 nM VLP in the absence of transfection reagent for 48 h. (b) Cell viability of VLP-RNAi$_{let-7}$ and VLP-RNAi$_{GFP}$. U87 cell viability was determined after treatment with various concentrations of VLP-RNAi$_{let-7}$ for 24 h (●) and 48 h (▼) and VLP-RNAi$_{GFP}$ for 24 h (■) and 48 h (▲). The level of viability of U87 cells is reported here as percentage survival. Values are expressed as means ±SD (n = 8).

3.4 Discussion

We have designed a general utility RNAi scaffold that spontaneously assembles with CP to form functional VLP-RNAi. The scaffold is a single RNA molecule containing the Qβ hairpin on the 5' end, a carrier strand, the miR-30 stem loop, and the silencing strand. The RNAi scaffold is designed to promote unimolecular pairing of the carrier and silencing strands, and contains a 3' terminus appropriately placed to direct dicer to release the single-stranded silencing strand. This RNAi scaffold can contain a broad variety of silencing sequences including miRNAs and siRNAs that can target essentially any mRNA. As a single RNA molecule, the scaffold folds efficiently, and readily assembles with CP to form Qβ VLPs containing functional RNA. Advantages of the VLP-RNAi system we describe here include ease of vector construction, assembly and packaging, purification, targeting and delivery, and in effectiveness of regulating gene expression.

Previous work identified a variant of human miR-30 that maximizes production of mature miRNA, and demonstrated function of RNAi in human cells by substituting the stems of miR-30 with artificial targeting sequences.[158] Ramratnam incorporated a siRNA sequence targeting the mRNA of HIV-1 transactivator protein *tat* into the miR-30 stem. The resulting artificial miRNA is 80% more potent in reducing target p24 antigen production than conventional *tat* shRNA.[159] The enhancement of gene silencing may be due in part to high stability of the miR-30 stem-

loop.[170] The miR-30 stem-loop provides a tool for intramolecular folding of shRNA, which is rapid and efficient, whereas formation of an intermolecular duplex by RNAs in unlinked strands is less efficient.[171]

We placed Qβ hairpin on the 5' end of scaffold, following Stockley, who synthesized a bimolecular aptamer-siRNA.[168] Our design of the RNAi scaffold presents a free 3' end for recognition by the PAZ domain of Dicer [164,172] and efficient transfer of the processed siRNA to Argonaute.[172] To facilitate one-step VLP-RNAi assembly in *E. coli* and to maximize activity, we co-express CP and cargo RNA,[151] which contains the packaging aptamer (the Qβ hairpin),[168] stabilizing the scaffold with miR-30.[158] The RNAi scaffold and Qβ CP were placed under control of T7 RNA polymerase promoters and are co-expressed in *E. coli*. The Qβ CP is transcribed and translated, packaging the transcribed RNAi scaffold, spontaneously forming functional VLPs *in vivo*. The assays and controls indicate that the RNAi scaffold is packaged within the VLPs.

We have incorporated several silencing sequences into the RNAi scaffold (Figure 3.1-1) and demonstrated function of these VLP-RNAi in a variety of human cell lines. The VLP-RNAi's inhibit expression of a reporter gene encoding GFP or expression of the Pan-Ras oncogene.
GFP expression in HeLa and U87 cells is inhibited by VLP-RNAi$_{GFP}$ (Figure 3.3-3). The VLP-RNAi$_{GFP}$ induces dose-dependent and time-dependent inhibition of GFP expression. The effect is specific: high concentrations of VLPs containing other RNAs do not decrease the level of GFP expression (Figure 3.3-3, Figure 5.2-4 and Figure 5.2-5).

Pan-Ras expression is suppressed by VLP-RNAi$_{let-7}$ (Figure 3.3-4). VLP-RNAi$_{let-7}$ attenuates U87 cell proliferation, promotes death in cell culture and down regulates Pan-Ras. Let-7 miRNAs function as tumor suppressors by decreasing expression of the Ras oncogene family at the level of translation,[166,173] reducing cell proliferation and invasion. Down-regulation of let-7 has been observed in lung cancer, colon cancer, and melanoma and is correlated with poor patient survival.[174-177] Restoration of let-7 expression may be a useful cancer therapy.[177] Ras proteins (K-Ras, N-Ras and Pan-Ras) are known to be up-regulated in these cancers.[178] Human Ras expression is regulated by let-7 miRNA by binding to the 3' UTR of Ras mRNA.[166] In human brain tumor cells, overexpression of let-7 miRNA leads to a decrease in Ras protein expression, inhibition of cell proliferation and reduced tumor growth, without harming normal astrocytes.[179]

Our control experiments confirm that Qβ VLPs containing non-specific RNAs are non-functional and benign. VLP-RNAi is active only when the RNAi scaffold contains functional RNAi sequences. In sum, the results show that the *in vivo* packaged VLP-RNAi containing the RNAi scaffold is efficient in inhibiting gene regulation and in promoting tumor cell death. The combined results demonstrate that undecorated Qβ VLPs enter cell lines in the absence of transfection reagent and surface decoration. Our results, along with earlier studies, demonstrate extended incubation times, allowing internalization of undecorated MS2[168] and Qβ VLPs. These results extend prior work in which surface decoration facilitates uptake of MS2 VLPs and Qβ VLPs in mammalian cells.[152,180-182] Previously, several groups showed that when surfaces of Qβ and the closely related MS2 VLPs are decorated with appropriate targeting ligands, the VLPs are quickly internalized by human cells via receptor-mediated endocytosis.[152,167,180,181,183] Stockley

showed that undecorated MS2 VLPs are also internalized, but more slowly.[168] Once internalized, VLPs disassemble and release their cargo, which is functional *in vivo* (in cell culture).[148,152,168]

Control and functional assays confirm that VLPs release their cargo intracellularly (Figures 3.3-3, 3.3-4, and Figures 5.2-5). Previous work has reported similar cytoplasmic release from bacteriophage MS2 VLPs.[152,168,180,182,184] The mechanism by which VLP-encapsidated RNA escapes from the endosome and enters cytoplasm remains unclear. Our results are consistent with previous work which show that ssRNA animal viruses can pass their viral genomes to the cytoplasm from the endosomes.[185]

The release mechanism of RNA from the VLP is most likely a combination of disulfide bond breakage and destabilization by low pH. Reducing agents such as glutathione that are important antioxidants in cells. The low pH in late endosomes and lysosomes may dissociate the coat proteins of the Qβ-VLPs. A combination of the above phenomena may result in the escape of encapsidated nucleic acid.

The efficiency of VLPs for delivering cargos to human cells depends on targeting, VLP uptake and endosome escape. Finn and Stockley both showed that covalent attachment of targeting peptides facilitates VLP uptake in human cell lines in short time periods at less than 50 nanomolar concentrations.[167,168,182] In addition, covalent attachment of a histidine-rich fusogenic peptide on the exterior surface VLPs can promote endosomal escape of internalized VLPs.[152] This histidine-rich peptide acts by a "proton sponge" effect. Histidine can sequester protons and buffer the acidification in the endosomes. The buffering induces osmotic swelling and bursting

of endosomes.[186,187] Impressively, the working concentration of siRNA-loaded VLPs with covalent attachment of both targeting and fusogenic peptides is less than 150 pM.[152] Comparison of our work with the results of several other groups who have decorated the MS2 or Qβ VLP external surface with different targeting ligands, suggests that undecorated VLP-RNAi requires higher concentrations and longer incubation times. Increasing the efficiency of VLP uptake and endosomal escape are future challenges for our one-step VLP-RNAi assembly method.

CHAPTER 4

4. USING CATIONIC QB VLPS FOR CO-DELIVERY OF DNA PLASMID AND PACKAGING RNA

4.1 Introduction & Motivation

Over the past 10 years, virus-like particles (VLPs) have been considered as new bio-nanoparticles, and have emerged as potential tools for therapeutic delivery and cell imaging.[188] VLPs are well known for their stability under thermal stress and various pH conditions, resistance to proteolytic degradation, and ease of surface modification.[4,18,24] Previous reports with peptide display on the exterior surface of VLPs demonstrated cell-specific delivery.[15,18] Toxin molecules and siRNA molecules can be loaded into VLPs using *in vitro* packaging method for delivery to specific cancer cells and achieve maximum cell death and gene silencing.[15,189] Previous studies have shown delivery of *in vivo* produced VLPs containing fluorescent proteins to mammalian cells.[23,190] We have designed a general utility RNAi scaffold that is able to co-assemble with Qβ coat proteins into VLPs in *E. coli* (Chapter 3.3-1). The Qβ VLP-RNAi platform has shown promising RNAi-mediated inhibition of target gene in mammalian cells (Chapter 3.3-3 and 3.3-4).

Besides RNAi-based therapeutic strategies, DNA gene therapy is another potential solution to genetic disorders and cancer. Plasmid DNA-based gene therapy with a suicide gene encoding thymidine kinase has demonstrated inhibition of tumor growth in mouse models.[191] The use of plasmid DNA vaccine has also shown promising results in the protection against human papillomavirus (HPV).[192] Although Qβ VLPs are extremely versatile bio-nanoparticles, the

VLPs originated from single-stranded RNA (ssRNA) bacteriophages (e.g., Qβ and MS2), and are not capable of packaging plasmid DNA *in vitro* and *in vivo* due to their natural limits.

Plasmid DNA delivery is usually accomplished by either viral vectors or cationic polymers. In general, viral vector systems (e.g., retroviruses and adenoviruses) show greater efficiencies for cellular delivery and gene expression, compared to non-viral mediated systems.[81] However, several safety concerns of viral vector systems regarding immunological response, specificity of transgene delivery, and unwanted mutagenesis must be addressed.[86] Non-viral alternatives have become increasingly in demand.

Many cationic polymers such as poly(β-amino esters) (PAEs), poly (L-lysine) (PLL), and poly(ethyleneimine) (PEI) are widely used as advance strategies to interact negatively charged phosphate backbone of DNA and RNA for nucleic acid delivery.[193,194] For example, PEIs have been designed as plasmid DNA carriers for cancer gene therapy (e.g., bladder, ovarian, and pancreatic cancer), and have been studied under clinical evaluation.[195] PAEs have been developed as an aerosol siRNA delivery system and show significant anticancer activity with low toxicity in lung tumor-bearing mice.[196]

Cationic polymers are composed of primary, secondary, and tertiary amine functional groups. Primary and secondary amines are strong nucleophiles that allow for covalent conjugation of different functional molecules to polymers with specific crosslinking agents (e.g. EDC/NHS or sulfo-SMCC).[197,198] At the physiological pH range, amines in cationic polymers are generally protonated and carry positive charges. The resulting protonated amines allow complexation of

polymers with anionic nucleic acids through electrostatic interaction [81,82] and are capable of inducing the proton sponge effect to enhance endosomal escape.[194,199] In addition, nanoparticles carrying positive charge, show higher cellular uptake efficiency than uncharged or negatively charged ones.[200-202]

Based on previous studies and current research in nucleic acid delivery, we report here a new delivery approach for the simultaneous delivery of DNA and RNA by combining cationic polymers and Qβ VLP (Figure 4.1-1). The method employs surface modification of RNA-containing VLPs that decorates by covalent conjugation of PEIs. The PEI-VLP (pVLP) complexes occur *in vitro* and form homogeneous particles with a positively charged surface. Our initial investigation shows that pVLP exhibits efficient DNA delivery in mammalian cells. We have successfully co-delivered plasmid DNA with Qβ VLP containing *in vivo* packaged RNA. Our results may provide a new insight into VLPs originated from the ssRNA bacteriophage as a DNA delivery systems. We believe this co-delivery strategy of plasmid DNA and functional RNA using Qβ VLP is likely to impact current cancer therapy.
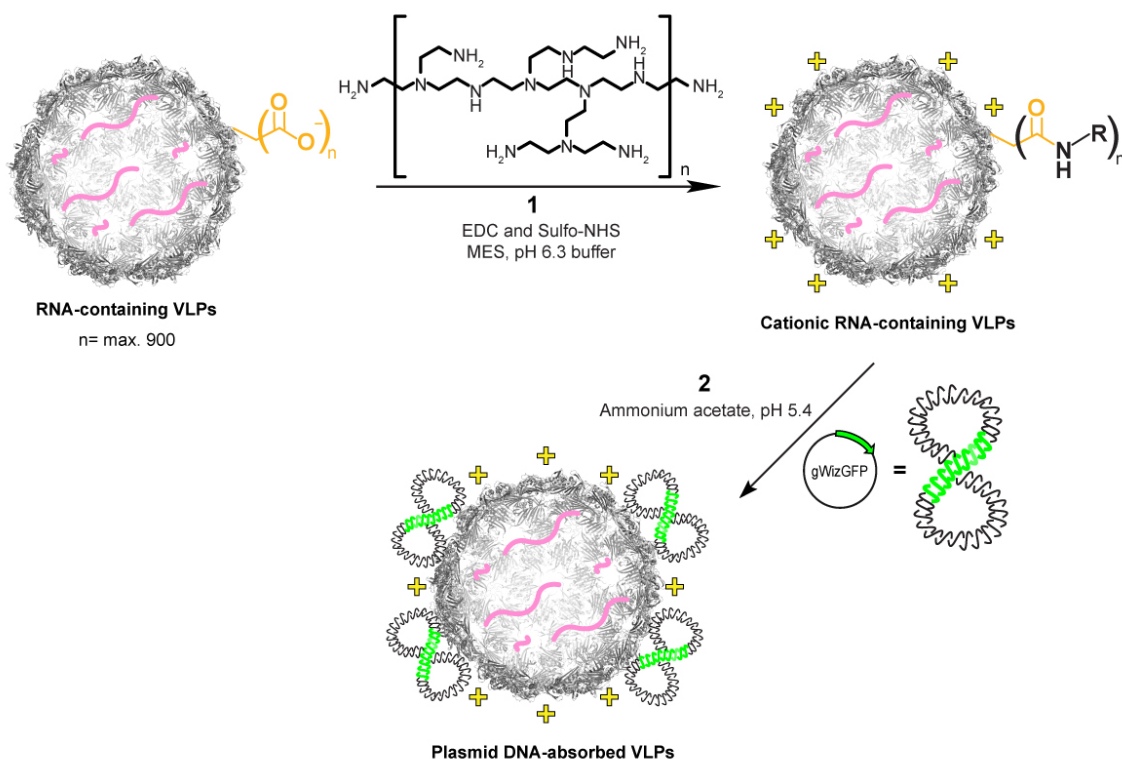
Figure 4.1-1 Preparation of plasmid DNA loaded RNA-containing VLPs.

4.2 Materials & Methods

4.2.1 *Reagents*

DNA oligos were ordered from Eurofins MWG Operon, Inc. NZY broth media was purchased from TEKNOVA. Sec-Butanol and Chloroform were purchased from Fisher Scientific. Ammonium sulfate was purchased from ICN Biomedicals. Sucrose, RNase- and DNase-free, was purchased from Amresco. Dithiothreitol (DTT) was purchased from Research Products International Corp. N-(3-Dimethylaminopropyl)-N′-ethylcarbodiimide hydrochloride (EDC), *N*-Hydroxysuccinimide (NHS), 2-(N-Morpholino)ethanesulfonic acid, 4-Morpholineethanesulfonic acid (MES), amd Cy®5 NHS ester were purchased from Sigma-Aldrich. Sodium dodecyl sulfate was purchased from Shelton Scientific, Inc. Polyethylene glycol 8000 was purchased from J. T.

Baker. 30% hydrogen peroxide was purchased from Fisher Scientific. BCA protein assay kit was purchased from Thermo Scientific. Polyallomer centrifuge tubes were purchased from Beckman Coulter. Amicon® Ultra centrifugal filters (100 kDa MWCO) were purchased from Millipore. Spectra/Por® dialysis tubing (15 KDa MWCO) was purchased from Spectrum® Laboratories, Inc. All other reagents were analytical grade.

4.2.2 *Construction of Qβ CP expression vector*

DNA encoding Qβ CP monomer (NCBI reference sequence: NC_001890.1) was synthesized by recursive-PCR (R-PCR)[121] and cloned into pCDF-1b (Novagen) to generate plasmid pCDF-CP previously. All constructs were sequence confirmed (MWG Operon).

4.2.3 *Expression of Qβ VLP-RNA complexes*

E. coli containing pCDF-Qβ CP vector was inoculated in NZY medium with streptomycin (50μg.mL^{-1}) and incubated overnight at 37°C. Qβ-VLP production started with the addition of 1% overnight culture to the ZYM-5052 auto-induction medium [123]. Production culture was incubated 24 h at 37°C. Cells were collected by centrifugation at 4°C and 6500xg for 30 min. Cells were resuspended in equal volume of Qβ buffer (10 mM MgCl$_2$ and 20 mM Tris-HCl, pH7.5) and lysed by sonication at 40 watts for three min with 10s on/off intervals. The lysate was centrifuged to remove cell debris for 30 minutes at 23,430xg. 2M Ammonium sulfate precipitation followed by 30-minute centrifugation at 23,430xg was performed to obtain crude VLP. Crude VLPs were then suspended in 1 mL Qβ buffer and extracted with 1:1 n-butanol:chloroform. Organic extraction was repeated three times. The aqueous layer was subsequently purified by step sucrose gradient ultracentrifugation (10-40% w:v) in a SW41Ti

rotor (Beckman) at 40K RPM for two hours. Qβ VLPs were precipitated from the sucrose fraction with 20% (w/v) PEG8000. Resuspended Qβ-VLPs were combined and dialyzed against 2 L dialysis buffer (20 mM Tris, pH 7.5 and 50 mM NaCl) for 2 h. This procedure was repeated three times prior to the use of particles in further analyses.

4.2.4 *Preparation of cationic VLP-Cy5 complexes*

The purified RNA-containing VLPs were mixed with NHS-mediated Cy5, and vortexed for two hours at 4°C in the dark. Cy5 immobilized on the surface of VLPs (VLPs-Cy5) was separated from the solution and washed with DI water. Cationic VLPs-Cy5 complexes were prepared by conjugation of PEI on the surface of VLPs-Cy5. Briefly, ethyl-3-(3-dimethylaminopropyl) carbodiimide hydrochloride (EDC, 12 mg) and sulfo-N-hydroxysulfosuccinimide sodium salt (sulfo-NHS, 27 mg) were dissolved in 2 mL of 0.5 M 2-(N-morpholino) ethanesulfonic acid (MES) buffer at pH 6.3) in the dark. A 0.1 mL aliquot of the above solution was mixed with 0.1 mL of a 45 μM VLPs-Cy5 at 25°C and reacted for 30 min in the dark then further mixed with 0.1 mL of PEI with different concentrations (i.e., 0.2 w/w% and 0.5 w/w%) for another three hour at 4°C in the dark to form pVLPs-Cy5. The produced pVLPs-Cy5 complexes were purified by Amicon® Ultra centrifugal filters (100 kDa MWCO) and suspended in PBS (pH = 7.4) for storage or 25 mM sodium acetate (pH = 5.4) for loading DNA plasmid.

4.2.5 *Fluorescence microscopy*

HEK 293 cells (2 x 10^5 cells) were seeded into glass bottom microwell dishes (MatTek) and grown for 24 h in DMEM with 2.2 mg mL^{-1} sodium carbonate, 10% fetal bovine serum, 50 μg mL^{-1} gentamicin, 50 μg mL^{-1} penicillin, and 50 μg mL^{-1} streptomycin at 37 °C and 5% CO_2.

Cationic VLPs-Cy5 complexes were added to cells to a final concentration of 1.25 μM. Treated cells were further incubated at 37 °C with 5% CO_2 for 0, 24, and 48 h. After incubation, cells were rinsed three times with PBS. Nuclei were stained with Hoechst for 20 min at 37 °C, and washed three times with PBS. Fluorescence images of HEK 293 cells were captured using a fluorescence microscope (Olympus U-LH100HG, Japan).

4.3 Results

4.3.1 *Strategies for conjugating branched PEI to Qβ VLP.*

Here, we initially investigated the conjugation of branched PEI (Figure 4.3-1a) to RNA-containing VLPs. The molecular weight (Mn) of PEI is up to 5,000 by gel permeation chromatography (GPC), relative to polystyrene standard. Carboxyl groups on the exterior surface of Qβ VLP (e.g., side chains of aspartic acid and glutamic acid and the C-terminus) are used to conjugate primary amine of branched PEI with zero-length crosslinking agents, carbodiimide and sulfo-*N*-hydroxysuccinimide (EDC and sulfo-NHS) *in vitro*. The conjugation of PEI to the exterior surface of VLPs proceeded in one step in 0.5 M MES buffer at pH 6.3 with EDC and sulfo-NHS at 4°C for 12 h (Figure 4.1-1, step 1). There are 12 carboxylic acid groups in each coat protein (CP) monomer (Figure 4.3-1b). We predict that less than four carboxylic groups react to branched PEI in each CP monomer due to steric hindrance. This effect may limit the number of accessible carboxylic groups to polymer.
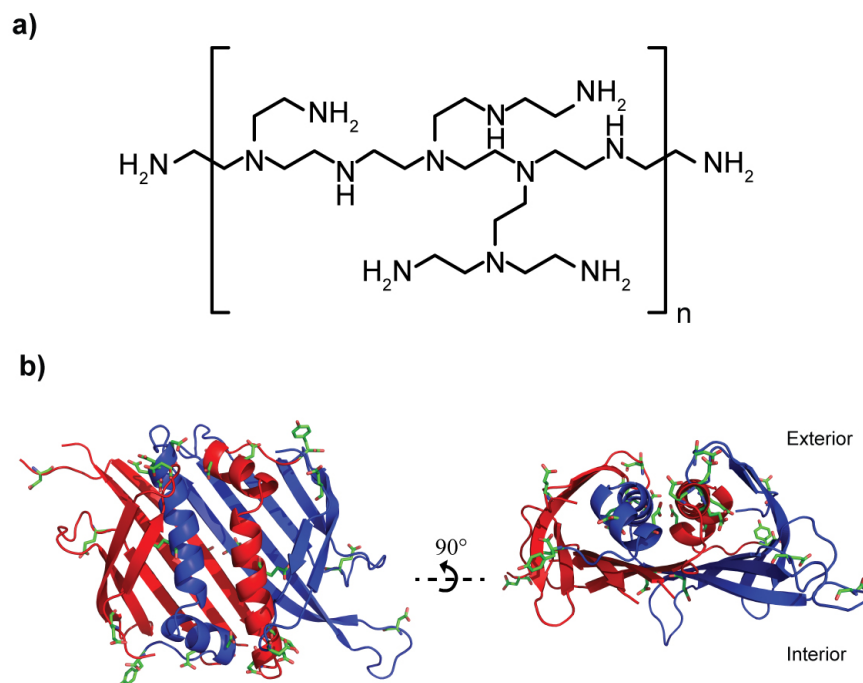
Figure 4.3-1 Structure of branched PEI and possible conjugation sites in CP dimer (a) Synthesized PEI used in this study. (b) Location of carboxylic acid in a Qβ CP dimer. Cartoon representation shows the structure of Qβ CP dimer. Carboxylic groups from aspartic acid, glutamic acid, and the C-terminus are highlighted in a stick representation.

4.3.2 *Characterization of PEI-conjugated VLPs*

Branched PEI was conjugated to the Qβ VLPs to form cationic bio-nanoparticles. The resulting pVLPs were subjected to dynamic light scattering, native agarose gel electrophoresis, and denaturing SDS-PAGE (Figure 4.3-2). Different degrees of PEI conjugation (0.1, 0.2, 0.5, and 1.0 wt% of PEI solution) to VLPs were analyzed. Conjugation of the PEI on the RNA-containing VLP increases the range of zeta potential from -2.8 ± 0.8 mV (wild-type) up to 14.3 ± 1.2 mV (0.2 wt% PEI solution). Conjugation of VLPs to higher concentration of PEI (0.5 wt% and 1 wt% PEI solution) exhibit moderate expansion in the diameter of capsid from 31.2 ± 1.7 nm (wild-type) to 43.1 ± 1.0 nm (1 wt%) at pH 7.4 (Figure 4.3-2a). We have not observed particle

aggregation after preparation of RNA-containing pVLPs. To further confirm that conjugated VLPs carry positive charges, we analyzed gel mobility for RNA-containing pVLPs and control wild-type VLPs. The results obtained from native agarose gel demonstrate that the mobility of pVLPs was retarded towards anode, relative to wild-type RNA-containing VLPs (Figure 4.3-2b). pVLPs with higher degree of PEI labeling (0.5 wt% PEI solution) do not migrate, remaining in the wells of the gel. The denatured SDS-PAGE results show smeared CP monomer bands appeared in both lower and higher (0.2 wt% and 0.5 wt% PEI solution) degree of labeling, but not in wild-type VLPs (Figure 4.3-2c). The protein band at 28 kDa represents CP dimers remaining noncovalently associated as noted previously.[203,204] The combined results suggest that RNA-containing VLPs have been successfully conjugated to branched PEI and carry positive charges on the exterior surface of particles.
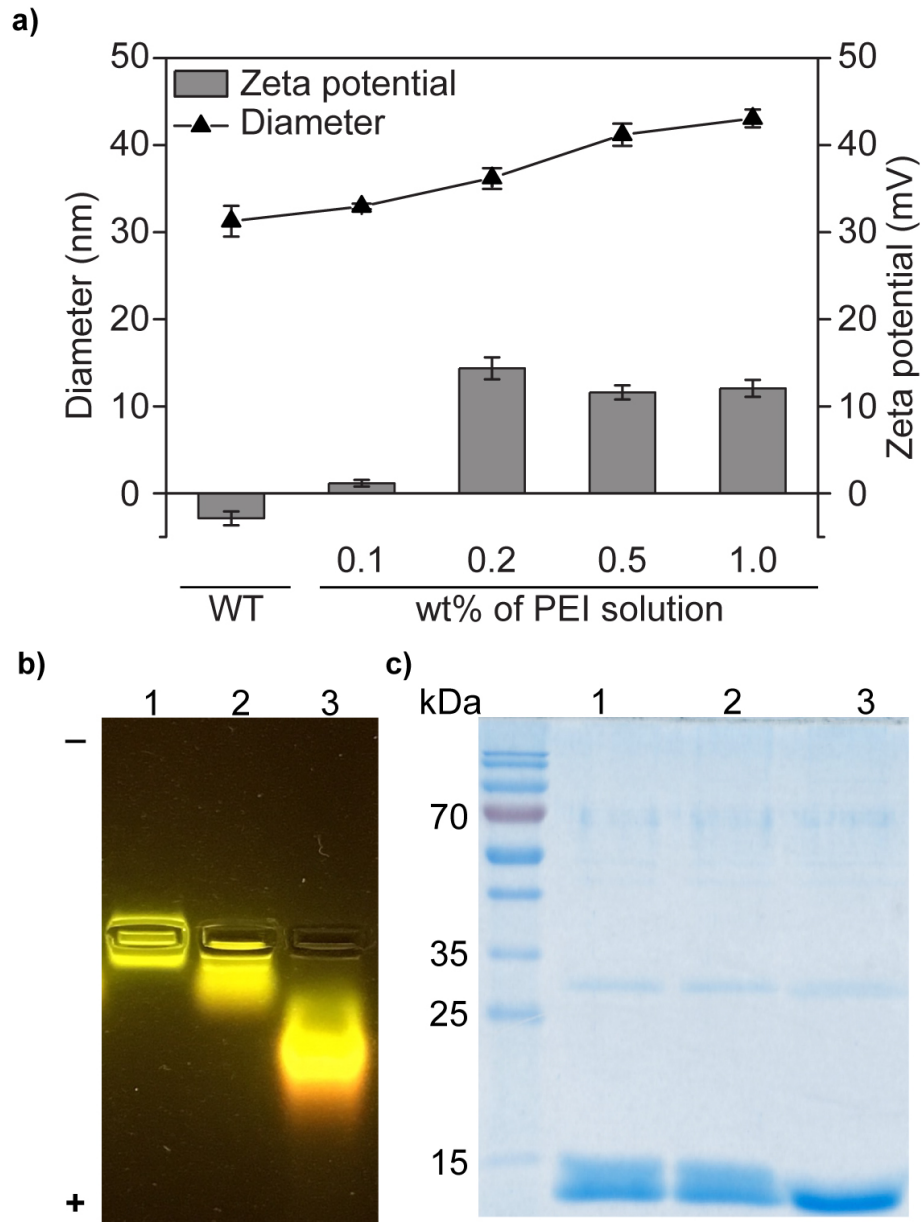
Figure 4.3-2 PEI is conjugated to the exterior surface of VLPs to form cationic VLP complexes. (a) Size and zeta potential of RNA-containing pVLPs and wild-type RNA containing VLPs by dynamic light scattering. Values are expressed mean ± SD (n=3). pVLPs and VLPs were subject to electrophoresis on (b) a native 1.2% agarose gel and visualized with GelStar[TM], and (c) a 12.5% denatureed SDS-PAGE and stained with Coomassie blue. Lane 1: conjugated Qβ-VLPs using 0.5 wt% PEI solution, Lane 2: conjugated Qβ-VLPs using 0.2 wt% PEI solution, Lane 3: purified Qβ-VLP without PEI conjugation. The Qβ CP monomer is 14.5 kDa.

4.3.3 *The Plasmid DNA is expressing upon delivery by cationic VLPs*

Cationic RNA-containing pVLPs deliver plasmid DNA into cultured human cells. To prove the pVLPs with plasmid DNA could be efficiently co-delivered to cells, the RNA-containing pVLPs were modified with Cy5 on the surface for tracking and monitoring. A 5.7 kb plasmid DNA encoding green fluorescent protein (GFP) was incubated with pVLP-Cy5 particles to form plasmid DNA loaded pVLP-Cy5 complexes (Figure 4.1-1, step 2). Cy5-labeled cationic VLPs (pVLP-Cy5) were prepared using PEI as mentioned above. Here, we asked cationic pVLP-Cy5 allow adsorption, delivery and release of plasmid DNA. The green and red fluorescent signals are observed after 48 h of co-culture using fluorescent microscopy. After incubation of 48 h with pVLP-Cy5, the cells exhibited red and green fluorescent signals, indicating that the pVLP-Cy5 was taken up into cells and then released plasmid DNA from plasmid loaded pVLP-Cy5 complexes to expression of GFP protein within the cytoplasm. The results indicate that plasmid DNA is adsorbed and delivered by cationic VLPs and is expressing in human embryonic kidney 293 cells (HEK293) (Figure 4.3-3). It implies cationic VLPs could be used as delivery vehicles for foreign plasmid DNA.
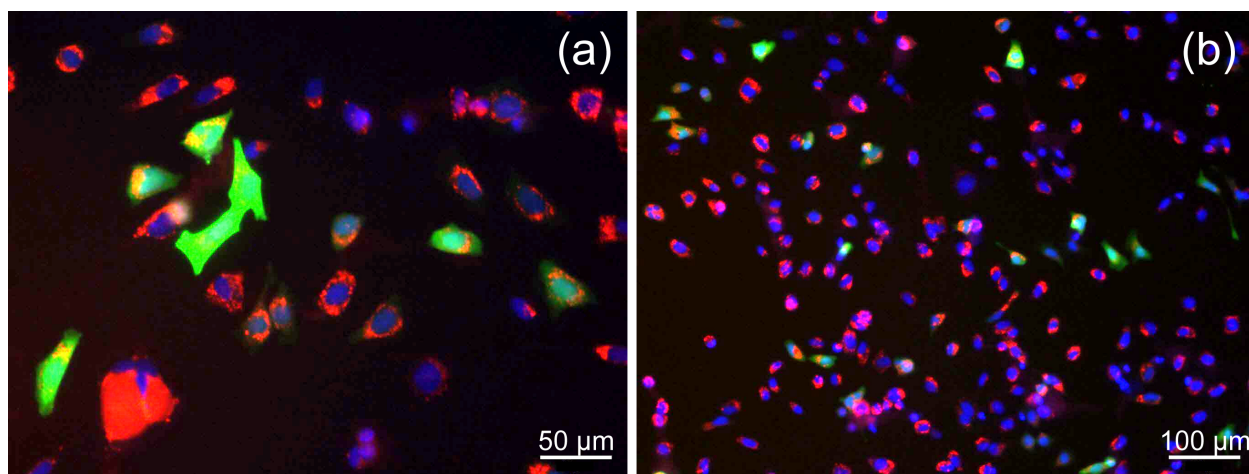
Figure 4.3-3 Cationic pVLP-Cy5 complexes can deliver and release plasmid DNA encoding GFP in cells. HEK293 cells were incubated with plasmid DNA loaded cationic pVLP-Cy5 complexes (1.25 μM) for 48 h. VLP conjugated with Cy5 is red, and GFP is green. Green color at 48 h indicates that the plasmid DNA has been released from particles. The nuclei are stained blue with DAPI.

4.4 Discussion

Here, we demonstrated an approach for co-delivery of plasmid DNA and RNA-containing VLPs. Commercially available branched PEI was used to conjugate on the exterior surface of Qβ VLPs to investigate the effects of cationic polymer on adsorption, delivery and release of plasmid DNA (Scheme 4.3-1). Our preliminary results indicate that conjugation of RNA-containing VLPs to cationic PEI polymer leads to an increase of the zeta potential from -2.8 ± 0.8 mV up to 14.3 ± 1.2 mV and an increase in the hydrodynamic diameter from 31.2 ± 1.7 nm to 43.1 ± 1.0 nm (Figure 4.3-2). We also show that adsorption of plasmid DNA on the surface of VLPs provides gene delivery and expression in mammalian cells (Figure 4.3-3).

Several groups have packaged foreign plasmid DNA into VLPs by *in vitro* methods and then delivered to eukaryotic cells.[205-207] By using this *in vitro* method, VLP disassembly and reassembly are required to achieve foreign plasmid DNA packaging into particles. Recently, JC virus-like particles (JC VLPs) originated from a double stranded DNA virus have been utilized

successfully to simultaneously package foreign plasmid DNA that was co-expressed in the *E. coli*.[208] The maximum size of foreign plasmid DNA packaging by JC VLPs in *E. coli* is up to 9.4 kilobases (kb).[209] The plasmid DNA-filled JC VLPs carrying the suicide gene have demonstrated efficient exogenous gene delivery to tumor cells and inhibition of tumor growth.[191]

Finn, et al, has recently demonstrated that Qβ VLPs incorporating the unnatural amino acid are able to conduct polymerization in the interior space of VLPs by atom-transfer radical polymerization.[203] The work shows that the cationic polymers inside a RNA-free VLPs offer substantial positive charge of the particles. Most importantly, the siRNA molecules may either be adsorbed on the surface of VLPs, or they may enter the particle to perform siRNA delivery into HeLa cells.

Our initial proof-of-concept experiments used an alternative method to combined natural biopolymer and synthetic cationic polymer to form cationic VLPs. The effects of an increasing PEI concentration during surface conjugation on particle size and surface charge were investigated. The particle size of VLPs increases linearly with increasing concentration of PEI. However, the zeta potential of RNA-containing pVLPs increases linearly with increasing concentration of PEI until it reaches a plateau between 0.2 wt% and 1 wt% PEI (Figure 4.3-2a). It suggests that conjugation of carboxylic acid group on the exterior surface of VLPs reaches the maximum at 0.2 wt% solution of PEI. When a higher wt% of PEI solution is used during the process of conjugation, excess amount of unreacted PEI molecules may accumulate on VLPs via non-covalent interaction to cause size expansion. This sterically crowded surface is likely to prevent exposure of the cationic amine groups on the exterior surface of VLPs. We have

observed two conjugated VLPs (0.2 wt% PEI vs. 0.5 wt% PEI) with similar zeta potentials seeing no results in similar migration pattern on native agarose gel (Figure 4.3-2b). The results indicate the size of both PEI conjugated VLPs is different which is consistent with data from dynamic light scattering experiments. Qβ coat protein monomer extracted from PEI conjugated VLPs streaks slightly to higher molecular weight on SDS-PAGE as previously observed (Figure 4.3-2c).[8,203] Detailed size characterization of RNA-containing pVLPs may be performed by transmission electron microscopy and size-exclusion chromatography.

RNA-containing pVLPs are capable of delivering and releasing plasmid DNA into mammalian cells (Figure 4.3-3). The image results from fluorescence microscopy demonstrated co-delivery of plasmid DNA encoding a green fluorescent protein and pVLP-Cy5 particles. The expression of green fluorescent protein in the cytoplasm indicates plasmid DNA adsorption and desorption on cationic pVLP-Cy5 particles. Maximum adsorption capacity of PEI-conjugated VLPs will be further investigated.

The hybrid pVLP system we developed here shows ease of plasmid DNA adsorption onto positive charged VLPs, plasmid DNA delivery for foreign gene expression. Ultimately, we would like to combine this pVLP system with our RNAi scaffold to achieve co-delivery of plasmid DNA, functional RNA, and fluorescent protein using Qβ VLPs to mammalian cells.

CHAPTER 5

5. RECOMMENDATIONS AND CONCLUSIONS

5.1 Recommendations

5.1.1 *Multiple RNAi target in single VLP*

As shown in **Chapter 3**, VLP-RNAi is capable of inhibiting mRNA translation of a single target in cancer cell culture. One of the goals of future work proposed here is to target multiple genes by *in vivo* produced VLP-RNAi complexes. We will develop new RNAi scaffolds that can silence multiple target genes. This new RNAi scaffold is inspired by a non-coding RNA (pRNA ring) derived from bacteriophage phi29.[210] The pRNAs assemble into three-membered or six-membered nanoparticles without covalent linkage and crosslinking. Previous studies have shown RNAi activity induced by pRNA/siRNA chimera *in vitro* and *in vivo*.[211-213] The self-assembly of pRNAs provide substantial stability to urea denaturation.[211] The new RNAi scaffold we designed can carry different target siRNAs and self-assemble into stable RNA nanoparticles. The RNA nanoparticles with Qβ hp can then be encapsulated into Qβ VLP. We will systematically determine the optimum RNA length, and RNA structure for efficient RNAi and self-assembly. In addition, we will design, construct and test RNA constructs with RNA aptamer for affinity purification.

5.1.2 *Continued development of multifunctional VLP for brain cancer*

As shown in **Chapter 4**, **Error! Reference source not found.**we have introduced a method to o-deliver DNA plasmid through a cationic polymer-VLP system (pVLP). The second proposal is to improve our multifunctional VLPs for brain tumor research. Brain tumor is one of the most

lethal cancers due to difficulties of delivering therapeutic agents across blood-brain barrier (BBB) and serious side effects. To overcome this hurdle, we propose a self-assembled VLP with cationic polymers and targeting ligands as multifunctional nanocarriers to deliver RNAi molecules, chemotherapeutics, suicide gene expression plasmid, and green fluorescence proteins (GFP) for RNA interference, gene therapy and imaging tracking. Qβ coat proteins and cargos including RNAi molecules and fluorescent proteins will be produced and self-assembled in *E. coli*. Previous study has shown APOE incorporated lysosomal enzymes enables delivery across the BBB.[214] The cationic polymer and APOE-peptide would be incorporated to the exterior surface of VLPs to carry DNA plasmid DNA on the exterior surface, enhance cellular uptake, and promote BBB penetration.

Our collaborator Dr. Hung-Wei Yang's group at the National Sun Yat-sen University, Taiwan has assessed pVLP by cell examination. pVLPs with APOE-peptide do not show cytotoxicity and can be internalized inside brain tumor cells efficiently. Based on these studies and our current finding, it is reasonable to propose *in vivo* experiments to confirm that APOE peptide-VLP conjugates can facilitate the crossing of BBB. We also expect to knockdown bioluminescence reporter gene in the brain of a transgenic mice model to confirm the efficiency of BBB penetration and protein inhibition. The ultimate goal is to deliver multifunctional VLPs against brain tumor growth in mice. We believe this multifunctional VLPs platform has potential to overcome impediments mentioned earlier and is well suited for nucleic acid-based tools.

5.2 Conclusions

We have made significant progress in solving RNA packaging, protection, and delivering functional RNA using VLPs. We have discovered ways to optimize packaging efficiency of

target RNAs in VLPs. We found RNA structure and Qβ hairpin to be the prevailing factor affecting the efficiency of non-viral RNA packaging within VLPs. The presence of a ribosome binding site (RBS) or absence of the Qβ hairpin sequence in the RNA affects packaging efficiency. We have shown that VLPs stabilize RNA and attenuate RNA degradation from high concentrations of Mg^{2+} ions, hydroxyl radicals generated from Fe^{2+} ions mediated Fenton chemistry, and nucleases (Chapter 2).

We have also designed and constructed VLP-RNAs containing novel chimeric RNA cargo and demonstrated functional RNA interference with target gene expression in HeLa and U-87 cancer cells. Other results, including direct confocal visualization of fluorescently tagged VLPs, and activity assays with VLP-RNAis, show that VLPs are readily taken up by a variety of human cells and perform RNA interference (Chapter 3).

We have demonstrated that PEI conjugated VLP complexes can be loaded with DNA plasmid on the exterior surface. We have shown that DNA plasmids can be adsorbed on the surface of PEI conjugated VLP complexes. DNA plasmids are spontaneously dissociated from VLP complexes and can drive target gene expression in the intracellular environment (Chapter 4).

This dissertation developed a number of VLP applications for target gene regulation and expression. Gene regulation can be achieved by *in vivo* produced VLP-RNAi complexes. Gene expression can be accomplished through pVLP-DNA plasmid complexes. Regardless of the function, the packaging efficiency of *in vivo* non-viral RNA to Qβ VLP in the field of recombinant RNA production makes this Qβ VLP system worthwhile investigating.

Appendix A

SUPPLEMENTARY INFORMATION FOR CHAPTER 2

A.1 Sequences

Table 5.2-1 Qβ coat protein primers and oligos used for coat protein gene construction by recursive PCR. Restriction sites are underlined: 1) CP-Fwd is the forward primer, which contains an *Nco*I site; 2) CP-Rev is the reverse primer, which contains an *Avr*II site.

Primer or oligo name	DNA sequence
CP-Fwd	5'- GTG GCC ATG GCA AAT TAG AGA CTG TTA CTT -3'
CP-Rev	5'- CAC CCC TAG GTC AAT ACG CTG GGT TC -3'
QβCP-F1	5'- GTG GGC TCA GCT CAA TAC GCT GGG TTC AGC TGA TCA ATA GCA TCG ATC AGC AGA GGA CTA -3'
QβCP-R1	5'- GCT TTT GTT CGT ACA GAG CTT GCT GCT CTG CTC GCT AGT CCT CTG CTG ATC GAT GCT ATT -3'
QβCP-F2	5'- GCA AGC TCT GTA CGA ACA AAA GCT CGT TCC TCA TCG GTA CTA TAC TGC GTG AAC GAA AAG GTC -3'
QβCP-R2	5'- TTG TGA CCC ATC CGT TAC TCG CCA GGC ATA TGC TGA CGT GAC CTT TTC GTT CAC GCA GTA TAG TA -3'
QβCP-F3	5'- CGA GTA ACG GAT GGG TCA CAA GAA CCG TTT GCA GTG CAA GCG GTC GGG TTC TGG ATC TTA ACC TGG ACC -3'
QβCP-R3	5'- CCG TTT CGG TAT CTC AGC CTT CTC GCA ATC GTA AGA ACT ACA AGG TCC AGG TTA AGA TCC AGA ACC -3'
QβCP-F4	5'- AAG GCT GAG ATA CCG AAA CGG TAA CAC GCT TCT CCA GCG CAG GAA CTG CAC CCG CTT GTG AAA GCG-3'
QβCP-R4	5'- TCT GGT CCT CAA TCC GCG TGG GGT AAA TCC CAC TAA CGG CGT TGC CTC GCT TTC ACA AGC GGG TG -3'
QβCP-F5	5'- ACG CGG ATT GAG GAC CAG AGT TTG TTT TCC ATC TTT CCC GAT GTT ACC TAA AGT AAC AGT C -3'
QβCP-R5	5'- CAC CCC ATG GGC AAA ATT AGA GAC TGT TAC TTT AGG TAA CAT CGG GAA -3'

Table 5.2-2 The Primers and oligos used for corresponding non-viral RNA gene construction. a) The Qβ hp is highlighted in blue. b) The spacer region highlighted in pink italics. c) The ribosomal binding site (RBS), highlighted in red. d) Overlapping recombinant RNA fragments, including a-rRNA, 23S rRNA, and GFP mRNA are highlighted in yellow. e) XbaI/BlpI sites underlined.

a-rRNA-hp[a,b,c,d,e]	Primer or oligomer sequence
a-rRNA-hp FWD	5'- GTG GTC TAG A*GT CCG AGT AAT TTA CGT TTT GA* -3'
a-rRNA-hp REV	5'- GGT GGC TCA GCG CGA AGA TGC TGT -3'
a-rRNA-hp oligo F1	5'- TCT AGA *GTC CGA GTA ATT TAC GTT TTG ATA CGG TTG CGG AAC TTG C*GG GGT GCC TAT TGA AGC ATG -3'
a-rRNA-hp oligo F2	5'- TCT CTA TCC GCC ACG GGC TTC CTC GTG CTT AGT AAC TAA GGA TGA AAT GCA TGT C -3'
a-rRNA-hp oligo R2	5'- GCT CAG CGC GAA GAT GCT GTC TTA GAC ATG CAT TTC ATC CTT AGT TAC TAA GC -3'

23S rRNA-hp hp[a,b,c,d,e]	Primer or oligomer sequence
23S rRNA-hp FWD	5'- GTG GTC TAG A*GT CCG AGT AAT TTA CGT TTT GA* -3'
23S rRNA-hp REV	5'- GGT GGC TCA GCG CGA AGA TGC TGT -3'
23S rRNA-hp oligo F1	5'-TCT AGA *GTC CGA GTA ATT TAC GTT TTG ATA CGG TTG CGG AAC TTG C* -3'
23S rRNA-hp oligo R1	5'- GCA TCC ACC GTG GGC CCT TAC CAT CTT GAC *GCA AGT TCC GC AAC CGT AT C* -3'
23S rRNA-hp oligo F2	5'- CCG AGG TCT TGA CCC CTC CTT CCT CGT GCT TAG TAA CTA AGG ATG AAA TG -3'
23S rRNA-hp oligo R2	5'- GCT CAG CGC GAA GAT GCT GTC TTA GAC ATG CAT TTC ATC CTT AGT TAC TAA GCA CGA G -3'

mRNA(GFP)-hp [d,e]	Primer or oligomer sequence
mRNA(GFP)-hp FWD	5'- GTG GTC TAG AAT GGC TAG CAA AGG AGA AGA ACT CT -3'
mRNA(GFP)-hp REV	5'- GGT GGC TCA GCG CGA AGA TGC TGT -3'

88

Table 5.2-2 continued

RBS-mRNA_{GFP}- hp[a,b,c]	Primer or oligomer sequence
RBS-mRNA$_{GFP}$-hp FWD	5'- GTG GTC TAG A AT GGC TAG CAA AGG AGA AGA ACT CT -3'
RBS-mRNA$_{GFP}$-hp REV	5'- GGT GGC TCA GCG CGA AGA TGC TGT -3'
RBS-mRNA$_{GFP}$-hp oligo F1	5'- TCT AGA ATA ATT TTG TTT AAC TTT AAG AAG GAG ATA TAC CAT GGC TAG CAA AGG AGA AGA ACT CT -3'

a-rRNA[a,b,d]	Primer or oligomer sequence
a-rRNA FWD	5'- GTG GTC TAG AGT CCG AGT AAT TTA CGT TTT GA -3'
a-rRNA REV	5'- GGT GGC TCA GCG CCC GTG GCG GAT AGA GA -3'

Appendix B

SUPPLEMENTARY INFORMATION FOR CHAPTER 3

B.1 Sequences

Table 5.2-3 Qβ coat protein, GFP, and RNAi scaffold primers used for production of GFP-containing VLPs and functional VLP-RNAi particles. Restriction sites are underlined: 1) CP-Fwd: NcoI; 2) CP-Rev: AvrII; 3) GFP-Fwd: BglII; 4) GFP-Rev: BlpI; 5) RNAi-Fwd: BglII; 6) RNAi-Rev: XhoI.

Primer name	Primer sequence
CP-Fwd	5'-GTGG<u>CCATGG</u>CAAATTAGAGACTGTTACTT-3'
CP-Rev	5'-CACC<u>CCTAGG</u>TCAATACGCTGGGTTC-3'
GFP-Fwd	5'-GTGG<u>TCTAGA</u>AATAATTTTGTTTAACTTTAAGAAGGAG ATATACCATGGCTAGCAAAGGAGAAGAACTCT-3'
GFP-Rev	5'-CACC<u>GCTCAGC</u>TCAGTTGTACAGTTCATCCATGCC-3'
RNAi-Fwd	5'-GTGG<u>AGATCT</u>TAATACGACTCACTATAGGG-*3'*
RNAi-Rev	5'-CACC<u>CTCGAG</u>CAAAAAACCC-3'

Table 5.2-4 The RNAi scaffold sequences used for GFP and Pan-Ras protein inhibition. T7 promoter and T7 terminator are noted in italics; Qβ RNA hairpin is noted in blue; stem and stem-loop derived from miR-30b is noted in green; targeting sequence and its complement are noted in red. BglII/XhoI sites are underlined.

RNAi_{GFP} sequence
5'-GTGG<u>AGATCT</u>*TAATACGACTCACTATAGGG*AAATGCATGTCTAAGACAGCATCTTCGCGCAACATTCTGGGACACAAATTGCTGTGAAGCCACAGATGGGCAATTTGTGTCCCAGAATGTTGTGC*CTAGCATAACCCCTTGGGGCCTCTAAACGGGTCTTGAGGGGTTTTTTG*<u>CTCGAG</u>GGTG-3'

RNAi_{let-7} sequence
5'-GTGG<u>AGATCT</u>*TAATACGACTCACTATAGGG*AAATGCATGTCTAAGACAGCATCTTCGCGAACTGTACAAACTACTACCTCACTGTGAAGCCACAGATGGGTGAGGTAGTAGTTTGTACAGTTTGC*CTAGCATAACCCCTTGGGGCCTCTAAACGGGTCTTGAGGGGTTTTTTG*<u>CTCGAG</u>GGTG-3'

B.2 Supplemental Data

1. Characterization of VLP-GFP uptake by human cells (Figure 5.2-1) and *in vivo*

packaging of GFP in VLP (Figure 5.2-2 and 5.2-3)

Qβ VLP_{647} lacking internal GFP enters DU-145 cells (Figure 5.2-1). In addition, co-expression of Qβ CP and GFP in *E. coli* produces GFP-containing VLPs (Figure 5.2-2). GFP is spontaneously packaged within the VLPs to levels sufficient to confer observable fluorescence (Figure 5.2-3), eliminating the need for *in vitro* packaging. These VLP-GFPs are internalized by PC3, human prostate cancer cells (Figure 3.3-2e-f) to similar extents with or without attachment of fluorescent probes on the surface (Figure 3.3-2b-c). Previous studies showed that *in vivo* packaging of GFP in VLP is mediated by RNA aptamers.[215] Here we show GFP packaging in VLP simply by expressing GFP and CP in *E. coli*.
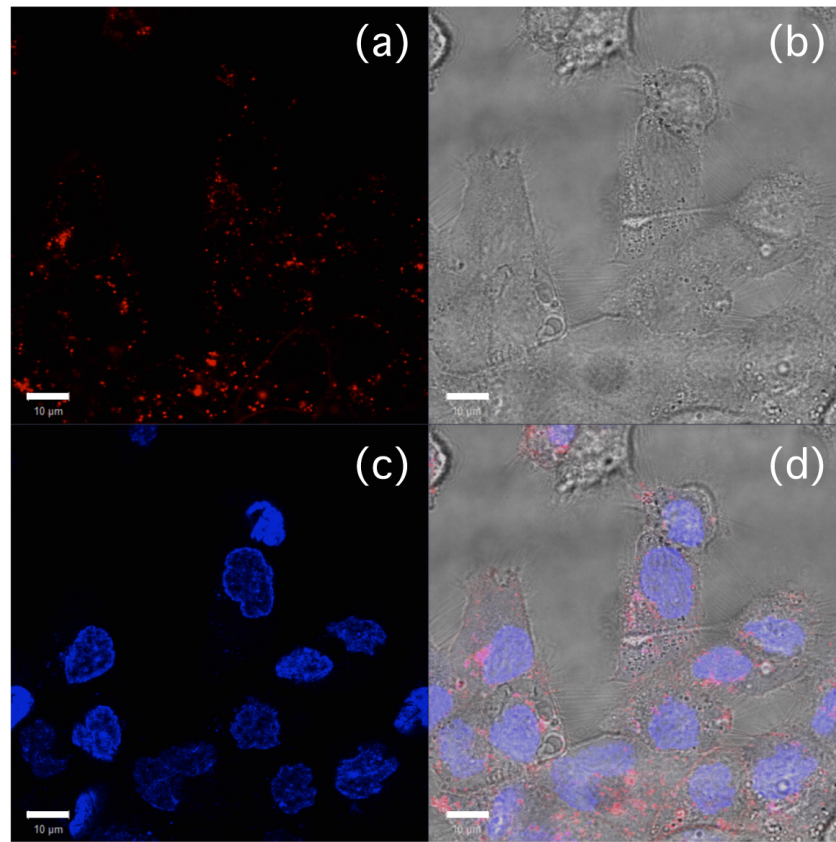
Figure 5.2-1 The internalization of VLP$_{647}$ by DU-145 cells: DU-145 cells were incubated with VLP$_{647}$ (100nM) for 24 h. Images were taken by confocal microscope. (a) DyLight-conjugated VLP, (b) bright field (c) nuclei, (d) merged confocal signals. The nuclei are stained blue with DAPI. VLP conjugated with Dylight 647 is magenta. Scale bar = 10 µm.
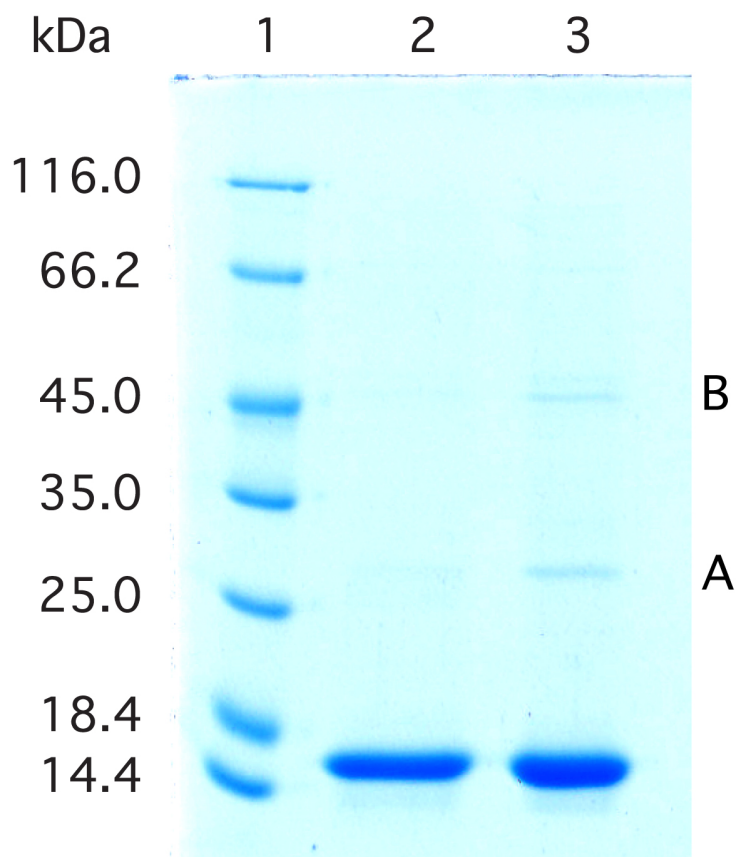
Figure 5.2-2 Characterization of *in vivo* prepared GFP-containing Qβ-VLPs with electrophoresis. The purified Qβ-VLP was analyzed by 10% SDS-PAGE. The molecular weight of Qβ CP monomer is 14.5 kDa. Lane 1: ladder, Lane 2: Qβ CP monomer from purified wild-type Qβ-VLP, Lane 3: *in vivo* –prepared, GFP-containing Qβ-VLPs. The molecular weight of GFP (A) is 28.3 kDa. Undefined *E. coli* protein (B) encapsidated simultaneously with GFP into VLPs.
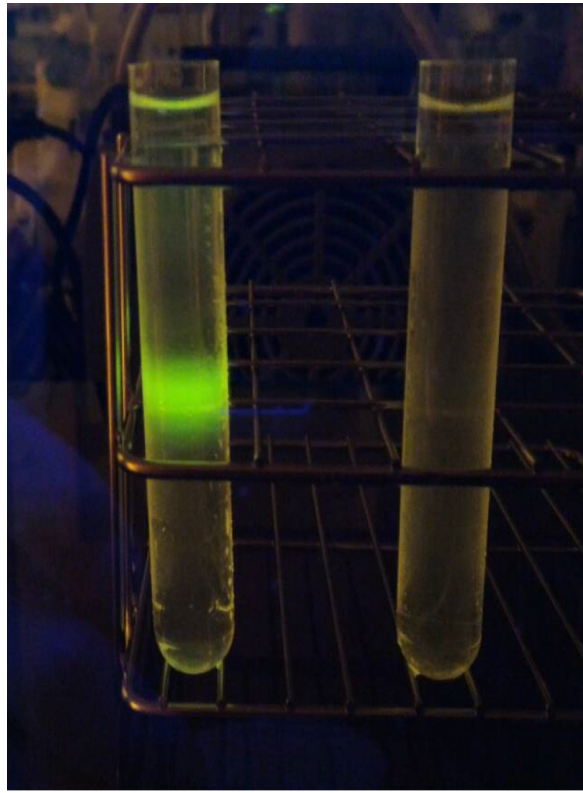
VLP-GFP   VLP

Figure 5.2-3 Characterization of *in vivo* prepared, GFP-containing Qβ VLPs by sucrose density gradient ultracentrifugation. *E. coli* produced GFP-containing VLPs form a discrete layer of green fluorescence signal after ultracentrifugation. The wild-type VLPs (control) do not have a fluorescent layer. Image was taken under blue LED transilluminator.

2. RNAi activity of *in vivo* VLP-RNAi$_{GFP}$ assembly (Figure 5.2-4 and 5.2-5)

Qβ-CP and RNAi$_{GFP}$ were co-expressed in *E. coli* to spontaneously assemble functional VLPs. The undecorated VLPs show RNAi activity to inhibit GFP expression in HeLa cells.
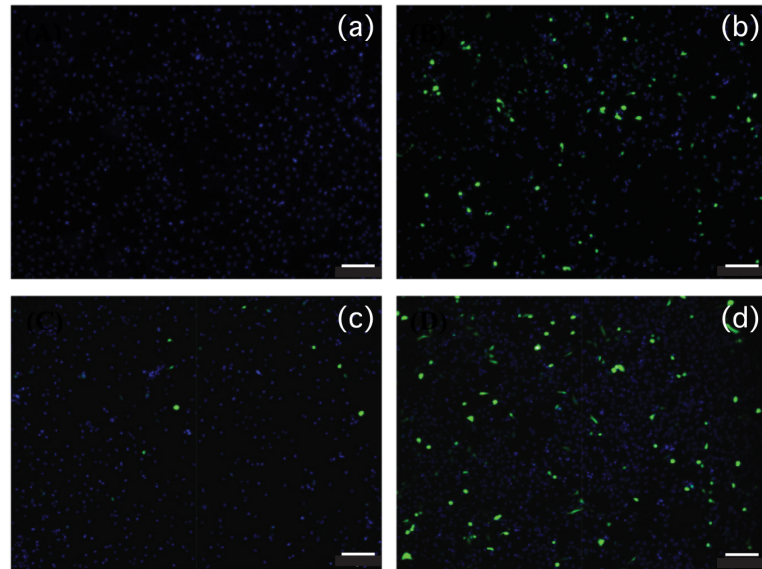
Figure 5.2-4 Suppression of gene expression by VLP-RNAi$_{GFP}$ in HeLa. HeLa cells were treated with (a) PBS, (b) GFP-expressing plasmid, (c) VLP-RNAi$_{GFP}$ after GFP -expressing plasmid transfection, or (d) VLP after GFP-expressing plasmid transfection. Cells were incubated with 360 nM VLP-RNAi$_{GFP}$ or VLP in the absence of transfection reagent for 24 h. The images were taken 24 h after addition of VLP-RNAi$_{GFP}$. In the images, green spots indicate cell with GFP expression; blue spots show the nuclei, stained by DAPI. The scale bar = 200 μm.
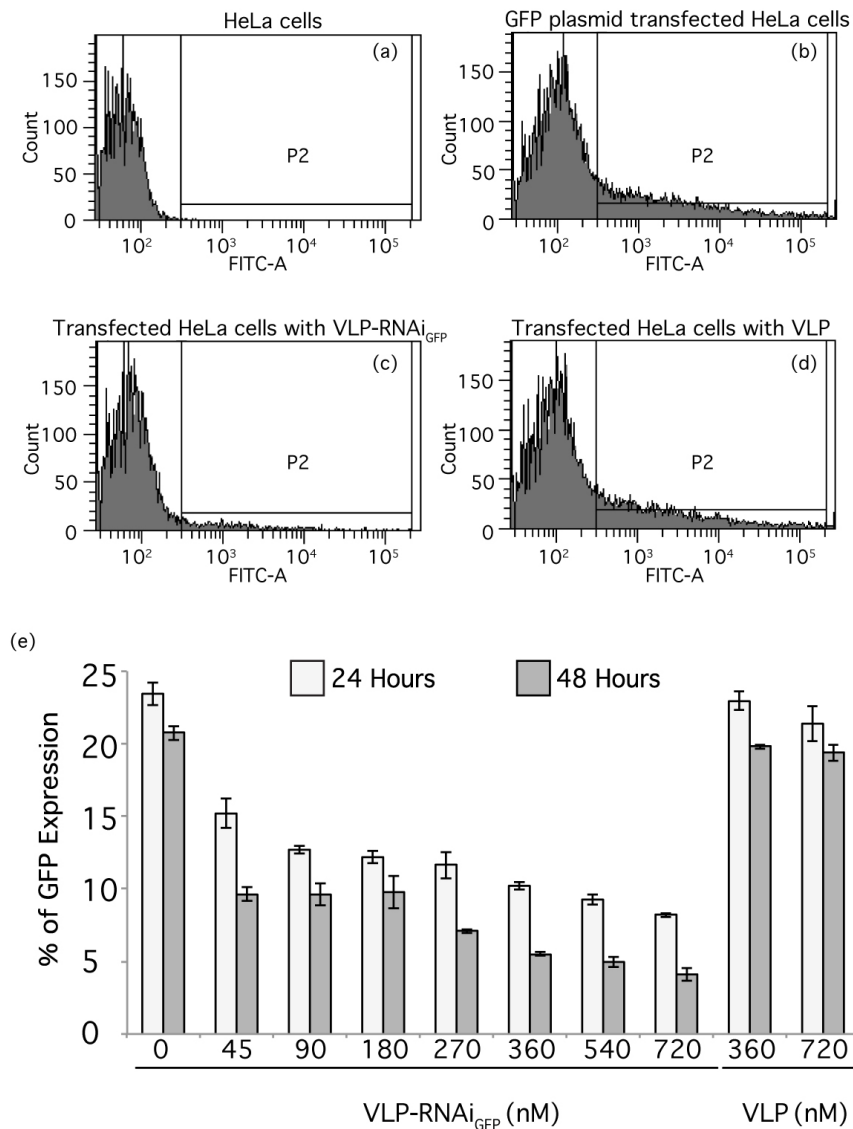
Figure 5.2-5 Inhibition of GFP expression in HeLa cells quantified by flow cytometry. (a) HeLa cells; (b) HeLa cells transfected with GFP expressing plasmid alone; (c) HeLa cells transfected with GFP expressing plasmid co-cultured with VLP-RNAiGFP; (d) HeLa cells transfected with GFP expressing plasmid co-cultured with VLP. P2 represents the fluorescent signal of GFP. The negative control is VLP that does not contain RNAiGFP. (e) Gene expression levels of GFP in HeLa cells were determined after treatment with various concentrations of VLP-RNAiGFP for 24 h (white) and 48 h (grey). The GFP gene expression levels are reported here as percentage of fluorescence positive cells. The negative control is VLP that does not contain RNAiGFP. Values are expressed as means ±SD (n = 3).

The *in vivo* transcribed RNA scaffold content of each VLP could not be quantified by analytical ultracentrifugation (AUC), since *E. coli* tRNAs, mRNAs, and rRNAs were encapsided in VLPs as well. Stockley has shown that MS2 VLPs reassemble *in vitro* with MS2 coat protein and an RNA conjugate (TR-siRNA) by AUC. The TR-siRNA conjugate content of each MS2 VLPs was 7.5 RNA molecules [189].

REFERENCES

1   Golmohammadi, R., Fridborg, K., Bundule, M., Valegard, K. & Liljas, L. The crystal structure of bacteriophage Q beta at 3.5 A resolution. *Structure* **4**, 543-554 (1996).

2   Fiedler, J. D. *et al.* Engineered mutations change the structure and stability of a virus-like particle. *Biomacromolecules* **13**, 2339-2348, doi:10.1021/bm300590x (2012).

3   Johnson, H. R., Hooker, J. M., Francis, M. B. & Clark, D. S. Solubilization and stabilization of bacteriophage MS2 in organic solvents. *Biotechnol Bioeng* **97**, 224-234, doi:10.1002/bit.21245 (2007).

4   Bundy, B. C., Franciszkowicz, M. J. & Swartz, J. R. Escherichia coli-based cell-free synthesis of virus-like particles. *Biotechnol Bioeng* **100**, 28-37, doi:10.1002/bit.21716 (2008).

5   Ashcroft, A. E. *et al.* Engineering Thermal Stability in RNA Phage Capsids via Disulphide Bonds. *Journal of Nanoscience and Nanotechnology* **5**, 2034-2041, doi:10.1166/jnn.2005.507 (2005).

6   Caldeira, J. C. & Peabody, D. S. Thermal Stability of RNA Phage Virus-Like Particles Displaying Foreign Peptides. *Journal of nanobiotechnology* **9**, 22-22, doi:10.1186/1477-3155-9-22 (2011).

7   Prasuhn, D. E. *et al.* Plasma Clearance of Bacteriophage Qβ Particles as a Function of Surface Charge. *J. Am. Chem. Soc.* **130**, 1328-1334, doi:10.1021/ja075937f (2008).

8   Steinmetz, N. F. *et al.* Buckyballs Meet Viral Nanoparticles: Candidates for Biomedicine. *J. Am. Chem. Soc.* **131**, 17093-17095, doi:10.1021/ja902293w (2009).

9   Kozlovska, T. M. *et al.* Recombinant RNA phage Q beta capsid particles synthesized and self-assembled in Escherichia coli. *Gene* **137**, 133-137 (1993).

10   Freivalds, J. *et al.* Assembly of bacteriophage Qbeta virus-like particles in yeast Saccharomyces cerevisiae and Pichia pastoris. *J. Biotechnol.* **123**, 297-303, doi:10.1016/j.jbiotec.2005.11.013 (2006).

11   Gillitzer, E., Willits, D., Young, M. & Douglas, T. Chemical modification of a viral cage for multivalent presentation. *Chem. Commun.*, 2390-2391, doi:10.1039/B207853H (2002).

12   Hooker, J. M., Kovacs, E. W. & Francis, M. B. Interior Surface Modification of Bacteriophage MS2. *J. Am. Chem. Soc.* **126**, 3718-3719, doi:10.1021/ja031790q (2004).

13   Garcea, R. L. & Gissmann, L. Virus-like particles as vaccines and vessels for the delivery of small molecules. *Curr. Opin. Biotechnol.* **15**, 513-517, doi:http://dx.doi.org/10.1016/j.copbio.2004.10.002 (2004).

14   Lee, L. A., Niu, Z. & Wang, Q. Viruses and virus-like protein assemblies—Chemically programmable nanoscale building blocks. *Nano Research* **2**, 349-364, doi:10.1007/s12274-009-9033-8 (2009).

15   Ashley, C. E. *et al.* Cell-specific delivery of diverse cargos by bacteriophage MS2 virus-like particles. *ACS nano* **5**, 5729-5745, doi:10.1021/nn201397z (2011).

16   Lee, L. A. & Wang, Q. Adaptations of nanoscale viruses and other protein cages for medical applications. *Nanomed. Nanotechnol. Biol. Med.* **2**, 137-149, doi:http://dx.doi.org/10.1016/j.nano.2006.07.009 (2006).

17   Canizares, M. C., Nicholson, L. & Lomonossoff, G. P. Use of viral vectors for vaccine production in plants. *Immunol Cell Biol* **83**, 263-270 (2005).

18   Pokorski, J. K., Hovlid, M. L. & Finn, M. G. Cell targeting with hybrid Qbeta virus-like particles displaying epidermal growth factor. *ChemBioChem* **12**, 2441-2447, doi:10.1002/cbic.201100469 (2011).

19   Brown, S. D., Fiedler, J. D. & Finn, M. G. Assembly of hybrid bacteriophage Qbeta virus-like particles. *Biochemistry* **48**, 11155-11157, doi:10.1021/bi901306p (2009).

20   Wei, B. *et al.* Development of an antisense RNA delivery system using conjugates of the MS2 bacteriophage capsids and HIV-1 TAT cell-penetrating peptide. *Biomedicine & pharmacotherapy = Biomedecine & pharmacotherapie* **63**, 313-318, doi:10.1016/j.biopha.2008.07.086 (2009).

21   Ponchon, L. *et al.* Co-expression of RNA-protein complexes in Escherichia coli and applications to RNA biology. *Nucleic Acids Res.* **41**, e150, doi:10.1093/nar/gkt576 (2013).

22   Lau, J. L. *et al.* Evolution and protein packaging of small-molecule RNA aptamers. *ACS nano* **5**, 7722-7729, doi:10.1021/nn2006927 (2011).

23   Rhee, J. K. *et al.* Colorful Virus-like Particles: Fluorescent Protein Packaging by the Q beta Capsid. *Biomacromolecules* **12**, 3977-3981, doi:Doi 10.1021/Bm200983k (2011).

24   Fiedler, J. D., Brown, S. D., Lau, J. L. & Finn, M. G. RNA-directed packaging of enzymes within virus-like particles. *Angew Chem Int Ed Engl* **49**, 9648-9651, doi:10.1002/anie.201005243 (2010).

25   Ren, Y., Wong, S. M. & Lim, L.-Y. Folic Acid-Conjugated Protein Cages of a Plant Virus: A Novel Delivery Platform for Doxorubicin. *Bioconj. Chem.* **18**, 836-843, doi:10.1021/bc060361p (2007).

26   Loo, L., Guenther, R. H., Lommel, S. A. & Franzen, S. Encapsidation of Nanoparticles by Red Clover Necrotic Mosaic Virus. *J. Am. Chem. Soc.* **129**, 11111-11117, doi:10.1021/ja071896b (2007).

27   Ross, J. mRNA stability in mammalian cells. *Microbiological reviews* **59**, 423-450 (1995).

28   Dam Mikkelsen, N. & Gerdes, K. Sok antisense RNA from plasmid R1 is functionally inactivated by RNase E and polyadenylated by poly (A) polymerase I. *Mol. Microbiol.* **26**, 311-320 (1997).

29   Milligan, J. F., Groebe, D. R., Witherell, G. W. & Uhlenbeck, O. C. Oligoribonucleotide synthesis using T7 RNA polymerase and synthetic DNA templates. *Nucleic Acids Res.* **15**, 8783-8798 (1987).

30   Marshall, W. S. & Kaiser, R. J. Recent advances in the high-speed solid phase synthesis of RNA. *Curr. Opin. Chem. Biol.* **8**, 222-229 (2004).

31   Nelissen, F. H. *et al.* Fast production of homogeneous recombinant RNA—towards large-scale production of RNA. *Nucleic Acids Res.* **40**, e102-e102 (2012).

32   Ponchon, L. *et al.* Co-expression of RNA–protein complexes in Escherichia coli and applications to RNA biology. *Nucleic Acids Res.*, gkt576 (2013).

33   Lago, B., Birnbaum, J. & Demain, A. Fermentation process for double stranded RNA an interferon inducer. *Appl. Microbiol* **18**, 430-436 (1972).

34   Studier, F. W. & Moffatt, B. A. Use of bacteriophage T7 RNA polymerase to direct selective high-level expression of cloned genes. *J. Mol. Biol.* **189**, 113-130 (1986).

35   Lopez, P. & Dreyfus, M. The lacZ mRNA can be stabilised by the T7 late mRNA leader in E coli. *Biochimie* **78**, 408-415 (1996).

36   Lau, J. L. *et al.* Evolution and Protein Packaging of Small-Molecule RNA Aptamers. *ACS Nano* **5**, 7722-7729, doi:10.1021/nn2006927 (2011).

37   Ashcroft, A. E. *et al.* Engineering thermal stability in RNA phage capsids via disulphide bonds. *J. Nanosci. Nanotechnol.* **5**, 2034-2041 (2005).

38   Witherell, G. W. & Uhlenbeck, O. C. Specific RNA binding by Q beta coat protein. *Biochemistry* **28**, 71-76 (1989).

39   Borodavka, A., Tuma, R. & Stockley, P. G. A two-stage mechanism of viral RNA compaction revealed by single molecule fluorescence. *RNA Biol.* **10**, 481-489, doi:10.4161/rna.23838 (2013).

40   Dykeman, E. C., Stockley, P. G. & Twarock, R. Packaging signals in two single-stranded RNA viruses imply a conserved assembly mechanism and geometry of the packaged genome. *J. Mol. Biol.* **425**, 3235-3249 (2013).

41   Hedenstierna, K. O., Lee, Y.-H., Yang, Y. & Fox, G. E. A prototype stable RNA identification cassette for monitoring plasmids of genetically engineered microorganisms. *Syst. Appl. Microbiol.* **16**, 280-286 (1993).

42   Umekage, S. & Kikuchi, Y. In vitro and in vivo production and purification of circular RNA aptamer. *J. Biotechnol.* **139**, 265-272 (2009).

43   Masson, J.-M. & Miller, J. H. Expression of synthetic suppressor tRNA genes under the control of a synthetic promoter. *Gene* **47**, 179-183, doi:http://dx.doi.org/10.1016/0378-1119(86)90061-2 (1986).

44   Meinnel, T., Mechulam, Y. & Fayat, G. Fast purification of a functional elongator tRNAmet expressed from a synthetic gene in vivo. *Nucleic Acids Res.* **16**, 8095 (1988).

45   Tisné, C., Rigourd, M., Marquet, R., Ehresmann, C. & Dardel, F. NMR and biochemical characterization of recombinant human tRNA (Lys) 3 expressed in Escherichia coli: identification of posttranscriptional nucleotide modifications required for efficient initiation of HIV-1 reverse transcription. *RNA* **6**, 1403-1412 (2000).

46   Ponchon, L. & Dardel, F. Recombinant RNA technology: the tRNA scaffold. *Nat. Methods* **4**, 571-576 (2007).

47   Fire, A. *et al.* Potent and specific genetic interference by double-stranded RNA in Caenorhabditis elegans. *Nature* **391**, 806-811, doi:10.1038/35888 (1998).

48   Elbashir, S. M. *et al.* Duplexes of 21-nucleotide RNAs mediate RNA interference in cultured mammalian cells. *Nature* **411**, 494-498, doi:10.1038/35078107 [doi] 35078107 [pii] (2001).

49   Pillai, R. S., Bhattacharyya, S. N. & Filipowicz, W. Repression of protein synthesis by miRNAs: how many mechanisms? *Trends Cell Biol.* **17**, 118-126, doi:http://dx.doi.org/10.1016/j.tcb.2006.12.007 (2007).

50   Jacque, J.-M., Triques, K. & Stevenson, M. Modulation of HIV-1 replication by RNA interference. *Nature* **418**, 435-438 (2002).

51   Lagos-Quintana, M., Rauhut, R., Lendeckel, W. & Tuschl, T. Identification of Novel Genes Coding for Small Expressed RNAs. *Science* **294**, 853-858, doi:10.1126/science.1064921 (2001).

52   Tang, G., Reinhart, B. J., Bartel, D. P. & Zamore, P. D. A biochemical framework for RNA silencing in plants. *Genes Dev.* **17**, 49-63, doi:10.1101/gad.1048103 (2003).

53   Mourelatos, Z. *et al.* miRNPs: a novel class of ribonucleoproteins containing numerous microRNAs. *Genes Dev.* **16**, 720-728, doi:10.1101/gad.974702 (2002).

54   Thermann, R. & Hentze, M. W. Drosophila miR2 induces pseudo-polysomes and inhibits translation initiation. *Nature* **447**, 875-878, doi:http://www.nature.com/nature/journal/v447/n7146/suppinfo/nature05878_S1.html (2007).

55   Kim, D. H. & Rossi, J. J. Strategies for silencing human disease using RNA interference. *Nature Reviews Genetics* **8**, 173-184 (2007).

56   Ozsolak, F. *et al.* Chromatin structure analyses identify miRNA promoters. *Genes Dev.* **22**, 3172-3183, doi:10.1101/gad.1706508 (2008).

57   Borchert, G. M., Lanier, W. & Davidson, B. L. RNA polymerase III transcribes human microRNAs. *Nat Struct Mol Biol* **13**, 1097-1101, doi:http://www.nature.com/nsmb/journal/v13/n12/suppinfo/nsmb1167_S1.html (2006).

58   Lee, Y. *et al.* The nuclear RNase III Drosha initiates microRNA processing. *Nature* **425**, 415-419, doi:http://www.nature.com/nature/journal/v425/n6956/suppinfo/nature01957_S1.html (2003).

59   Gregory, R. I. *et al.* The Microprocessor complex mediates the genesis of microRNAs. *Nature* **432**, 235-240, doi:http://www.nature.com/nature/journal/v432/n7014/suppinfo/nature03120_S1.html (2004).

60   Kim, D.-H. *et al.* Synthetic dsRNA Dicer substrates enhance RNAi potency and efficacy. *Nat Biotech* **23**, 222-226, doi:http://www.nature.com/nbt/journal/v23/n2/suppinfo/nbt1051_S1.html (2005).

61   Siolas, D. *et al.* Synthetic shRNAs as potent RNAi triggers. *Nat Biotech* **23**, 227-231, doi:http://www.nature.com/nbt/journal/v23/n2/suppinfo/nbt1052_S1.html (2005).

62   Elbashir, S. M., Lendeckel, W. & Tuschl, T. RNA interference is mediated by 21- and 22-nucleotide RNAs. *Genes Dev* **15**, 188-200 (2001).

63   Akao, Y., Nakagawa, Y. & Naoe, T. let-7 microRNA functions as a potential growth suppressor in human colon cancer cells. *Biol. Pharm. Bull.* **29**, 903-906, doi:Doi 10.1248/Bpb.29.903 (2006).

64   Yu, F. *et al.* let-7 regulates self renewal and tumorigenicity of breast cancer cells. *Cell* **131**, 1109-1123, doi:10.1016/j.cell.2007.10.054 (2007).

65   Trang, P. *et al.* Regression of murine lung tumors by the let-7 microRNA. *Oncogene* **29**, 1580-1587, doi:10.1038/onc.2009.445 (2010).

66   Brummelkamp, T. R., Bernards, R. & Agami, R. Stable suppression of tumorigenicity by virus-mediated RNA interference. *Cancer Cell* **2**, 243-247, doi:http://dx.doi.org/10.1016/S1535-6108(02)00122-8 (2002).

67   Li, Y., Lu, J., Han, Y., Fan, X. & Ding, S.-W. RNA Interference Functions as an Antiviral Immunity Mechanism in Mammals. *Science* **342**, 231-234, doi:10.1126/science.1241911 (2013).

68   Alvarez, R. *et al.* RNA Interference-Mediated Silencing of the Respiratory Syncytial Virus Nucleocapsid Defines a Potent Antiviral Strategy. *Antimicrob. Agents Chemother.* **53**, 3952-3962, doi:10.1128/aac.00014-09 (2009).

69   Neff, C. P. *et al.* An Aptamer-siRNA Chimera Suppresses HIV-1 Viral Loads and Protects from Helper CD4+ T Cell Decline in Humanized Mice. *Science Translational Medicine* **3**, 66ra66-66ra66, doi:10.1126/scitranslmed.3001581 (2011).

70   Stein, E. A. *et al.* Combination of RNA Interference and Virus Receptor Trap Exerts Additive Antiviral Activity in Coxsackievirus B3-induced Myocarditis in Mice. *J. Infect. Dis.* **211**, 613-622, doi:10.1093/infdis/jiu504 (2015).

71   Flenniken, M. L. & Andino, R. Non-Specific dsRNA-Mediated Antiviral Response in the Honey Bee. *PLoS ONE* **8**, e77263, doi:10.1371/journal.pone.0077263 (2013).

72   Brutscher, L. M., Daughenbaugh, K. F. & Flenniken, M. L. Antiviral defense mechanisms in honey bees. *Current Opinion in Insect Science* **10**, 71-82, doi:http://dx.doi.org/10.1016/j.cois.2015.04.016 (2015).

73   Davidson, B. L. & McCray, P. B. Current prospects for RNA interference-based therapies. *Nat Rev Genet* **12**, 329-340 (2011).

74   Kanasty, R., Dorkin, J. R., Vegas, A. & Anderson, D. Delivery materials for siRNA therapeutics. *Nat Mater* **12**, 967-977, doi:10.1038/nmat3765 (2013).

75   Kanasty, R., Dorkin, J. R., Vegas, A. & Anderson, D. Delivery materials for siRNA therapeutics. *Nature materials* **12**, 967-977 (2013).

76   Alabi, C., Vegas, A. & Anderson, D. Attacking the genome: emerging siRNA nanocarriers from concept to clinic. *Curr. Opin. Pharm.* **12**, 427-433, doi:http://dx.doi.org/10.1016/j.coph.2012.05.004 (2012).

77   Burnett, J. C., Rossi, J. J. & Tiemann, K. Current Progress of siRNA/shRNA Therapeutics in Clinical Trials. *Biotechnology Journal* **6**, 1130-1146, doi:10.1002/biot.201100054 (2011).

78   Geisbert, T. W. *et al.* Postexposure protection of non-human primates against a lethal Ebola virus challenge with RNA interference: a proof-of-concept study. *The Lancet* **375**, 1896-1905, doi:http://dx.doi.org/10.1016/S0140-6736(10)60357-1.

79   McNamara, J. O. *et al.* Cell type-specific delivery of siRNAs with aptamer-siRNA chimeras. *Nat Biotech* **24**, 1005-1015, doi:http://www.nature.com/nbt/journal/v24/n8/suppinfo/nbt1223_S1.html (2006).

80   Zhou, J. *et al.* Selection, characterization and application of new RNA HIV gp 120 aptamers for facile delivery of Dicer substrate siRNAs into HIV infected cells. *Nucleic Acids Res.* **37**, 3094-3109, doi:10.1093/nar/gkp185 (2009).

81   Luo, D. & Saltzman, W. M. Synthetic DNA delivery systems. *Nat Biotech* **18**, 33-37 (2000).

82   Lemkine, G. & Demeneix, B. Polyethylenimines for in vivo gene delivery. *Current opinion in molecular therapeutics* **3**, 178-182 (2001).

83   Wu, Y. *et al.* The investigation of polymer-siRNA nanoparticle for gene therapy of gastric cancer in vitro. *International Journal of Nanomedicine* **5**, 129-136 (2010).

84   Yang, H. W. *et al.* Gadolinium-functionalized nanographene oxide for combined drug and microRNA delivery and magnetic resonance imaging. *Biomaterials* **35**, 6534-6542, doi:10.1016/j.biomaterials.2014.04.057 (2014).

85   Järver, P. *et al.* Peptide-mediated cell and in vivo delivery of antisense oligonucleotides and siRNA. *Molecular therapy. Nucleic acids* **1**, e27 (2012).

86   Thomas, C. E., Ehrhardt, A. & Kay, M. A. Progress and problems with the use of viral vectors for gene therapy. *Nat Rev Genet* **4**, 346-358 (2003).

87   Heilbronn, R. & Weger, S. in *Drug Delivery* Vol. 197 *Handbook of Experimental Pharmacology* (ed Monika Schäfer-Korting) Ch. 5, 143-170 (Springer Berlin Heidelberg, 2010).

88   Matrai, J., Chuah, M. K. L. & VandenDriessche, T. Recent Advances in Lentiviral Vector Development and Applications. *Mol Ther* **18**, 477-490 (2010).

89   Morenweiser, R. Downstream processing of viral vectors and vaccines. *Gene Ther.* **12**, S103-S110 (2005).

90   Crystal, R. G. Transfer of genes to humans: early lessons and obstacles to success. *Science* **270**, 404-410 (1995).

91   Tripathy, S. K., Black, H. B., Goldwasser, E. & Leiden, J. M. Immune responses to transgene–encoded proteins limit the stability of gene expression after injection of replication–defective adenovirus vectors. *Nat. Med.* **2**, 545-550 (1996).

92   Kay, M. A., Glorioso, J. C. & Naldini, L. Viral vectors for gene therapy: the art of turning infectious agents into vehicles of therapeutics. *Nat. Med.* **7**, 33-40 (2001).

93   Milligan, J. F., Groebe, D. R., Witherell, G. W. & Uhlenbeck, O. C. Oligoribonucleotide Synthesis Using T7 Rna-Polymerase and Synthetic DNA Templates. *Nucleic Acids Res.* **15**, 8783-8798, doi:Doi 10.1093/Nar/15.21.8783 (1987).

94   Marshall, W. S. & Kaiser, R. J. Recent advances in the high-speed solid phase synthesis of RNA. *Curr. Opin. Chem. Biol.* **8**, 222-229, doi:10.1016/j.cbpa.2004.04.012 (2004).

95   Nelissen, F. H. T. *et al.* Fast production of homogeneous recombinant RNA—towards large-scale production of RNA. *Nucleic Acids Res.*, doi:10.1093/nar/gks292 (2012).

96   Lopez, P. J. & Dreyfus, M. The lacZ mRNA can be stabilised by the T7 late mRNA leader in E coli. *Biochimie* **78**, 408-415, doi:Doi 10.1016/0300-9084(96)84747-X (1996).

97   Lago, B. D., Birnbaum, J. & Demain, A. L. Fermentation Process for Double-Stranded Ribonucleic Acid, an Interferon Inducer. *Applied Microbiology* **24**, 430-436 (1972).

98   Li, Z. & Deutscher, M. P. Analyzing the Decay of Stable RNAs in E. coli. *Methods Enzymol.* **447**, 31-45, doi:10.1016/S0076-6879(08)02202-7 (2008).

99   Hedenstierna, K. O., Lee, Y. H., Yang, Y. & Fox, G. E. A prototype stable RNA identification cassette for monitoring plasmids of genetically engineered microorganisms. *Syst Appl Microbiol* **16**, 280-286, doi:D - NASA: 00020724 OTO - NASA (1993).

100   Umekage, S. & Kikuchi, Y. In vitro and in vivo production and purification of circular RNA aptamer. *J. Biotechnol.* **139**, 265-272, doi:10.1016/j.jbiotec.2008.12.012 (2009).

101   Meinnel, T., Mechulam, Y. & Fayat, G. Fast purification of a functional elongator tRNAmet expressed from a synthetic gene in vivo. *Nucleic Acids Res.* **16**, 8095-8096 (1988).

102   Tisné, C., Rigourd, M., Marquet, R., Ehresmann, C. & Dardel, F. NMR and biochemical characterization of recombinant human tRNA(Lys)3 expressed in Escherichia coli: identification of posttranscriptional nucleotide modifications required for efficient initiation of HIV-1 reverse transcription. *RNA* **6**, 1403-1412 (2000).

103   Ponchon, L. & Dardel, F. Recombinant RNA technology: the tRNA scaffold. *Nat Methods* **4**, 571-576, doi:10.1038/nmeth1058 (2007).

104   Lee, Y. H., Dsouza, L. & Fox, G. E. Experimental investigation of an RNA sequence space. *Orig Life Evol Biosph* **23**, 365-372 (1993).

105   Zhang, Z., D'Souza Lm Fau - Lee, Y.-H., Lee Yh Fau - Fox, G. E. & Fox, G. E. Common 5S rRNA variants are likely to be accepted in many sequence contexts. *J. Mol. Evol.* **56**, 69-76, doi:10.1007/s00239-002-2381-6 (2003).

106   Pitulle, C., Hedenstierna Ko Fau - Fox, G. E. & Fox, G. E. A novel approach for monitoring genetically engineered microorganisms by using artifical, stbale RNAs. *Appl Environ Microbiol.* **61**, 3661-3666 (1995).

107   D'Souza, L. M., Larios-Sanz, M., Setterquist, R. A., Willson, R. C. & Fox, G. E. Small RNA sequences are readily stabilized by inclusion in a carrier rRNA. *Biotechnol Prog* **19**, 734-738, doi:10.1021/bp025755j (2003).

108   Pitulle, C., Dsouza, L. & Fox, G. E. A Low Molecular Weight Artificial RNA of Unique Size with Multiple Probe Target Regions. *Syst. Appl. Microbiol.* **20**, 133-136, doi:http://dx.doi.org/10.1016/S0723-2020(97)80057-4 (1997).

109   Liu, Y. *et al.* DNAzyme-mediated recovery of small recombinant RNAs from a 5S rRNA-derived chimera expressed in Escherichia coli. *BMC Biotechnol* **10**, 85, doi:10.1186/1472-6750-10-85 (2010).

110   Zhang, X. *et al.* Engineered 5S ribosomal RNAs displaying aptamers recognizing vascular endothelial growth factor and malachite green. *J Mol Recognit* **22**, 154-161, doi:10.1002/jmr.917 (2009).

111   Deutscher, M. P. Degradation of RNA in bacteria: comparison of mRNA and stable RNA. *Nucleic Acids Res.* **34**, 659-666, doi:10.1093/nar/gkj472 (2006).

112   Puerta-Fernández, E., Romero-López, C., Barroso-delJesus, A. & Berzal-Herranz, A. Ribozymes: recent advances in the development of RNA tools. *FEMS Microbiol. Rev.* **27**, 75-97 (2003).

113   Pelechano, V. & Steinmetz, L. M. Gene regulation by antisense transcription. *Nature Reviews Genetics* **14**, 880-893 (2013).

114   Davidson, B. L. & McCray, P. B. Current prospects for RNA interference-based therapies. *Nature Reviews Genetics* **12**, 329-340 (2011).

115   Goodchild, J. in *Therapeutic Oligonucleotides*   1-15 (Springer, 2011).

116   Geller, B. L., Deere, J., Tilley, L. & Iversen, P. L. Antisense phosphorodiamidate morpholino oligomer inhibits viability of Escherichia coli in pure culture and in mouse peritonitis. *J. Antimicrob. Chemother.* **55**, 983-988 (2005).

117   Warren, T. K. *et al.* Advanced antisense therapies for postexposure protection against lethal filovirus infections. *Nat. Med.* **16**, 991-994 (2010).

118   Machida, K. & Imataka, H. Production methods for viral particles. *Biotechnol. Lett.* **37**, 753-760 (2015).

119   Golmohammadi, R., Fridborg, K., Bundule, M., Valegård, K. & Liljas, L. The crystal structure of bacteriophage Qβ at 3.5 å resolution. *Structure* **4**, 543-554, doi:http://dx.doi.org/10.1016/S0969-2126(96)00060-3 (1996).

120   Fiers, W. *et al.* Complete nucleotide sequence of bacteriophage MS2 RNA: primary and secondary structure of the replicase gene. *Nature* **260**, 500-507 (1976).

121   Bowman, J. C., Azizi, B., Lenz, T. K., Roy, P. & Williams, L. D. in *Recombinant and In Vitro RNA Synthesis: Methods and Protocols, Methods in Molecular Biology* Vol. 941 *Methods in Molecular Biology* (ed G. L. Conn) 19-41 (Springer Science, LLC, 2012).

122   Hsiao, C. *et al.* Molecular paleontology: a biochemical model of the ancestral ribosome. *Nucleic Acids Res.* **41**, 3373-3385, doi:10.1093/nar/gkt023 (2013).

123   Studier, F. W. Protein production by auto-induction in high density shaking cultures. *Protein Expr Purif* **41**, 207-234 (2005).

124   Tullius, T. D. & Dombroski, B. A. Hydroxyl radical" footprinting": high-resolution information about DNA-protein contacts and application to lambda repressor and Cro protein. *Proc. Natl. Acad. Sci. U. S. A.* **83**, 5469-5473 (1986).

125   Regulski, E. & Breaker, R. in *Post-Transcriptional Gene Regulation* Vol. 419 *Methods In Molecular Biology™* (ed Jeffrey Wilusz) Ch. 4, 53-67 (Humana Press, 2008).

126   Hsiao, C. *et al.* Molecular paleontology: a biochemical model of the ancestral ribosome. *Nucleic Acids Res.* **41**, 3373-3385, doi:10.1093/nar/gkt023 (2013).

127   Calogero, R. A., Pon, C. L., Canonaco, M. A. & Gualerzi, C. O. Selection of the mRNA translation initiation region by Escherichia coli ribosomes. *Proc. Natl. Acad. Sci. U.S.A.* **85**, 6427-6431 (1988).

128   Yi, Q.-M. & Wong, K.-P. The effects of magnesium ions on the hydrodynamic shape, conformation, and stability of the ribosomal 23S RNA from E. coli. *Biochem. Biophys. Res. Commun.* **104**, 733-739 (1982).

129   Pasloske, B. L., Walkerpeach, C. R., Obermoeller, R. D., Winkler, M. & DuBois, D. B. Armored RNA technology for production of ribonuclease-resistant viral RNA controls and standards. *J. Clin. Microbiol.* **36**, 3590-3594 (1998).

130   Prousek, J. Fenton chemistry in biology and medicine. *Pure Appl. Chem.* **79**, 2325-2338 (2007).

131   Forconi, M. & Herschlag, D. Metal ion-based RNA cleavage as a structural probe. *Methods Enzymol.* **468**, 91-106, doi:10.1016/s0076-6879(09)68005-8 (2009).

132   Regulski, E. E. & Breaker, R. R. In-line probing analysis of riboswitches. *post-transcriptional gene regulation*, 53-67 (2008).

133   WalkerPeach, C. R., Winkler, M., DuBois, D. B. & Pasloske, B. L. Ribonuclease-resistant RNA controls (Armored RNA) for reverse transcription-PCR, branched DNA, and genotyping assays for hepatitis C virus. *Clin. Chem.* **45**, 2079-2085 (1999).

134   Peabody, D. Role of the coat protein-RNA interaction in the life cycle of bacteriophage MS2. *Molecular and General Genetics MGG* **254**, 358-364 (1997).

135   Hirao, I., Spingola, M., Peabody, D. & Ellington, A. D. The limits of specificity: an experimental analysis with RNA aptamers to MS2 coat protein variants. *Mol. Divers.* **4**, 75-89 (1998).

136   Mills, D., Priano, C., Merz, P. & Binderow, B. Q beta RNA bacteriophage: mapping cis-acting elements within an RNA genome. *J. Virol.* **64**, 3872-3881 (1990).

137   Borodavka, A., Tuma, R. & Stockley, P. G. Evidence that viral RNAs have evolved for efficient, two-stage packaging. *Proc. Natl. Acad. Sci. U. S. A.* **109**, 15769-15774, doi:10.1073/pnas.1204357109 (2012).

138   Horn, W. T. *et al.* Structural Basis of RNA Binding Discrimination between Bacteriophages Qβ and MS2. *Structure* **14**, 487-495, doi:http://dx.doi.org/10.1016/j.str.2005.12.006 (2006).

139   Peabody, D. S. The RNA binding site of bacteriophage MS2 coat protein. *The EMBO journal* **12**, 595 (1993).

140   Lim, F., Spingola, M. & Peabody, D. S. The RNA-binding site of bacteriophage Qβ coat protein. *J. Biol. Chem.* **271**, 31839-31845 (1996).

141   Beckett, D., Wu, H.-N. & Uhlenbeck, O. C. Roles of operator and non-operator RNA sequences in bacteriophage R17 capsid assembly. *J. Mol. Biol.* **204**, 939-947, doi:http://dx.doi.org/10.1016/0022-2836(88)90053-8 (1988).

142   Beckett, D. & Uhlenbeck, O. C. Ribonucleoprotein complexes of R17 coat protein and a translational operator analog. *J. Mol. Biol.* **204**, 927-938, doi:http://dx.doi.org/10.1016/0022-2836(88)90052-6 (1988).

143   Stockley, P. G. *et al.* A simple, RNA-mediated allosteric switch controls the pathway to formation of a T= 3 viral capsid. *J. Mol. Biol.* **369**, 541-552 (2007).

144   Gott, J. M., Wilhelm, L. J. & Olke, C. U. RNA binding properties of the coat protein from bacteriophage GA. *Nucleic Acids Res.* **19**, 6499-6503 (1991).

145   Muriaux, D., Mirro, J., Harvin, D. & Rein, A. RNA is a structural element in retrovirus particles. *Proc. Natl. Acad. Sci. U.S.A.* **98**, 5246-5251, doi:10.1073/pnas.091000398 (2001).

146   Belyi, V. A. & Muthukumar, M. Electrostatic origin of the genome packing in viruses. *Proc. Natl. Acad. Sci. U.S.A.* **103**, 17174-17178 (2006).

147   Devkota, B. *et al.* Structural and electrostatic characterization of pariacoto virus: implications for viral assembly. *Biopolymers* **91**, 530-538 (2009).

148   Hovlid, M. L. *et al.* Encapsidated Atom-Transfer Radical Polymerization in Q beta Virus-like Nanoparticles. *ACS Nano* **8**, 8003-8014, doi:10.1021/nn502043d (2014).

149   Latham, J. A. & Cech, T. R. Defining the inside and outside of a catalytic RNA molecule. *Science* **245**, 276-282 (1989).

150   Dent, K. C. *et al.* The asymmetric structure of an icosahedral virus bound to its receptor suggests a mechanism for genome release. *Structure* **21**, 1225-1234 (2013).

151   Fiedler, J. D., Brown, S. D., Lau, J. L. & Finn, M. G. RNA-Directed Packaging of Enzymes within Virus-like Particles. *Angew. Chem. Int. Ed.* **49**, 9648-9651, doi:10.1002/anie.201005243 (2010).

152   Ashley, C. E. *et al.* Cell-Specific Delivery of Diverse Cargos by Bacteriophage MS2 Virus-like Particles. *ACS Nano* **5**, 5729-5745, doi:10.1021/nn201397z (2011).

153   Golmohammadi, R., Fridborg, K., Bundule, M., Valegard, K. & Liljas, L. The crystal structure of bacteriophage Q beta at 3.5 angstrom resolution. *Structure* **4**, 543-554, doi:10.1016/s0969-2126(96)00060-3 (1996).

154   Bajaj, S. & Banerjee, M. Engineering Virus Capsids Into Biomedical Delivery Vehicles: Structural Engineering Problems in Nanoscale. *J. Biomed. Nanotechnol.* **11**, 53-69, doi:10.1166/jbn.2015.1959 (2015).

155   Drude, I., Dombos, V., Vauleon, S. & Muller, S. Drugs made of RNA: development and application of engineered RNAs for gene therapy. *Mini-Rev. Med. Chem.* **7**, 912-931 (2007).

156   Fire, A. *et al.* Potent and specific genetic interference by double-stranded RNA in Caenorhabditis elegans. *Nature* **391**, 806-811 (1998).

157   Meister, G. & Tuschl, T. Mechanisms of gene silencing by double-stranded RNA. *Nature* **431**, 343-349 (2004).

158   Zeng, Y., Wagner, E. J. & Cullen, B. R. Both natural and designed micro RNAs can inhibit the expression of cognate mRNAs when expressed in human cells. *Mol. Cell* **9**, 1327-1333 (2002).

159   Boden, D. *et al.* Enhanced gene silencing of HIV‑1 specific siRNA using microRNA designed hairpins. *Nucleic Acids Res.* **32**, 1154-1158 (2004).

160   Silva, J. M. *et al.* Second-generation shRNA libraries covering the mouse and human genomes. *Nat Genet* **37**, 1281-1288, doi:10.1038/ng1650 (2005).

161   Puglisi, J. D. & Tinoco, I., Jr. Absorbance melting curves of RNA. *Methods Enzymol.* **180**, 304-325 (1989).

162   Marky, L. A. & Breslauer, K. J. Calculating thermodynamic data for transitions of any molecularity from equilibrium melting curves. *Biopolymers* **26**, 1601-1620, doi:10.1002/bip.360260911 [doi] (1987).

163   MacRae, I. J. *et al.* Structural basis for double-stranded RNA processing by Dicer. *Science* **311**, 195-198 (2006).

164   MacRae, I. J., Zhou, K. & Doudna, J. A. Structural determinants of RNA recognition and cleavage by Dicer. *Nat. Struct. Mol. Biol.* **14**, 934-940 (2007).

165   Kozlovska, T. M. *et al.* Recombinant RNA phage Qβ capsid particles synthesized and self-assembled in Escherichia coli. *Gene* **137**, 133-137 (1993).

166   Johnson, S. M. *et al.* RAS is regulated by the let-7 microRNA family. *Cell* **120**, 635-647, doi:10.1016/j.cell.2005.01.014 (2005).

167   Pokorski, J. K., Hovlid, M. L. & Finn, M. G. Cell Targeting with Hybrid Q beta Virus-Like Particles Displaying Epidermal Growth Factor. *ChemBioChem* **12**, 2441-2447, doi:10.1002/cbic.201100469 (2011).

168   Galaway, F. A. & Stockley, P. G. MS2 Viruslike Particles: A Robust, Semisynthetic Targeted Drug Delivery Platform. *Mol. Pharm.* **10**, 59-68, doi:10.1021/mp3003368 (2013).

169   Yang, H.-W. *et al.* Gadolinium-functionalized nanographene oxide for combined drug and microRNA delivery and magnetic resonance imaging. *Biomaterials* **35**, 6534-6542 (2014).

170   Shan, Z. *et al.* An efficient method to enhance gene silencing by using precursor microRNA designed small hairpin RNAs. *Mol. Biol. Rep.* **36**, 1483-1489 (2009).

171   Yu, J.-Y., DeRuiter, S. L. & Turner, D. L. RNA interference by expression of short-interfering RNAs and hairpin RNAs in mammalian cells. *Proc. Natl. Acad. Sci. U.S.A.* **99**, 6047-6052 (2002).

172   Macrae, I., Li, F., Zhou, K., Cande, W. & Doudna, J. in *Cold Spring Harbor Symp. Quant. Biol.* 73-80 (Cold Spring Harbor Laboratory Press).

173   Roush, S. & Slack, F. J. The let-7 family of microRNAs. *Trends Cell Biol.* **18**, 505-516 (2008).

174   Akao, Y., Nakagawa, Y. & Naoe, T. let-7 microRNA functions as a potential growth suppressor in human colon cancer cells. *Biol. Pharm. Bull.* **29**, 903-906 (2006).

175   Schultz, J., Lorenz, P., Gross, G., Ibrahim, S. & Kunz, M. MicroRNA let-7b targets important cell cycle molecules in malignant melanoma cells and interferes with anchorage-independent growth. *Cell Res.* **18**, 549-557 (2008).

176   Trang, P. *et al.* Regression of murine lung tumors by the let-7 microRNA. *Oncogene* **29**, 1580-1587 (2010).

177   Takamizawa, J. *et al.* Reduced expression of the let-7 microRNAs in human lung cancers in association with shortened postoperative survival. *Cancer Res.* **64**, 3753-3756 (2004).

178   Yu, F. *et al.* let-7 regulates self renewal and tumorigenicity of breast cancer cells. *Cell* **131**, 1109-1123 (2007).

179   Lee, S.-T. *et al.* Let-7 microRNA inhibits the proliferation of human glioblastoma cells. *Journal of neuro-oncology* **102**, 19-24 (2011).

180   Pan, Y. *et al.* Development of a microRNA delivery system based on bacteriophage MS2 virus-like particles. *The FEBS journal* **279**, 1198-1208, doi:10.1111/j.1742-4658.2012.08512.x (2012).

181   Wei, B. *et al.* Development of an antisense RNA delivery system using conjugates of the MS2 bacteriophage capsids and HIV-1 TAT cell penetrating peptide. *Biomedicine & Pharmacotherapy* **63**, 313-318 (2009).

182   Wu, M., Brown, W. L. & Stockley, P. G. Cell-specific delivery of bacteriophage-encapsidated ricin A chain. *Bioconjugate Chem.* **6**, 587-595 (1995).

183   Wu, M., Sherwin, T., Brown, W. L. & Stockley, P. G. Delivery of antisense oligonucleotides to leukemia cells by RNA bacteriophage capsids. *Nanomed. Nanotechnol. Biol. Med.* **1**, 67-76 (2005).

184   Ida, R. & Wu, G. Direct NMR detection of alkali metal ions bound to G-quadruplex DNA. *J. Am. Chem. Soc.* **130**, 3590-3602, doi:10.1021/ja709975z (2008).

185   Tuthill, T. J., Bubeck, D., Rowlands, D. J. & Hogle, J. M. Characterization of early steps in the poliovirus infection process: receptor-decorated liposomes

induce conversion of the virus to membrane-anchored entry-intermediate particles. *J. Virol.* **80**, 172-180 (2006).

186   Nel, A. E. *et al.* Understanding biophysicochemical interactions at the nano–bio interface. *Nature materials* **8**, 543-557 (2009).

187   Lächelt, U. *et al.* Fine-tuning of proton sponges by precise diaminoethanes and histidines in pDNA polyplexes. *Nanomed. Nanotechnol. Biol. Med.* **10**, 35-44 (2014).

188   Brunel, F. M. *et al.* Hydrazone ligation strategy to assemble multifunctional viral nanoparticles for cell imaging and tumor targeting. *Nano Lett* **10**, 1093-1097, doi:10.1021/nl1002526 (2010).

189   Galaway, F. A. & Stockley, P. G. MS2 viruslike particles: a robust, semisynthetic targeted drug delivery platform. *Mol Pharm* **10**, 59-68, doi:10.1021/mp3003368 (2013).

190   Kaczmarczyk, S. J., Sitaraman, K., Young, H. A., Hughes, S. H. & Chatterjee, D. K. Protein delivery using engineered virus-like particles. *Proc. Natl. Acad. Sci. U. S. A.* **108**, 16998-17003, doi:10.1073/pnas.1101874108 (2011).

191   Chao, C.-N. *et al.* Inhibition of human diffuse large B-cell lymphoma growth by JC polyomavirus-like particles delivering a suicide gene. *Journal of translational medicine* **13**, 1-9 (2015).

192   Stanley, M. Prophylactic HPV vaccines. *J. Clin. Pathol.* **60**, 961-965 (2007).

193   Lynn, D. M. & Langer, R. Degradable Poly(β-amino esters): Synthesis, Characterization, and Self-Assembly with Plasmid DNA. *J. Am. Chem. Soc.* **122**, 10761-10768, doi:10.1021/ja0015388 (2000).

194   Akinc, A., Thomas, M., Klibanov, A. M. & Langer, R. Exploring polyethylenimine‐mediated DNA transfection and the proton sponge hypothesis. *The journal of gene medicine* **7**, 657-663 (2005).

195   Yin, H. *et al.* Non-viral vectors for gene-based therapy. *Nature Reviews Genetics* **15**, 541-555 (2014).

196   Jiang, H.-L. *et al.* Aerosol delivery of spermine-based poly (amino ester)/Akt1 shRNA complexes for lung cancer gene therapy. *Int. J. Pharm.* **420**, 256-265 (2011).

197   Ali, M., Hicks, A. E., Hellewell, P. G., Thoma, G. & Norman, K. E. Polymers bearing sLex-mimetics are superior inhibitors of E-selectin-dependent leukocyte rolling in vivo. *The FASEB journal* **18**, 152-154 (2004).

198   Zanta, M.-A., Boussif, O., Adib, A. & Behr, J.-P. In vitro gene delivery to hepatocytes with galactosylated polyethylenimine. *Bioconj. Chem.* **8**, 839-844 (1997).

199   Chou, L. Y., Ming, K. & Chan, W. C. Strategies for the intracellular delivery of nanoparticles. *Chem. Soc. Rev.* **40**, 233-245 (2011).

200   Fröhlich, E. The role of surface charge in cellular uptake and cytotoxicity of medical nanoparticles. *International journal of nanomedicine* **7**, 5577 (2012).

201   Villanueva, A. *et al.* The influence of surface functionalization on the enhanced internalization of magnetic nanoparticles in cancer cells. *Nanotechnology* **20**, 115103 (2009).

202 Yue, Z.-G. *et al.* Surface charge affects cellular uptake and intracellular trafficking of chitosan-based nanoparticles. *Biomacromolecules* **12**, 2440-2446 (2011).

203 Hovlid, M. L. *et al.* Encapsidated atom-transfer radical polymerization in Qbeta virus-like nanoparticles. *ACS nano* **8**, 8003-8014, doi:10.1021/nn502043d (2014).

204 Banerjee, D., Liu, A. P., Voss, N. R., Schmid, S. L. & Finn, M. Multivalent display and receptor-mediated endocytosis of transferrin on virus-like particles. *ChemBioChem* **11**, 1273-1279 (2010).

205 Touze, A. & Coursaget, P. In vitro gene transfer using human papillomavirus-like particles. *Nucleic Acids Res.* **26**, 1317-1323 (1998).

206 Takamura, S. *et al.* DNA vaccine-encapsulated virus-like particles derived from an orally transmissible virus stimulate mucosal and systemic immune responses by oral administration. *Gene Ther.* **11**, 628-635 (2004).

207 Jariyapong, P. *et al.* Encapsulation and delivery of plasmid DNA by virus-like nanoparticles engineered from Macrobrachium rosenbergii nodavirus. *Virus Res.* **179**, 140-146 (2014).

208 Chen, L. S. *et al.* Efficient gene transfer using the human JC virus-like particle that inhibits human colon adenocarcinoma growth in a nude mouse model. *Gene Ther* **17**, 1033-1041 (2010).

209 Fang, C.-Y. *et al.* Analysis of the size of DNA packaged by the human JC virus-like particle. *J. Virol. Methods* **182**, 87-92 (2012).

210 Guo, P., Erickson, S. & Anderson, D. A small viral RNA is required for in vitro packaging of bacteriophage phi 29 DNA. *Science* **236**, 690-694 (1987).

211 Shu, D., Shu, Y., Haque, F., Abdelmawla, S. & Guo, P. Thermodynamically stable RNA three-way junction for constructing multifunctional nanoparticles for delivery of therapeutics. *Nature nanotechnology* **6**, 658-667 (2011).

212 Khaled, A., Guo, S., Li, F. & Guo, P. Controllable self-assembly of nanoparticles for specific delivery of multiple therapeutic molecules to cancer cells using RNA nanotechnology. *Nano Lett.* **5**, 1797-1808 (2005).

213 Shu, Y., Cinier, M., Fox, S. R., Ben-Johnathan, N. & Guo, P. Assembly of therapeutic pRNA-siRNA nanoparticles using bipartite approach. *Mol. Ther.* **19**, 1304-1311 (2011).

214 Wang, D. *et al.* Engineering a lysosomal enzyme with a derivative of receptor-binding domain of apoE enables delivery across the blood–brain barrier. *Proc. Natl. Acad. Sci. U. S. A.* **110**, 2999-3004, doi:10.1073/pnas.1222742110 (2013).

215 Rhee, J. K. *et al.* Colorful virus-like particles: fluorescent protein packaging by the Qbeta capsid. *Biomacromolecules* **12**, 3977-3981, doi:10.1021/bm200983k (2011).

VITA

PO-YU FANG

Po-Yu was born in Miaoli, Taiwan. When he was eighteen-year-old, he came to Los Angeles, California and was accepted to the California State University, Fullerton. Po-Yu was accepted to the Chemistry and Biochemistry program accidently instead of Business program and graduate with Cum Laude. He then pursued a doctoral degree at Georgia Institute of Technology within the school of Chemistry & Biochemistry.